Doctoral Dissertation

Numerical study on local pressure components and interfacial tensions of liquid film in the vicinity of solid surface by classical molecular dynamics method

Kunio Fujiwara

January 2015

Graduate School of Engineering

Osaka University

Abstract

A general perturbative method on the basis of statistical thermodynamics is proposed for a fluid-solid interfacial system in the canonical and grand canonical ensembles. This method allows us to obtain local pressure components and interfacial tensions acting on the fluid at a fluid-solid interface, which includes contributions of pressure components tangential to the interface affected by interactions with solid atoms. Furthermore, an instantaneous expression of the local pressure components and interfacial tensions, which is based on a volume perturbation, is presented to investigate time-dependent phenomena in molecular simulations.

Numerical analyses are conducted by the classical molecular dynamics method for a liquid film on a flat solid surface and in the vicinity of a structured solid surface, where all the interactions between particles are described by the 12-6 Lennard-Jones potential. The purpose is to reveal local thermodynamic quantities: pressure components and interfacial tensions, based on the proposed method, and the molecular transition mechanism between the two states of the liquid film: (a) liquid film on the slit and (b) liquid film in the slit, based on the local thermodynamic quantities.

Comparisons between the numerical results of the liquid film on a flat solid surface obtained by the proposed perturbative method and by the alternative two methods, indicate that the proposed perturbative method is applicable and suitable for practical use in molecular simulations, to obtain the local pressure components and interfacial tensions at a fluid-solid interface in equilibrium states.

The numerical results of the liquid film in the vicinity of a structured solid surface, show that wetting phenomena of the slit pore, i.e., whether the inside of the slit pore is filled with liquid molecules within a definite time, as well as the characteristic time of the phenomena, are dependent on the intensity of the fluid molecule-solid atom interaction. The time-averaged local pressure components and interfacial tensions in the vicinity of the corner of the slit, are different from those obtained in other areas, for cases where the fluid-solid interaction intensities are relatively strong. The difference between the integrated vapor-solid and liquid-solid interfacial tensions acting on the fluid outside the slit, predicts for the most part the occurrence of the liquid film in one state or the other. However, it does not determine a definite threshold between the two states on a molecular temporal-spatial scale, i.e., it does not predict fluctuations of the liquid film and variations of the local quantities in the vicinity of the corner of the slit. The local interfacial tensions, defined in this thesis, reveal that the minimum values of the local interfacial tensions inside the slit, in the vicinity of the 2nd and 3rd layers of solid atoms from the entrance of the slit respectively, act as a trigger to cause the transition between the two states. These results reveal that there exist the phenomena on a molecular temporal-spatial scale which are not comprehended through the thermodynamic quantities based on the macroscopic concept, and which lead to the transport of the condensed matter.

Acknowledgements

I would like to express my sincere gratitude to Professor Masahiko Shibahara for giving me an opportunity to do my research freely, and for his guidance and support during my research.

I am also grateful to my thesis committee members: Professor Takeru Yano, Professor Fumiteru Akamatsu, and Professor Shohji Tsushima, for their valuable comments and advice.

I would like to thank Professor Nobumasa Sugimoto, Associate Professor Takao Yoshinaga, and Dr. Kentaro Kan, for giving me a seed for the research, when I was a student in the Master's course of Graduate School of Engineering Science in Osaka University.

I also acknowledge the members in Shibahara Laboratory: Assistant professor Y. Ueki, Ms. Y. Saito, and the students, who kindly supported my research.

I couldn't have done this work without the help of the members in my company. I would especially like to thank Dr. M. Arita, Dr. S. Nadahara, Mr. K. Terashima, Mr. K. Kinose, Mr. T. Funayoshi, Mr. Y. Nakazawa, Mr. I. Kajino, Mr. T. Kawamura, and Mr. J. Yoshida of SCREEN Holdings Co., Ltd. for supporting this work.

Finally, I thank my family for supporting this work.

Table of contents

Nomenclature

A	Interfacial area
A_s	Interfacial area
A_{s,V_k}	Interfacial area in local volume, V_k
$A_{s,0}$	Interfacial area in system 0
$A_{s,1}$	Interfacial area in system 1
$A_{s,0,V_k}$	Interfacial area in local volume, V_k in system 0
$A_{s,1,V_k}$	Interfacial area in local volume, V_k in system 1
A_η	Plane perpendicular to η coordinate
A_{η,V_k}	Plane perpendicular to η coordinate in local volume, V_k
$A_{\eta,0}$	Plane perpendicular to η coordinate in system 0
$A_{\eta,1}$	Plane perpendicular to η coordinate in system 1
$A_{\eta,0,V_k}$	Plane perpendicular to η coordinate in local volume, V_k in system 0
$A_{\eta,1,V_k}$	Plane perpendicular to η coordinate in local volume, V_k in system 1
A_ξ	Plane perpendicular to ξ coordinate
A_{ξ,V_k}	Plane perpendicular to ξ coordinate in local volume, V_k
$A_{\xi,0}$	Plane perpendicular to ξ coordinate in system 0
$A_{\xi,1}$	Plane perpendicular to ξ coordinate in system 1
$A_{\xi,0,V_k}$	Plane perpendicular to ξ coordinate in local volume, V_k in system 0
$A_{\xi,1,V_k}$	Plane perpendicular to ξ coordinate in local volume, V_k in system 1
$\mathrm{d}x_k$	Length in the x direction of local volume, V_k
$\mathrm{d}y_k$	Length in the y direction of local volume, V_k
$\mathrm{d}z_k$	Length in the z direction of local volume, V_k
$\mathrm{d}z_{ij,0}$	z component of distance between particles in local volume, $V_{k,}$ in system 0
$\mathrm{d}z_{ij,1}$	z component of distance between particles in local volume, V_k in system 1
$\mathrm{d}\xi_k$	Length in the ξ direction of local volume, V_k
$\mathrm{d}\xi_{k,0}$	Length in the ξ direction of local volume, V_k in system 0
$\mathrm{d}\xi_{k,1}$	Length in the ξ direction of local volume, V_k in system 1
$f_{ij\xi}$	ξ component of the intermolecular force acting on ith fluid particle due to jth fluid particle
f_ξ	Total ξ component of intermolecular force between fluid particles through the local area A_{ξ,V_k} in V_k
$f_{ij\xi}^{'}$	ξ component of the intermolecular force acting on ith fluid particle due to jth solid particle
$f_\xi^{'}$	Total ξ component of the intermolecular force acting on fluid particles due to the interactions with solid atoms, through the local area A_{ξ,V_k}

	in V_k.
$\mathbf{f}_i$	Force vector of ith particle
F	Helmholtz free energy
h	Planck constant
H	Hamiltonian
I	Impregnation parameter
$\hat{I}$	Instantaneous expression of impregnation parameter
k_B	Boltzmann constant
K	Kinetic energy
L_x	Length in the x direction of volume
$L_{x,0}$	Length in the x direction of volume in system 0
$L_{x,1}$	Length in the x direction of volume in system 1
L_y	Length in the y direction of volume
$L_{y,0}$	Length in the y direction of volume in system 0
$L_{y,1}$	Length in the y direction of volume in system 1
L_z	Length in the z direction of volume
$L_{z,0}$	Length in the z direction of volume in system 0
$L_{z,1}$	Length in the z direction of volume in system 1
L_ξ	Length in the ξ direction of volume
$L_{\xi,0}$	Length in the ξ direction of volume in system 0
$L_{\xi,1}$	Length in the ξ direction of volume in system 1
$L_{\neq\xi}$	Length in the direction($\neq\xi$) of volume
L_x^u	Length in the x direction of volume above the slit
L_y^u	Length in the y direction of volume above the slit
L_z^u	Length in the z direction of volume above the slit
m	Mass of a particle
m_i	Mass of ith particle
N	Number of particles
N_f	Number of fluid particles
N_s	Number of solid particles
N_{V_k}	Number of particles in local volume, V_k
$\mathbf{p}$	Momentum vector of a particle
$\mathbf{p}_i$	Momentum vector of ith particle
p_{ix}	x component of momentum of ith particle
p_{iy}	y component of momentum of ith particle
p_{iz}	z component of momentum of ith particle
$p_{i\xi}$	ξ component of momentum of ith particle
P	Pressure
P_N	Pressure component normal to interface
P_T	Pressure component tangential to interface
$P_{\xi\xi}$	ξ component of pressure acting on a plane perpendicular to ξ coordinate
$P_{\xi\eta}$	ξ component of pressure acting on a plane perpendicular to η coordinate
P_{xx,V_k}	x component of pressure acting on a plane perpendicular to x

	coordinate at local volume, V_k
P_{yy,V_k}	y component of pressure acting on a plane perpendicular to y coordinate at local volume, V_k
P_{zz,V_k}	z component of pressure acting on a plane perpendicular to z coordinate at local volume, V_k
$P_{\eta\eta,V_k}$	η component of pressure acting on a plane perpendicular to η coordinate at local volume, V_k
$P_{\xi\xi,V_k}$	ξ component of pressure acting on a plane perpendicular to ξ coordinate at local volume, V_k
$P_{\xi\eta,V_k}$	ξ component of pressure acting on a plane perpendicular to η coordinate at local volume, V_k
$\hat{P}_{\xi\xi,V_k}$	Instantaneous expression of ξ component of pressure acting on a plane perpendicular to ξ coordinate at local volume, V_k
$\hat{P}_{\eta\eta,V_k}$	Instantaneous expression of η component of pressure acting on a plane perpendicular to η coordinate at local volume, V_k
Q_{NVT}	Canonical partition function
$Q_{NVT,0}$	Canonical partition function of system 0
$Q_{NVT,1}$	Canonical partition function of system 1
r_{ij}	Distance between ith particle and jth particle
$\mathbf{r}$	Positional vector of a particle
$\mathbf{r}_i$	Positional vector of ith particle
$\mathbf{r}_j$	Positional vector of jth particle
$\mathbf{r}_{ij}$	$\mathbf{r}_{ij}=\mathbf{r}_i-\mathbf{r}_j$
$\mathbf{r}_0$	Positional vector of a particle in system 0
$\mathbf{r}_1$	Positional vector of a particle in system 1
t	Time
T	Absolute temperature
T_{V_k}	Temperature in V_k
$\hat{T}_{V_k}$	Instantaneous temperature in V_k
u_{ff}	Potential energy between fluid particles
u_{fs}	Potential energy between fluid particle and solid particle
u_{ext}	External potential energy due to solid atoms
U	Potential energy, or Potential energy between fluid particles
$U_{Ar\text{-}Pt}$	Potential energy between Ar molecules and Pt atoms
U_{V_k}	Potential energy between fluid particles in local volume, V_k
U_0	Potential energy between fluid particles in system 0
U_{0,V_k}	Potential energy between fluid particles in local volume, V_k, in system 0
U_1	Potential energy between fluid particles in system 1
U_{1,V_k}	Potential energy between fluid particles in local volume, V_k, in system 1
$\mathbf{v}_i$	Velocity vector of ith particle

V	Volume
V_k	kth local Volume
V_0	Volume of system 0
V_1	Volume of system 1
V^{u}	Volume above the slit
x	Coordinate in the direction of width in system
$x_{f,0}$	x component of positional vector of a fluid particle in system 0
$x_{fs,0}$	x component of distance between fluid particle and solid particle in system 0
$x_{fs,1}$	x component of distance between fluid particle and solid particle in system 1
$x_{s,0}$	x component of positional vector of a solid particle in system 0
x_{ij}	x component of distance between ith particle and jth particle
y	Coordinate in the direction of depth in system
$y_{f,0}$	y component of positional vector of a fluid particle
$y_{fs,0}$	y component of distance between fluid particle and solid particle in system 0
$y_{fs,1}$	y component of distance between fluid particle and solid particle in system 1
$y_{s,0}$	y component of positional vector of a solid particle
y_{ij}	y component of distance between ith particle and jth particle
z	Coordinate in the direction of height in system
$z_{f,0}$	z component of positional vector of a fluid particle in system 0
$z_{fs,0}$	z component of distance between fluid particle and solid particle in system 0
$z_{fs,1}$	z component of distance between fluid particle and solid particle in system 1
$z_{s,0}$	z component of positional vector of a solid particle in system 0
z_{ij}	z component of distance between ith particle and jth particle
$z_{ij,0}$	z component of distance between ith particle and jth particle in system 0
$z_{ij,1}$	z component of distance between ith particle and jth particle in system 1

α	Fluid-solid interaction intensity
β	$\beta=1/(k_BT)$
γ	Interfacial tension
γ_{ls}	Liquid-solid interfacial tension
γ_{vs}	Vapor-solid interfacial tension
$\hat{\gamma}_{ls}$	Instantaneous expression of liquid-solid interfacial tension
$\hat{\gamma}_{vs}$	Instantaneous expression of vapor-solid interfacial tension
γ_{V_k}	Local interfacial tension at local volume, V_k
$\hat{\gamma}_{\xi-\eta}$	Instantaneous expression of interfacial tension at local volume, V_k,

	defined by difference of the pressure components between normal(ξ) and tangential(η) to an interface
ΔA_s	$A_{s,1}$-$A_{s,0}$
$\Delta A_{s,V_k}$	$A_{s,1,V_k} - A_{s,0,V_k}$
$\Delta A_{\eta,V_k}$	$A_{\eta,1,V_k} - A_{\eta,0,V_k}$
$\Delta A_{\xi,V_k}$	$A_{\xi,1,V_k} - A_{\xi,0,V_k}$
$\Delta(\mathrm{d}\xi_k)$	$\mathrm{d}\xi_{k,1}$-$\mathrm{d}\xi_{k,0}$
ΔF	F_1- F_0
ΔL_ξ	$L_{\xi,1}$- $L_{\xi,0}$
Δt	Time step interval
ΔU	U_1- U_0
ΔU_{V_k}	$U_{1,V_k} - U_{0,V_k}$
ΔV	V_1- V_0
$\Delta \Phi$	Φ_1- Φ_0
$\Delta \Phi_{V_k}$	$\Phi_{1,V_k} - \Phi_{0,V_k}$
ε	Lennard-Jones parameter
ε_{Ar}	Lennard-Jones parameter between Ar molecules
$\varepsilon_{Ar\text{-}Pt}$	Lennard-Jones parameter between Ar molecules and Pt atoms
ε_{ff}	Lennard-Jones parameter between fluid particles
ε_{fs}	Lennard-Jones parameter between fluid and solid particles, fluid-solid interaction intensity
ε_{Pt}	Lennard-Jones parameter between Pt atoms
ε_{ss}	Lennard-Jones parameter between solid particles
η	Coordinate(=x, y, or z)
Θ	Heaviside step function
λ	Perturbation parameter
Λ	de Broglie thermal wavelength
μ	Chemical potential
ξ	Coordinate(=x, y, or z)
$\Xi_{\mu VT}$	Grand canonical partition function
$\Xi_{\mu VT,0}$	Grand canonical partition function in system 0
$\Xi_{\mu VT,1}$	Grand canonical partition function in system 1
π	Circular constant($\cong$3.14)
ρ	Density of fluid
σ	Lennard-Jones parameter
σ_{Ar}	Lennard-Jones parameter between Ar molecules
$\sigma_{Ar\text{-}Pt}$	Lennard-Jones parameter between Ar molecules and Pt atoms
σ_{ff}	Lennard-Jones parameter between fluid particles
σ_{fs}	Lennard-Jones parameter between fluid and solid particles
σ_{Pt}	Lennard-Jones parameter between Pt atoms
σ_{ss}	Lennard-Jones parameter between solid particles
Φ	Potential energy between fluid and solid particles

Φ_{V_k}	Potential energy between fluid and solid particles in local volume, V_k
Φ_{0,V_k}	Potential energy between fluid and solid particles in local volume, V_k in system 0
Φ_{1,V_k}	Potential energy between fluid and solid particles in local volume, V_k in system 1
Φ_0	Potential energy between fluid and solid particles in system 0
Φ_1	Potential energy between fluid and solid particles in system 1
$\Omega_{\mu VT}$	Grand canonical potential
$\Omega_{\mu VT,0}$	Grand canonical potential in system 0
$\Omega_{\mu VT,1}$	Grand canonical potential in system 1

$\mathfrak{U}$	Total potential energy in system

1. Introduction

Liquid-solid interface where the solid surface has nanometer-scale structures, allows room to study, not only complicated molecular systems, for instance, which consist of polymer molecules interacting with solid surfaces having terminations under quantum effects, but also simple systems consisting of spherical particles interacting by the Lennard-Jones potential. However, phenomena at the structured liquid-solid interface such as evaporation, condensation, diffusion, and wetting, are related to complex physics and chemistry over a wide range of temporal-spatial scale, and hence it is difficult to obtain a complete picture of the phenomena (e.g. Schoch *et al.* 2008; Plawsky *et al.* 2014).

In the semiconductor industry, with the help of the photolithographic technique which enable us to produce structures of a few nanometers (e.g. Ito *et al.* 2006), controlling those phenomena in the vicinity of the liquid-solid interface with the nanometer-scale structures is a crucial issue especially in the wet cleaning process used to manufacture semiconductor devices (see Fig. 1.1) as reported by the recent paper of Choi (2014), and a precise understanding of those phenomena is also beneficial in the engineering fields such as the thermal engineering and chemical engineering, to design surfaces to control the mass, momentum, and energy transport phenomena which occur at and through the interface.

Such non-equilibrium transport phenomena including the liquid-solid interface with the nanostructures are difficult to understand on the basis of the common non-equilibrium thermodynamics (e.g. de Groot & Mazur 1984), because the concept of the local equilibrium assumption (Prigogine 1955) is difficult to accept, particularly in nanoscale. As a promising theory, there is the statistical mechanics which explains the relationship between the macroscopic thermodynamics and microscopic pictures of matter in an equilibrium state (e.g. Hill 1986), but the extension to a generalized description which is not based on the local equilibrium assumption in non-equilibrium systems, has yet to be established (Zubarev 1974; Evans & Morriss 2008). Hence, elucidations of those molecular temporal-spatial phenomena at the nano-structured liquid-solid interface and of connections with the macroscopic transport phenomena, are still beyond rigorous theoretical frameworks.

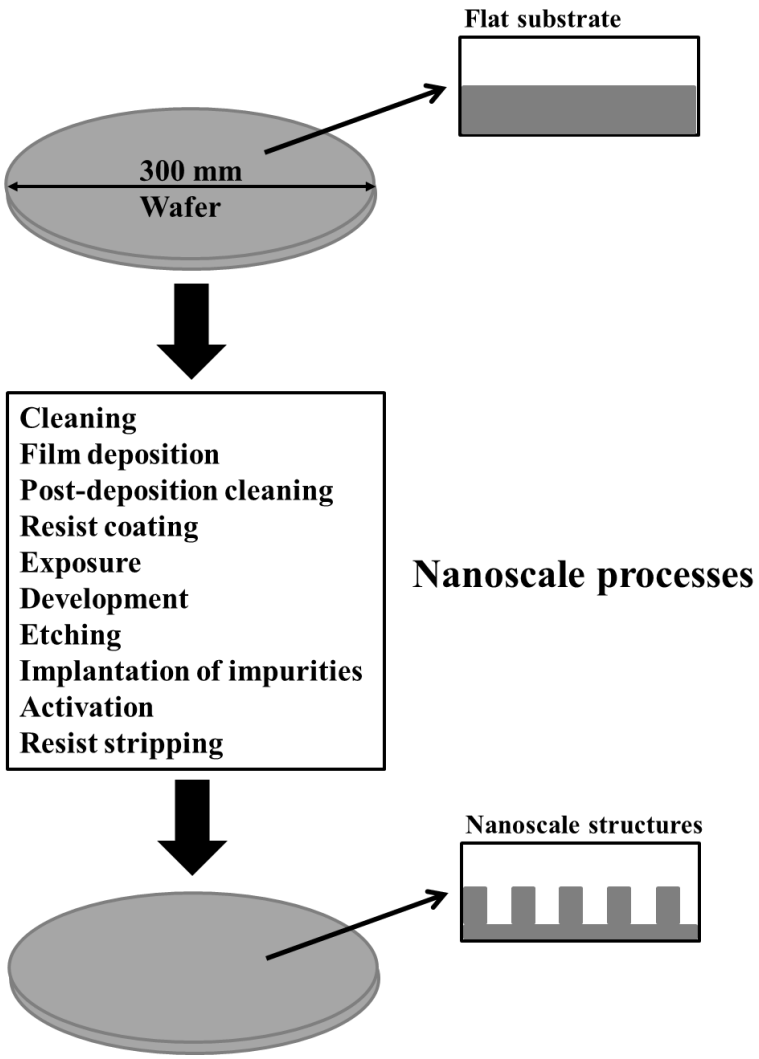

Fig. 1.1 Semiconductor manufacturing processes.

One way of accessing the microscopic physics and chemistry in relation to states of atoms and molecules is to use numerical analyses by molecular simulations such as Monte Carlo and molecular dynamics methods (e.g. Allen & Tildesley 1987), which have been developed with the progress of the semiconductor devices, and widely used in equilibrium and non-equilibrium systems. These techniques in the framework of the classical mechanics assume that the atoms and molecules interact with each other

through implicitly-defined potential functions. Of the two methods, the molecular dynamics method allows us to obtain information on instantaneous positions and velocities of atoms or molecules, therefore the method has been also applied to non-equilibrium systems, for instance, to elucidate the momentum and energy transport mechanism in a liquid phase and through a liquid-solid interface (e.g. Ohara 1999; Torii & Ohara 2007). Shibahara *et al.* (2008, 2011) conducted molecular dynamics simulations to elucidate energy transfer mechanism through a liquid-solid interfacial system with structures, and showed possibilities of energy transfer enhancements by the structures at the liquid-solid interface. However, through those studies, the local thermodynamics quantities in the vicinity of the liquid-solid interface, and its relations to the imposed momentum and energy fluxes, have yet to be elucidated.

The state of a structured liquid-solid interface can be classified into the two situations shown in Fig. 1.2, where we consider an ideal model of a liquid film in the vicinity of a solid surface with a slit pore. One is the state of (a) liquid film on the slit pore, and the other is (b) liquid film in the slit pore. These two states are historically called Cassie-Baxter (Cassie & Baxter 1944) and Wenzel (Wenzel 1936) states respectively if the shape of the liquid on the solid surface is a droplet, and the difference of the states has a potential to control the macroscopic phenomena at and through the structured liquid-solid interface in relation to the wetting (e.g. Choi & Kim 2011). As a result, from macro- to nano-scale, numerous studies related to the two states have been devoted for many years using theories, numerical analyses, and experiments (e.g. Mickel *et al.* 2011; Bohlen *et al.* 2008; Kumar *et al.* 2011; Verplanck *et al.* 2007; Ma *et al.* 2012).

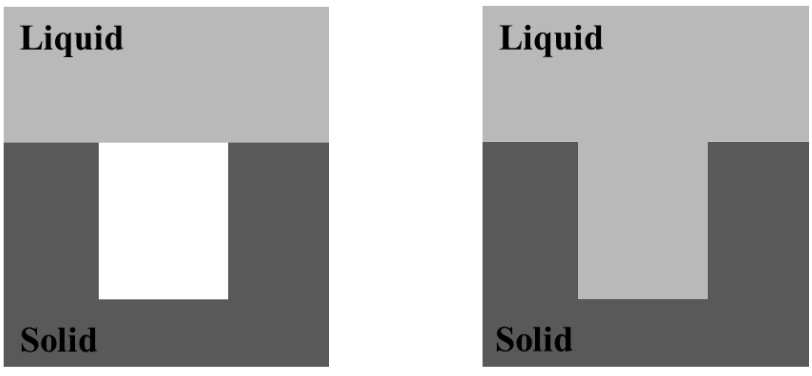

(a) Liquid film on the slit pore. (b) Liquid film in the slit pore.

Fig. 1.2 Schematic illustration of the two states of the liquid-solid interface with a slit pore.

Macroscopic thermodynamics (e.g. Callen 1985) tells that the state of (b) liquid film in the slit is implemented through the lower free energy than that of the state of (a) liquid film on the slit, in a macroscopic scale. However, it doesn't tell whether the macroscopic thermodynamic quantities such as the pressure, interfacial tension, temperature, entropy, chemical potential, are allowable in a nanoscopic local volume even in an equilibrium state. Furthermore, the molecular transition process from one state to the other is beyond the framework of the theory.

In particular, in molecular systems, it is known by the results of the molecular dynamics simulations that the fluid-solid interaction intensity has a dominant influence on the wetting phenomena (Shi & Dhir 2009; Koishi *et al.* 2009; Ould-Kaddour & Levesque 2011). However, under the influence of a varying fluid-solid interaction, the local thermodynamic states of the liquid in the vicinity of the solid surface having nanometer-scale structures, which is intimately involved in the interfacial phenomena, and the transition mechanism between the two states based on the local thermodynamic quantities, have yet to be revealed from a molecular point of view.

The intensive variable, pressure, one of the fundamental thermodynamic quantities and directly connected to the interfacial tension, is indispensable for discussion of such interfacial phenomenon. Irving & Kirkwood (1950) derived microscopic expression for the pressure tensor, based on the statistical mechanics, and the derived expression is widely spread through the time-averaged formalism in an equilibrium state (e.g. Walton *et al.* 1982; Varnik *et al.* 2000). Later, Todd *et al.* (1995) derived microscopic expressions to obtain instantaneous quantitiy of the pressure tensor, by evaluating intermolecular forces acting on a plane. These expressions have been applied in molecular simulations to obtain pressure components based on the states of the atoms and molecules.

On the other hand, attempts to obtain thermodynamic quantities based on the differential forms of free energies have been made, but not received a great deal of attention, compared with the above expressions. Zwanzig (1954) performed a perturbation expansion on the partition function of the system, and obtained a relationship between the difference of the configurational free energy and the paritition function. Later, Bennett (1976) evaluated the free energy difference by a multistage approach called "The acceptance ratio method" in the Monte Carlo method. On the other hand, based on a numerical evaluation of the free energy difference of Eppenga & Frenkel (1984), Harismiadis *et al.* (1996) generalized their calculation method to obtain

the vapor pressure for the Lennard-Jones fluid. The generalized method has been called "Volume perturbation(VA) method". Recently, aiming at calculating the surface tension of a vapor-liquid interface, Gloor *et al.* (2005) published a detailed paper, in which the "Test-area(TA) method" is presented on the basis of the constant-volume perturbation. These perturbative methods may be applied to vapor-liquid interfaces, and the results provide details not only for the overall liquid-vapor interface tension but also the local interface tension (de Miguel & Jackson 2006; Ibergay *et al.* 2007; Biscay *et al.* 2009). However application of these methods to the liquid-solid interface has been limited to a few studies. In the paper of Nair & Sathian (2012), the TA method was applied to obtain the liquid-solid interfacial tension for a system composed of fluid molecules sandwiched between two flat solid surfaces consisting of solid atoms, although the paper gives no details about the method and the results are not fully examined. Míguez *et al.* (2012) extended the TA methodology to the grand canonical ensemble and applied it to a system of fluid molecules confined in a pore. The results showed the consistency of the Irving-Kirkwood(IK) method including only the normal pressure component affected by the fluid-solid interaction because of the integrated form of the fluid-solid interaction function. Throughout the studies mentioned above, a perturbative method to obtain the local pressure components and interfacial tension at a liquid-solid interface has not been established, i.e., a general perturbative method that includes the effects of the tangential pressure components affected by the solid atoms has not been presented. It should be also noted that the previous studies have focused on obtaining results in one dimension (namely, perpendicular to the interfaces), and the pressure components and interfacial tension at a liquid-solid interface were not obtained in two dimensions.

In this thesis, a general perturbative method on the basis of statistical thermodynamics is proposed for a fluid-solid interfacial system in the canonical and grand canonical ensembles. The method allows us to obtain local pressure components and interfacial tensions acting on the fluid at a fluid-solid interface, which includes contributions of pressure components tangential to the interface affected by interactions with solid atoms. Furthermore, an instantaneous expression of the local pressure components and interfacial tensions, which is based on a volume perturbation, is presented to investigate time-dependent phenomena in molecular simulations.

Numerical analyses are conducted by the classical molecular dynamics method for a liquid film on a flat solid surface and in the vicinity of a structured solid surface, where all the interactions between particles are described by the 12-6 Lennard-Jones potential. The purpose is to reveal local thermodynamic quantities: pressure components and

interfacial tensions, based on the proposed method, and the molecular transition mechanism between the two states of the liquid film: (a) liquid film on the slit and (b) liquid film in the slit, based on the local thermodynamic quantities. This thesis is organized as follows:

In Chapter 2, theories of the perturbative method are presented. As described above, a general perturbative method that includes the effects of the tangential pressure components affected by the solid atoms has not been presented. First, in Sec. 2.1, a description of the perturbative method which includes the effect of an external potential, is derived to obtain pressure components and interfacial tension acting on the fluid at a fluid-solid interface on the basis of statistical thermodynamics for the canonical and grand canonical ensembles. Later, in Sec. 3.2, the treatment of the derived description in molecular simulation is explained to include the effects of the tangential pressure components affected by the solid atoms. The description is assumed to be applicable in subsystems in Sec. 2.2.1 to obtain local pressure components and interfacial tension. Two alternative methods are presented in Sec. 2.2.2 and Sec. 2.2.3 respectively to compare the results of the local interfacial tension calculation: the first method evaluates the intermolecular force acting on a plane, and the second is the conventional virial expression based on the Irving and Kirkwood definition. In Sec. 2.3 an instantaneous expression of the local pressure components and interfacial tensions, which is based on a volume perturbation, is presented to investigate time-dependent phenomena in molecular simulations.

In Chapter 3, methods for the numerical analyses are presented. First, the classical molecular dynamics method is introduced in Sec. 3.1. In Sec. 3.2.1, the procedure to evaluate energy difference in the perturbative method presented in Chapter 2, is proposed for fluid-solid interfacial systems consisting of flat and structured interfaces. Finally, Sec. 3.2.2 proposes the method to evaluate the energy difference in the local volume by using the perturbative method.

In Chapter 4, before detailed analyses of the liquid film on a flat solid surface (Chapter5) and in the vicinity of a structured solid surface (Chapters 6 and 7), a phenomenological analysis of wetting phenomena at a solid surface with a slit pore is conducted by the molecular dynamics method, in order to understand dynamic characteristics of a liquid film consisting of fluid molecules. Through the analyses, effects of the fluid-solid interaction intensity on the dynamic wetting phenomena are examined. First, in Sec. 4.1, the calculation system and numerical details used in this

Chapter are described. Sec. 4.2 shows results of the effects of the fluid-solid interaction intensity on the dynamic wetting phenomena.

In Chapter 5, the molecular dynamics simulation is conducted for the calculation system in which fluid molecules are confined between two planar solid surfaces, in order to obtain in particular local pressure components, interfacial tension of the liquid film which exists on a flat solid surface, and check the validity of the proposed perturbative method. The calculation system and numerical details are described in Sec. 5.1. In Sec. 5.2, the local pressure components and interfacial tension of the liquid in the vicinity of the solid surface are obtained by the proposed perturbative method in one dimension, and the results are compared with those obtained by two alternative methods: the first method evaluates the intermolecular force acting on a plane, and the second is the conventional method based on the virial expression. The quantities are also obtained in two dimensions and the results are shown in Sec. 5.3.

In Chapter 6, as the local thermodynamic quantities, the time-averaged local density and pressure components of the fluid are obtained for the two states of the liquid film: (a) liquid film on the slit and (b) liquid film in the slit, based on the instantaneous expression of the pressure components. Sec. 6.1 describes the system and numerical details used in this Chapter. The results of the density and pressure distributions of the liquid film on the slit are given in a two dimensional plane in Sec. 6.2 and the results of the liquid film in the slit are given in Sec. 6.3.

In Chapter 7, the molecular transition mechanism is examined between the two states: (a) liquid film on the slit and (b) liquid film in the slit, based on the thermodynamic states of the liquid film in the vicinity of the slit. First, in Sec. 7.1, effects of the fluid-solid interaction intensity on the states of the liquid film are investigated for the calculation model introduced in Sec. 6.1. Next, the relationship between interfacial tensions based on a macroscopic concept and the states of the liquid film are examined under a varying fluid-solid interaction intensity. In Sec. 7.2, as the local thermodynamic quantities, the local pressure components, and interfacial tensions of the liquid film in the vicinity of the slit, are obtained as the time-averaged values of the instantaneous expression of the pressure components and interfacial tensions, and which are investigated in detail, to reveal a beginning of the transition process between the two states of the condensed matter from a molecular point of view.

At the end, summaries and conclusions of this thesis are described in Chapter 8 and Chapter 9, respectively.

2. Theories

In this Chapter, theories of the perturbative method are presented. As described in Chapter 1, a general perturbative method that includes the effects of the tangential pressure components affected by the solid atoms has not been presented. First, in Sec. 2.1, a description of the perturbative method which includes the effect of an external potential, is derived to obtain the pressure components and interfacial tension acting on the fluid at a fluid-solid interface on the basis of statistical thermodynamics for the canonical and grand canonical ensembles. Later, in Sec. 3.2, the treatment of the derived description in molecular simulation is explained to include the effects of the tangential pressure components affected by the solid atoms. The description is assumed to be applicable in subsystems in Sec. 2.2.1 to obtain local pressure components and interfacial tension. Two alternative methods are presented in Sec. 2.2.2 and Sec. 2.2.3 respectively to compare the results of the local interfacial tension calculation: the first method evaluates the intermolecular force acting on a plane, and the second is the conventional virial expression based on the Irving and Kirkwood definition. In Sec. 2.3 an instantaneous expression of the local pressure components and interfacial tensions, which is based on a volume perturbation, is presented to investigate time-dependent phenomena in molecular simulations.

2.1 Derivation based on statistical thermodynamics

2.1.1 Canonical ensemble

Consider a classical inhomogeneous system which consists of N identical and spherical particles in a volume V interacting with an external field (Hansen & McDonald 2013). In addition, the system consists of flat interfaces which exist parallel in the system. The state of the system is specified by the $3N$ coordinates and $3N$ momenta, and then the Hamiltonian of the system H is written as

$$H(\mathbf{r}^N, \mathbf{p}^N) = K(\mathbf{p}^N) + U(\mathbf{r}^N) + \Phi(\mathbf{r}^N), \tag{2.1}$$

where K is the kinetic energy of the particles, U is the potential energy between particles in the system, and Φ is the potential energy contributed from the external field. For the canonical ensemble in which the system is described by Eq. (2.1), the Helmholtz free energy F is expressed as

$$F = -\frac{1}{\beta} \ln Q_{NVT}, \tag{2.2}$$

where

$$Q_{NVT} = \frac{1}{\Lambda^{3N} N!} \int \mathrm{d}\mathbf{r}^N \exp\left(-\beta\left(U(\mathbf{r}^N) + \Phi(\mathbf{r}^N)\right)\right) \tag{2.3}$$

is the canonical partition function, and $\beta=1/(k_B T)$ with the Boltzmann constant k_B and the absolute temperature T. The de Broglie thermal wavelength Λ is defined as $\Lambda = \sqrt{h^2/(2\pi m k_B T)}$ with the Planck constant h and mass of the particle m. Harismiadis *et al.* (1996), Gloor *et al.* (2005), and Miguel *et al.* (2006) proposed the equation: $Q_{NVT} = \frac{1}{\Lambda^{3N} N!} \int \mathrm{d}\mathbf{r}^N \exp\left(-\beta U(\mathbf{r}^N)\right)$, which includes no contributions of $\Phi(\mathbf{r}^N)$ in Eq. (2.3), and the expressions of the pressure components and interfacial tension shown below are also proposed by them. In this Section, the expressions of the pressure components and interfacial tension based on their proposition are extended to expressions applicable at a fluid-solid interface by using Eq. (2.3) which includes the effect of the external potential. The ξ component of pressure acting on a plane A_η which is perpendicular to the η coordinate, $P_{\xi\eta}$ ($\xi,\eta=x,y,z$) and the interfacial tension γ are defined as the partial derivatives of the Helmholtz free energy with respect to the volume and interfacial area, respectively:

$$P_{\xi\eta} = -\left(\frac{\partial F}{\partial V}\right)_{L_{\neq\xi} NT}, \quad \gamma = \left(\frac{\partial F}{\partial A_s}\right)_{NVT}, \tag{2.4}$$

where V is defined as $V=L_x L_y L_z$ ($L_x=L_y=L_z$), and A_s indicates the interfacial area in the system. Describing the partition functions of the initial and perturbed states as $Q_{NVT,0}$ and $Q_{NVT,1}$ respectively, it follows from Eq. (2.3) that

$$\begin{aligned}\frac{Q_{NVT,1}}{Q_{NVT,0}} &= \frac{\int \mathrm{d}\mathbf{r}_1^N \exp\left(-\beta\left(U(\mathbf{r}_1^N)+\Phi(\mathbf{r}_1^N)\right)\right)/\left(\Lambda^{3N}N!\right)}{\int \mathrm{d}\mathbf{r}_0^N \exp\left(-\beta\left(U(\mathbf{r}_0^N)+\Phi(\mathbf{r}_0^N)\right)\right)/\left(\Lambda^{3N}N!\right)}, \\ &= \frac{\int \mathrm{d}\mathbf{r}^{*N} V_1^N \exp\left(-\beta\left(U_0+\Phi_0\right)\right)\exp\left(-\beta\Delta(U+\Phi)\right)/\left(\Lambda^{3N}N!\right)}{\int \mathrm{d}\mathbf{r}^{*N} V_0^N \exp\left(-\beta\left(U_0+\Phi_0\right)\right)/\left(\Lambda^{3N}N!\right)}, \\ &= \left\langle \left(1+\frac{\Delta V}{V_0}\right)^N \exp\left(-\beta\Delta(U+\Phi)\right)\right\rangle_0 .\end{aligned} \tag{2.5}$$

In the above equation, $\Delta V = V_1 - V_0$, $\Delta U = U_1 - U_0$, $\Delta\Phi = \Phi_1 - \Phi_0$, the subscripts 0 and 1 indicate values of the initial and perturbed states respectively, $\mathbf{r}^*$ is a coordinate scaled with the size of the system, and $\langle\ \rangle$ represents the ensemble average. Then the free energy difference from F_0 at the initial state to F_1 at the perturbed state, $\Delta F(=F_1-F_0)$ is expressed from Eqs. (2.2) and (2.5) as

$$\begin{aligned}\Delta F &= -\frac{1}{\beta}\ln\left(\frac{Q_{NVT,1}}{Q_{NVT,0}}\right), \\ &= -\frac{1}{\beta}\ln\left\langle \left(1+\frac{\Delta V}{V_0}\right)^N \exp\left(-\beta\Delta(U+\Phi)\right)\right\rangle_0 .\end{aligned} \tag{2.6}$$

Assuming the free energy difference from the initial state to the perturbed state by infinitesimal variation of the volume ($\Delta V = V_1 - V_0$) and of the area ($\Delta A_s = A_{s,1} - A_{s,0}$), the substitution of Eq. (2.6) into Eq. (2.4) gives

$$P_{\xi\eta} = -\left(\frac{\partial F}{\partial V}\right)_{L_{\neq\xi}NT} = \frac{1}{\beta\Delta L_\xi A_{\eta,0}}\ln\left\langle \left(1+\frac{\Delta V}{V_0}\right)^N \exp\left(-\beta\Delta(U+\Phi)\right)\right\rangle_0 , \tag{2.7}$$

and

$$\gamma = \left(\frac{\partial F}{\partial A_s}\right)_{NVT} = -\frac{1}{\beta\Delta A_s}\ln\left\langle \exp\left(-\beta\Delta(U+\Phi)\right)\right\rangle_0 , \tag{2.8}$$

where $\Delta L_\xi = L_{\xi,1} - L_{\xi,0}$. It is to be remarked that in Eq. (2.7) ΔF is evaluated at $A_{\eta,0}$, and

the kinetic part: $\ln(1+\Delta V/V_0)^N/(\beta\Delta L_\xi A_{\eta,0})$, is not considered appropriately in the case of $\xi \neq \eta$.

2.1.2 Grand canonical ensemble

For a system of constant chemical potential μ, V, and T, the grand canonical potential is defined as

$$\Omega_{\mu VT} = -\frac{1}{\beta}\ln \Xi_{\mu VT}, \tag{2.9}$$

where the grand canonical partition function $\Xi_{\mu VT}$ is

$$\Xi_{\mu VT} = \sum_{N=0}^{+\infty} \frac{\exp(N\beta\mu)}{\Lambda^{3N} N!} \int \mathrm{d}\mathbf{r}^N \exp\left(-\beta\left(U(\mathbf{r}^N)+\Phi(\mathbf{r}^N)\right)\right). \tag{2.10}$$

Ibergay *et al.* (2006) proposed the equation: $\Xi_{\mu VT} = \sum_{N=0}^{+\infty} \frac{\exp(N\beta\mu)}{\Lambda^{3N} N!} \int \mathrm{d}\mathbf{r}^N \exp\left(-\beta U(\mathbf{r}^N)\right)$, which includes no contributions of $\Phi(\mathbf{r}^N)$ in Eq. (2.10), and the expressions of the pressure components and interfacial tension shown below are also proposed by them. In this Section, the expressions of the pressure components and interfacial tension based on their proposition are extended to expressions applicable at a fluid-solid interface by using Eq. (2.10) which includes the effect of the external potential. The pressure components and the interfacial tension are defined as the partial derivatives of the grand potential with respect to the volume and interfacial area, respectively:

$$P_{\xi\eta} = -\left(\frac{\partial\Omega}{\partial V}\right)_{\mu L_{\neq\xi} T}, \quad \gamma = \left(\frac{\partial\Omega}{\partial A_\mathrm{s}}\right)_{\mu VT}. \tag{2.11}$$

Then, the ratio of the grand canonical partition function of the perturbed state $\Xi_{\mu VT,1}$ to $\Xi_{\mu VT,0}$ at the initial state is given by

$$\frac{\Xi_{\mu VT,1}}{\Xi_{\mu VT,0}} = \frac{\sum_{N=0}^{+\infty} \frac{\exp(N\beta\mu)}{\Lambda^{3N} N!} \int \mathrm{d}\mathbf{r}_1^{\,N} \exp\left(-\beta\left(U(\mathbf{r}_1^{\,N}) + \Phi(\mathbf{r}_1^{\,N})\right)\right)}{\sum_{N=0}^{+\infty} \frac{\exp(N\beta\mu)}{\Lambda^{3N} N!} \int \mathrm{d}\mathbf{r}_0^{\,N} \exp\left(-\beta\left(U(\mathbf{r}_0^{\,N}) + \Phi(\mathbf{r}_0^{\,N})\right)\right)},$$

$$= \frac{\sum_{N=0}^{+\infty} \frac{\exp(N\beta\mu)}{\Lambda^{3N} N!} \int \mathrm{d}\mathbf{r}^{*N} V_1^{\,N} \exp\left(-\beta\left(U_0 + \Phi_0\right)\right) \exp\left(-\beta\Delta(U+\Phi)\right)}{\sum_{N=0}^{+\infty} \frac{\exp(N\beta\mu)}{\Lambda^{3N} N!} \int \mathrm{d}\mathbf{r}^{*N} V_0^{\,N} \exp\left(-\beta\left(U_0 + \Phi_0\right)\right)}, \tag{2.12}$$

$$= \left\langle \left(1 + \frac{\Delta V}{V_0}\right)^N \exp\left(-\beta\Delta(U+\Phi)\right) \right\rangle_0 .$$

This expression enables $\Delta\Omega_{\mu VT}$ (=$\Omega_{\mu VT,1}$ - $\Omega_{\mu VT,0}$) to be expressed as the same form of ΔF of the canonical ensemble:

$$\Delta\Omega_{\mu VT} = -\frac{1}{\beta} \ln\left(\frac{\Xi_{\mu VT,1}}{\Xi_{\mu VT,0}}\right),$$

$$= -\frac{1}{\beta} \ln\left\langle \left(1 + \frac{\Delta V}{V_0}\right)^N \exp\left(-\beta\Delta(U+\Phi)\right) \right\rangle_0 . \tag{2.13}$$

Thus, the final equations become

$$P_{\xi\eta} = -\left(\frac{\partial\Omega}{\partial V}\right)_{\mu L_{\neq\xi} T} = \frac{1}{\beta\Delta L_\xi A_{\eta,0}} \ln\left\langle \left(1 + \frac{\Delta V}{V_0}\right)^N \exp\left(-\beta\Delta(U+\Phi)\right) \right\rangle_0 , \tag{2.14}$$

and

$$\gamma = \left(\frac{\partial\Omega}{\partial A_s}\right)_{\mu VT} = -\frac{1}{\beta\Delta A_s} \ln\left\langle \exp\left(-\beta\Delta(U+\Phi)\right) \right\rangle_0 . \tag{2.15}$$

Equations, (2.7), (2.8), (2.14), and (2.15) indicate that in an equilibrium state, the pressure components and the interfacial tension can be evaluated by the same expressions whether the system is defined as the canonical ensemble or grand canonical ensemble.

2.2 Methodology to obtain local quantities

2.2.1 Perturbative method

In order to obtain the pressure components and interfacial tension in subsystems based on the derived perturbative method, it is reasonable to use Eqs. (2.14) and (2.15) which are derived in the μVT ensemble. This requires the assumption that the system is in equilibrium, keeping μ, V, and T constant in each subsystem. Under this assumption, the thermodynamic properties in each subsystem can be evaluated appropriately. For a system in a volume V which consists of subsystems with volumes V_k(V_k =dx_k ×dy_k ×dz_k, dx_k =dy_k =dz_k, and $V = \Sigma_k V_k$), the local pressure components $P_{\xi\eta,V_k}$ (ξ,η=x,y,z) and interfacial tension γ_{V_k} are described on the basis of Eqs. (2.14) and (2.15) as

$$P_{\substack{\xi\eta \\ (x,y,z)\in V_k}}(x,y,z) \equiv P_{\xi\eta,V_k} = \frac{1}{\beta\Delta(\mathrm{d}\xi_k)A_{\eta,V_k}} \ln\left\langle \left(1+\frac{\Delta V_k}{V_k}\right)^{N_{V_k}} \exp\left(-\beta\Delta\left(U_{V_k}+\Phi_{V_k}\right)\right)\right\rangle, \qquad (2.16)$$

and

$$\gamma_{\substack{(x,y,z)\in V_k}}(x,y,z) \equiv \gamma_{V_k} = -\frac{1}{\beta\Delta A_{\mathrm{s},V_k}} \ln\left\langle \exp\left(-\beta\Delta\left(U_{V_k}+\Phi_{V_k}\right)\right)\right\rangle, \qquad (2.17)$$

where $\Delta(\mathrm{d}\xi_k) = \mathrm{d}\xi_{k,1} - \mathrm{d}\xi_{k,0}$, $\Delta A_{\mathrm{s},V_k} = A_{\mathrm{s},1,V_k} - A_{\mathrm{s},0,V_k}$, and the subscript V_k indicates that the quantity is defined in V_k. It should be noted that in Eq. (2.16) the pressure components at the volume V_k are obtained by considering only the interactions through the area A_{η,V_k} which is perpendicular to the η coordinate. The definition of the energy in V_k is presented in 3.2.2. These equations are the same forms as those derived by using Eqs. (2.7) and (2.8) in the canonical ensemble, which suggests that the pressure components and interfacial tension are obtained in subsystems based on Eqs. (2.16) and (2.17) respectively in the canonical ensemble simulation if the system is in equilibrium.

2.2.2 Evaluation of the force acting on a plane

Todd *et al.* (1995) have presented a method to consider contributions of the interactions between the particles to the pressure components by evaluating the intermolecular forces acting on a plane, and this method is used as one of the methods to calculate the pressure components (Varnik *et al.* 2000). This approach can be extended to formalism applicable to subsystems. Consider a plane in the volume V_k : A_{η,V_k} , which is perpendicular to the axis η, and through which the ith particle and jth particle may interact. For a region in the vicinity of the fluid-solid interface, in which a substrate is located below fluid molecules, it follows that the contributions of the interactions to the pressure components of the fluid exerted on the plane are straightforwardly calculated by the evaluation of the intermolecular forces, and the pressure components are given by

$$
\begin{aligned}
P_{\substack{\xi\eta \\ (x,y,z)\in V_k}}(x,y,z) \equiv P_{\xi\eta,V_k} = & \frac{1}{V_k}\left\langle \sum_{i\in V_k} \frac{p_{i\xi}p_{i\eta}}{m_i} \right\rangle \\
& + \frac{1}{2A_{\eta,V_k}}\left\langle \sum_{(i\neq j),\mathbf{r}_{ij}\cap A_{\eta,V_k}} f_{ij\xi}\left[\Theta(\eta_i-\eta)\Theta(\eta-\eta_j)-\Theta(\eta_j-\eta)\Theta(\eta-\eta_i)\right] \right\rangle \\
& + \frac{1}{A_{\eta,V_k}}\left\langle \sum_{(i,j),\mathbf{r}_{ij}\cap A_{\eta,V_k}} f'_{ij\xi}\left[\Theta(\eta_i-\eta)\Theta(\eta-\eta_j)+\Theta(\eta_j-\eta)\Theta(\eta-\eta_i)\right] \right\rangle,
\end{aligned}
\tag{2.18}
$$

where $V_k = (\mathrm{d}\eta_k)A_{\eta,V_k}$, $\mathbf{r}_{ij} = \mathbf{r}_i - \mathbf{r}_j$, m_i is the mass of ith particle, $p_{i\xi}$ and $p_{i\eta}$ are the ξ and η components of the momentum of the ith particle in the volume V_k respectively, $f_{ij\xi}$ represents the ξ component of the intermolecular force acting on the ith fluid particle due to the jth fluid particle, $f'_{ij\xi}$ is the ξ component of the intermolecular force acting on the ith fluid particle due to the jth solid atom, and Θ is the Heaviside step function. In Eq. (2.18), the first term on the right hand side is the volume-averaged expression, the third term is obtained considering only the forces acting on the ith fluid particles, and the second part in the third term, $f'_{ij\xi}\Theta(\eta_j-\eta)\Theta(\eta-\eta_i)$ is needed to include effects of the components of the fluid-solid interaction force which are tangential to the fluid-solid interface. Then, the local interfacial tension at the volume V_k is defined in the present

study as

$$\gamma_{V_k} = dz_k \left(P_{zz,V_k} - \frac{P_{xx,V_k} + P_{yy,V_k}}{2} \right), \tag{2.19}$$

for the system in which z is the component normal to the interface, and x and y are the tangential components. Eq. (2.19) is based on the formula,

$$\gamma = \int \left(P_\xi - P_\eta \right) \mathrm{d}\xi, \tag{2.20}$$

which is defined in an equilibrium state (Kirkwood & Buff 1949; Rowlinson & Widom 1982; Nijmeijer *et al.* 1990).

2.2.3 Irving and Kirkwood definition

The normal and tangential pressure components, $P_N(z)=P_{zz}(z)$ and $P_T(z)=(P_{xx}(z)+P_{yy}(z))/2$, which depend only on the direction normal to the interface in a planar system, are expressed by the conventional virial equations which are based on the Irving and Kirkwood definition (Irving & Kirkwood 1950; Walton *et al.* 1982; Varnik *et al.* 2000). For a region in the vicinity of the fluid-solid interface, in which a substrate is located below fluid molecules,

$$\begin{aligned} P_N(z) = \rho(z) k_B T - \frac{1}{2A} \left\langle \sum_{i \neq j} \frac{|z_{ij}|}{r_{ij}} \frac{\partial u(r_{ij})}{\partial r_{ij}} \Theta\left(\frac{z - z_i}{z_{ij}} \right) \Theta\left(\frac{z_j - z}{z_{ij}} \right) \right\rangle \\ + \frac{1}{A} \left\langle \sum_{i,j} f_{ijz}^{'} \Theta(z_i - z) \Theta(z - z_j) \right\rangle, \end{aligned} \tag{2.21}$$

$$P_T(z) = \rho(z) k_B T - \frac{1}{4A} \left\langle \sum_{i \neq j} \frac{x_{ij}^2 + y_{ij}^2}{r_{ij}} \frac{\partial u(r_{ij})}{\partial r_{ij}} \frac{1}{|z_{ij}|} \Theta\left(\frac{z - z_i}{z_{ij}} \right) \Theta\left(\frac{z_j - z}{z_{ij}} \right) \right\rangle, \tag{2.22}$$

where ρ is the density, A is the interfacial area, and u and $r_{ij} = \sqrt{x_{ij}^2 + y_{ij}^2 + z_{ij}^2}$ are the potential energy and distance between the particles, respectively. In Eqs. (2.21) and

(2.22), the first and second terms on the right hand side are the respective contributions of the fluid molecules' kinetic part and the intermolecular forces between fluid molecules. In Eq. (2.21), the third term on the right hand side is the contribution of the intermolecular forces acting on fluid molecules due to the solid atoms. A number of published studies have calculated the pressure components by using these equations (e.g. Míguez *et al.* 2000; Varnik *et al.* 2000). The local interfacial tension for the planar system is defined in the present study as

$$\gamma_{V_k} = \gamma_{\mathrm{d}z_k} = \mathrm{d}z_k \left(P_N(z) - P_T(z) \right). \tag{2.23}$$

2.3 An instantaneous expression of the local pressure components based on a volume perturbation

The perturbative method based on the statistical thermodynamics introduced in Sec. 2.1 is applicable in an equilibrium system, which requires the time average of the Boltzmann factor: $\exp(-\beta\Delta(U+\Phi))$, in the molecular dynamics simulation. For investigations of the time dependent phenomena such as transport phenomena of condensed matters, it cannot be used. In this section, an instantaneous expression of the local pressure components, is transformed to a volume-perturbed expression, and the relationship with the formula established in an equilibrium state is discussed. This expression is used in Chapters 6 and 7, to obtain local pressure components and interfacial tensions of the liquid film in the vicinity of the slit pore.

Consider fluid particles in the local volume V_k, which interact with the other fluid particles through the local area A_{ξ,V_k} in V_k. Based on Eq. (2.18), the $\xi\xi$ component of the instantaneous pressure, $\hat{P}_{\xi\xi,V_k}$ are expressed as

$$\hat{P}_{\substack{\xi\xi\\(x,y,z)\in V_k}}(x,y,z) \equiv \hat{P}_{\xi\xi,V_k} = \frac{1}{V_k}\sum_{i\in V_k}\frac{p_{i\xi}^2}{m_i} + \frac{1}{A_{\xi,V_k}}\left(f_\xi + f_\xi^{'}\right). \tag{2.24}$$

Here, f_ξ is the total ξ component of the intermolecular force between fluid particles through the local area A_{ξ,V_k} in V_k, and $f_\xi^{'}$ is the total ξ component of the intermolecular force acting on the fluid particles due to the interactions with solid atoms, through the local area A_{ξ,V_k} in V_k. The value of the hydrodynamic velocity is assumed to be small, and is ignored in Eq. (2.24). The first and second terms on the right hand side in Eq. (2.24) represent contributions of the kinetic and intermolecular parts, respectively. The first term on the right hand side in Eq. (2.24) is expressed using ΔV_k as below,

$$\frac{1}{V_k}\sum_{i\in V_k}\frac{p_{i\xi}^2}{m_i}=\frac{1}{\Delta(\mathrm{d}\xi_k)A_{\xi,V_k}}\sum_{i\in V_k}\frac{p_{i\xi}^2}{m_i}\frac{\Delta V_k}{V_k}, \tag{2.25}$$

where the relationship, $\Delta V_k=\Delta(\mathrm{d}\xi_k)A_{\xi,V_k}$ is used. On the other hand, the second term is expressed as the numerical evaluation of forces acting on a plane, that is,

$$\frac{1}{A_{\xi,V_k}}\left(f_\xi+f_\xi^{'}\right)=-\frac{\Delta\left(U_{V_k}+\Phi_{V_k}\right)}{\Delta(\mathrm{d}\xi_k)A_{\xi,V_k}}. \tag{2.26}$$

Thus, the instantaneous pressure $\hat{P}_{\xi\xi,V_k}$ is represented as a volume-perturbed expression,

$$\hat{P}_{\xi\xi,V_k}=\frac{1}{\Delta(\mathrm{d}\xi_k)A_{\xi,V_k}}\left[\sum_{i\in V_k}\frac{p_{i\xi}^2}{m_i}\frac{\Delta V_k}{V_k}-\Delta\left(U_{V_k}+\Phi_{V_k}\right)\right]. \tag{2.27}$$

The relationship between Eq. (2.16) applicable in an equilibrium state and Eq. (2.27), is shown as follows. First, in an equilibrium state, the relationship below is assumed to be satisfied (Evans & Morriss 2008),

$$\frac{3}{2}N_{V_k}k_B\hat{T}_{V_k}=\sum_{i\in V_k}\frac{1}{2}\frac{\left|\mathbf{p}_i\right|^2}{m_i}, \tag{2.28}$$

where $\hat{T}_{V_k}$ represents the instantaneous temperature in V_k, and its time-averaged value is equal to the temperature in V_k: $T_{V_k}=\left\langle\hat{T}_{V_k}\right\rangle$. Considering only the ξ component of the momentum in Eq. (2.28), and the approximation: $\ln(1+\Delta V_k/V_k)\approx\Delta V_k/V_k$, the time-averaged expression of Eq. (2.27) becomes

$$
\begin{aligned}
\left\langle \hat{P}_{\xi\xi,V_k} \right\rangle &= \left\langle \frac{1}{\Delta(\mathrm{d}\xi_k) A_{\xi,V_k}} \left[\sum_{i \in V_k} \frac{p_{i\xi}^2}{m_i} \frac{\Delta V_k}{V_k} - \Delta\left(U_{V_k} + \Phi_{V_k} \right) \right] \right\rangle, \\
&= \frac{1}{\Delta(\mathrm{d}\xi_k) A_{\xi,V_k}} \left\langle N_{V_k} k_B \hat{T}_{V_k} \ln\left(1 + \frac{\Delta V_k}{V_k} \right) + k_B \hat{T}_{V_k} \ln\left[\exp\left(- \frac{\Delta(U_{V_k} + \Phi_{V_k})}{k_B \hat{T}_{V_k}} \right) \right] \right\rangle, \\
&= \frac{k_B}{\Delta(\mathrm{d}\xi_k) A_{\xi,V_k}} \left\langle \hat{T}_{V_k} \ln\left[\left(1 + \frac{\Delta V_k}{V_k} \right)^{N_{V_k}} \exp\left(- \frac{\Delta(U_{V_k} + \Phi_{V_k})}{k_B \hat{T}_{V_k}} \right) \right] \right\rangle, \\
&\cong \frac{1}{\beta \Delta(\mathrm{d}\xi_k) A_{\xi,V_k}} \left\langle \ln\left[\left(1 + \frac{\Delta V_k}{V_k} \right)^{N_{V_k}} \exp\left(-\beta \Delta(U_{V_k} + \Phi_{V_k}) \right) \right] \right\rangle.
\end{aligned}
\tag{2.29}
$$

The final form in Eq. (2.29) is approximately obtained by using the relationship of $T = \left\langle \hat{T}_{V_k} \right\rangle$ in an equilibrium state. Eq. (2.29) is similar to Eq. (2.16), but the bracket in Eq. (2.29) includes "ln", which can avoid the time average of only the Boltzmann factor in molecular dynamics simulation.

From Eq. (2.27), the local interfacial tension is defined in the present study as

$$
\underset{(x,y,z) \in V_k}{\hat{\gamma}_{\xi-\eta}(x,y,z)} \equiv \hat{\gamma}_{\xi-\eta,V_k} = \mathrm{d}\xi_k \left(\hat{P}_{\xi\xi,V_k} - \hat{P}_{\eta\eta,V_k} \right), \tag{2.30}
$$

where normal and tangential directions to an interface are described as ξ and η, respectively. From a strict point of view, the interfacial tension is not defined in non-equilibrium states, hence the validity of applications to the non-equilibrium states is not assured.

3. Methods for numerical analyses

In this Chapter, methods for the numerical analyses are presented. First, the classical molecular dynamics method is introduced in Sec. 3.1. This study adopts the common techniques in the molecular dynamics method, and each technique is explained in brief. Further information is available, for instance, in the book of Allen & Tildesley (1987). Molecules and atoms are assumed to be simple particles which interact with each other through the 12-6 Lennard-Jones potential. In Sec. 3.2.1, the procedure to evaluate energy difference in the perturbative method presented in Chapter 2, is proposed for fluid-solid interfacial systems consisting of flat and structured interfaces. Finally, Sec. 3.2.2 proposes the method to evaluate the energy difference in the local volume by using the perturbative method.

3.1 Classical molecular dynamics method

3.1.1 Newton's second law and numerical integration

In this study, molecules or atoms are assumed to be classical particles. The equation of motion of the *i*th particle is described by the Newton's second law,

$$m_i \frac{\mathrm{d}^2 \mathbf{r}_i}{\mathrm{d}t^2} = \mathbf{f}_i , \tag{3.1}$$

where m_i is the mass of the *i*th particle, $\mathbf{r}_i$ is the positional vector of the *i*th particle, $\mathbf{f}_i$ is the force vector on the *i*th particle, and t denotes the time. The force on the *i*th particle due to the *j*th particle, $\mathbf{f}_{ij}$ is described as below, in the case of the pairwise additive potential U between the *i*th and *j*th particles,

$$\mathbf{f}_{ij} = -\frac{\partial U(r_{ij})}{\partial \mathbf{r}_i} = -\frac{\partial U(r_{ij})}{\partial r_{ij}}\frac{\partial r_{ij}}{\partial \mathbf{r}_i} = -\frac{\partial U(r_{ij})}{\partial r_{ij}}\frac{\mathbf{r}_{ij}}{r_{ij}}. \tag{3.2}$$

Here, U is the function which depends only on the distance between the ith and jth particles, $r_{ij} = |\mathbf{r}_i - \mathbf{r}_j|$. For the numerical integration, the 'velocity Verlet algorithm' is adopted, which is derived using the expansion of Eq. (3.1) by the Taylor series, then the final forms are given as,

$$\begin{aligned} \mathbf{r}_i(t+\Delta t) &= \mathbf{r}_i(t) + \Delta t \mathbf{v}_i(t) + \frac{\Delta t^2}{2m_i}\mathbf{f}_i(t) + O(\Delta t^4), \\ \mathbf{v}_i(t+\Delta t) &= \mathbf{v}_i(t) + \frac{\Delta t}{2m_i}\left[\mathbf{f}_i(t) + \mathbf{f}_i(t+\Delta t)\right] + O(\Delta t^2). \end{aligned} \tag{3.3}$$

In Eq. (3.3), Δt denotes the time step interval in simulations, and $\mathbf{v}_i$ is the velocity vector of the ith particle. Eq. (3.3) enables us to calculate the positions and velocities of the particles at each time step.

3.1.2 Potential function

In a molecular system consisting of N particles, the total potential energy $\mathfrak{U}$ is expressed as,

$$\mathfrak{U} = \mathfrak{U}(\mathbf{r}^N). \tag{3.4}$$

In the classical molecular dynamics method, a fundamental assumption is usually adopted, as below,

$$\mathfrak{U} \equiv \frac{1}{2}\sum_{i}^{N}\sum_{j(j\neq i)}^{N} U(r_{ij}), \tag{3.5}$$

that is, the total potential energy in the system is described by the sum of the pairwise additive potential. In the present study, all the interactions between molecules or atoms

are assumed to obey the 12-6 Lennard-Jones(LJ) potential, of the form,

$$U(r_{ij}) = 4\varepsilon\left[\left(\frac{\sigma}{r_{ij}}\right)^{12} - \left(\frac{\sigma}{r_{ij}}\right)^{6}\right], \tag{3.6}$$

where σ and ε are constants, and the first and second terms on the right hand side respectively represent the repulsive and attractive forces between the particles. The calculation of the interactions between the particles is conducted by using the cutoff distance, which truncates the long-range effects at a finite distance. As the cutoff distance, 3σ is used in the numerical analysis in Chapter 4, and 5σ is adopted in Chapters 5, 6, and 7. The fluid molecules and solid atoms are assumed to be argon (Ar) and platinum (Pt) respectively, and the parameters used in Eq. (3.6) are described in Chapters 4 and 5.

3.1.3 Temperature control

For a system of the volume V which consists of N particles, the temperature T is defined in an equilibrium state, as,

$$\frac{3}{2}Nk_BT = \left\langle \sum_{i\in V}\frac{1}{2}\frac{|\mathbf{p}_i|^2}{m_i} \right\rangle, \tag{3.7}$$

where $\mathbf{p}_i$ is the momentum vector ($\mathbf{p}_i^2 = p_{ix}^2 + p_{iy}^2 + p_{iz}^2$) of the ith particle and $\langle\ \rangle$ represents the ensemble average. The temperature of the fluid molecules is kept constant by the velocity scaling control to make the initial states of the calculation systems, and the Lanvegin method (Tully 1980; Maruyama 2000) is applied for the temperature control of the solid atoms through the simulations. The controlled solid atoms in the Langevin method are described for each calculation system, in Chapters. 4, 5, and 6.

3.1.4 Computational efficiencies

For improving computational efficiencies, the book keeping method is applied to calculations of the interactions between particles, which keeps the pairs of the particles' interactions for a few time steps and allows us to cut computational time remarkably. Furthermore, the parallel computing method, OpenMP, is used to speed up the calculation.

3.2 Perturbative method

3.2.1 Evaluation of energy difference

The procedures to evaluate ΔU in Eqs. (2.7), (2.8), (2.14), (2.15), and (2.27) are as follows. For instance, P_{zz} is given by the perturbation of the system from the initial state of $V_0 = L_{x,0}L_{y,0}L_{z,0}$ to the final state of $V_1 = L_{x,1}L_{y,1}L_{z,1}$, where $L_{z,1} = L_{z,0}(1+\lambda)$, keeping the $L_{x,1}$ and $L_{y,1}$ constant: $L_{x,1} = L_{x,0}$ and $L_{y,1} = L_{y,0}$ (see Figs. 3.1(a,b)). Here, perturbation parameter λ is the infinitesimal quantity, but it actually expresses a small finite quantity in simulations. In order to obtain the interfacial tension γ, it is not necessary to change the volume: the alternative method uses a constant volume through the perturbation such that $L_{z,1} = L_{z,0}/(1+\lambda)$, $L_{x,1} = L_{x,0}\sqrt{(1+\lambda)}$, and $L_{y,1} = L_{y,0}\sqrt{(1+\lambda)}$ where z is the direction normal to the interface, while x and y are the tangential directions. It should be noted that the pressure components and interfacial tension are defined as the partial derivatives expressed in Eqs. (2.4) and (2.11), which can be evaluated in simulations by the forward, backward, and central difference methods.

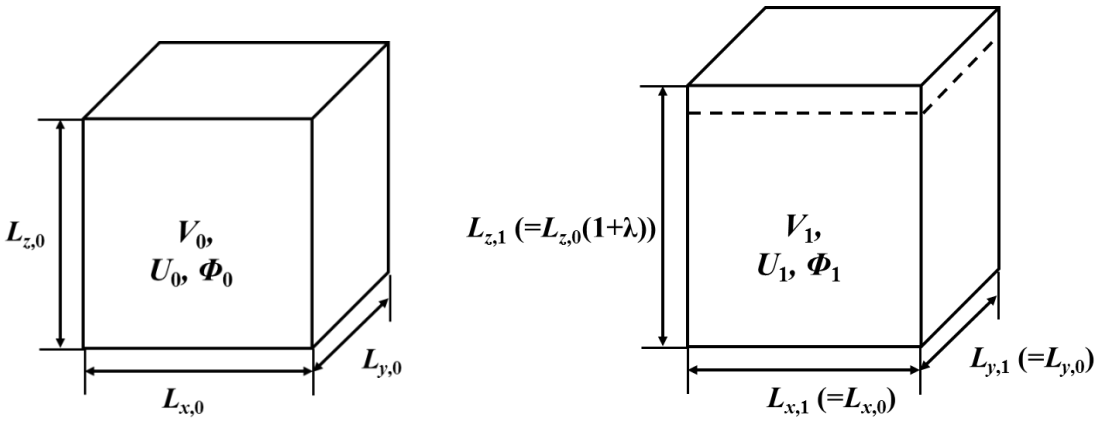

(a) System 0. (b) System 1.

Fig. 3.1 Illustration of the initial state (system 0) and the perturbed state (system 1).

In order to obtain the pressure components tangential to the interface, a new method is proposed in the present study. Special attention is required to deal with $\Delta\Phi$ in Eqs. (2.7), (2.8), (2.14), (2.15), and (2.27) due to the fact that the volume of the system is defined as the region of fluid particles. This means the distance between fluid particles and solid atoms should be extended or shortened, depending on the relative positions of the fluid particles to the solid atoms in the x and y directions (i.e., the tangential directions to the solid surface). The transformation of positions of the fluid particles in the system through the volume perturbation in the x and y directions imposes the conditions:

$$\begin{aligned} x_{fs,1} &= x_{fs,0}(1+\lambda) \quad \text{for} \quad x_{f,0} > x_{s,0}, \\ x_{fs,1} &= x_{fs,0}(1-\lambda) \quad \text{for} \quad x_{f,0} < x_{s,0}, \end{aligned} \tag{3.8}$$

and

$$\begin{aligned} y_{fs,1} &= y_{fs,0}(1+\lambda) \quad \text{for} \quad y_{f,0} > y_{s,0}, \\ y_{fs,1} &= y_{fs,0}(1-\lambda) \quad \text{for} \quad y_{f,0} < y_{s,0}, \end{aligned} \tag{3.9}$$

where x_{fs} and y_{fs} respectively represent the x and y components of the distance between the fluid particles and solid atoms. The subscripts f and s indicate the values for the fluid particles and the solid atoms, respectively. In the case of the constant volume, it follows that

$$\begin{aligned} x_{fs,1} &= x_{fs,0}\sqrt{1+\lambda} \quad \text{for} \quad x_{f,0} > x_{s,0}, \\ x_{fs,1} &= x_{fs,0}\sqrt{1-\lambda} \quad \text{for} \quad x_{f,0} < x_{s,0}, \end{aligned} \tag{3.10}$$

and

$$\begin{aligned} y_{fs,1} &= y_{fs,0}\sqrt{1+\lambda} \quad \text{for} \quad y_{f,0} > y_{s,0}, \\ y_{fs,1} &= y_{fs,0}\sqrt{1-\lambda} \quad \text{for} \quad y_{f,0} < y_{s,0}. \end{aligned} \tag{3.11}$$

The z component normal to the solid surface can be treated in the same manner as the usual transformation, since the relative positions of the fluid particles to the solid atoms are the same in the direction normal to the interface.

Next, consider a fluid-solid interfacial system with a slit pore as shown in Fig. 1.2,

where the height, width, and depth directions of the slit are defined as *z*, *x*, and *y* coordinates respectively, and whose solid particles are arranged just below *z*=0.0. The imposed conditions for the fluid-solid interfacial system with a slit pore, in the vicinity of the left side of the slit, are

$$\begin{aligned} x_{fs,1} &= x_{fs,0}(1+\lambda) \quad \text{for} \quad x_{f,0} > x_{s,0} \ \text{ and } \ z_{f,0} > 0, \\ x_{fs,1} &= x_{fs,0}(1-\lambda) \quad \text{for} \quad x_{f,0} < x_{s,0} \ \text{ and } \ z_{f,0} > 0, \end{aligned} \tag{3.12}$$

and

$$\begin{aligned} y_{fs,1} &= y_{fs,0}(1+\lambda) \quad \text{for} \quad y_{f,0} > y_{s,0} \ \text{ and } \ z_{f,0} > 0, \\ y_{fs,1} &= y_{fs,0}(1-\lambda) \quad \text{for} \quad y_{f,0} < y_{s,0} \ \text{ and } \ z_{f,0} > 0. \end{aligned} \tag{3.13}$$

These are identical to Eqs. (3.8) and (3.9). Furthermore, in the slit, the additional conditions below are added,

$$\begin{aligned} z_{fs,1} &= z_{fs,0}(1+\lambda) \quad \text{for} \quad z_{f,0} > z_{s,0} \ \text{ and } \ z_{f,0} < 0, \\ z_{fs,1} &= z_{fs,0}(1-\lambda) \quad \text{for} \quad z_{f,0} < z_{s,0} \ \text{ and } \ z_{f,0} < 0, \end{aligned} \tag{3.14}$$

and

$$\begin{aligned} y_{fs,1} &= y_{fs,0}(1+\lambda) \quad \text{for} \quad y_{f,0} > y_{s,0} \ \text{ and } \ z_{f,0} < 0, \\ y_{fs,1} &= y_{fs,0}(1-\lambda) \quad \text{for} \quad y_{f,0} < y_{s,0} \ \text{ and } \ z_{f,0} < 0. \end{aligned} \tag{3.15}$$

3.2.2 Evaluation of local energy difference

A method to evaluate the energy difference in the local volume is proposed in this Section. Consider a situation shown in Fig. 3.2(a), where the *i*th and *j*th particles are interacting with each other through a local volume V_k. Figure 3.2(a) shows the line segment between the *i*th and *j*th particles whose part of the line segment is inside the volume. The part inside the volume is evaluated by the variation of the volume. Now consider the evaluation of the energy difference by the volume perturbation of the local volume in the *z* direction. In reference to Figs. 3.2(b,c), the potential energy in the local volume in the initial state, U_{0,V_k}, between the *i*th and *j*th particles, is

$$U_{0,V_k} = U_{0,V_k}(\mathrm{r}_{ij,0}) \times \frac{\mathrm{dz}_{ij,0}}{z_{ij,0}}. \tag{3.16}$$

Meanwhile, the potential energy in the perturbed local volume, U_{1,V_k} is

$$U_{1,V_k} = U_{1,V_k}(\mathrm{r}_{ij,1}) \times \frac{\mathrm{dz}_{ij,1}}{z_{ij,1}}. \tag{3.17}$$

Then, the energy difference is evaluated as below,

$$\Delta U_{V_k} = U_{1,V_k} - U_{0V_k} = \left(U_{1,V_k}(\mathrm{r}_{ij,1}) - U_{0,V_k}(\mathrm{r}_{ij,0})\right) \times \frac{\mathrm{dz}_{ij,0}}{z_{ij,0}}. \tag{3.18}$$

In Eq. (3.18), $z_{ij,1} = (1+\lambda) z_{ij,0}$ and $\mathrm{dz}_{ij,1} = (1+\lambda)\mathrm{dz}_{ij,0}$ are considered. The other components of the pressure are evaluated in the same manner.

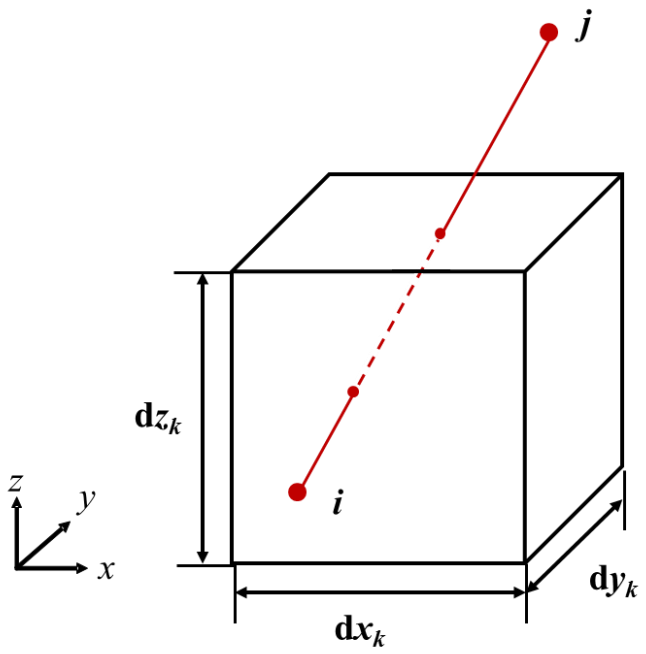

(a) The *i*th and *j*th particles interacting through a local volume.

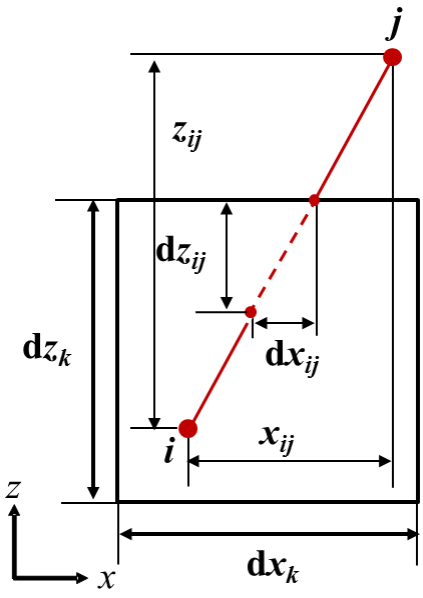

(b) View from the *y* direction.

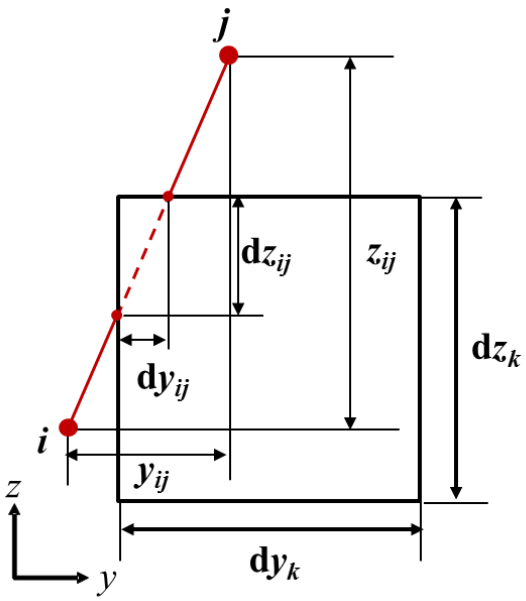

(c) View from the *x* direction.

Fig. 3.2 Definition of line segment between the *i*th and *j*th particles inside and outside a local volume.

4. Wetting phenomena at a solid surface with a structure

Before detailed analyses of the liquid film on a flat solid surface (Chapter5) and in the vicinity of a structured solid surface (Chapters 6 and 7), in this Chapter, a phenomenological analysis of wetting phenomena at a solid surface with a slit pore is conducted by the molecular dynamics method, in order to understand dynamic characteristics of a liquid film consisting of fluid molecules. Through the analyses, effects of the fluid-solid interaction intensity on the dynamic wetting phenomena are examined. First, in Sec. 4.1, the calculation system and numerical details used in this Chapter are described. Sec. 4.2 shows results of the effects of the fluid-solid interaction intensity on the dynamic wetting phenomena.

4.1 System and numerical details

Figure 4.1 shows the calculation model in the present study. The calculation region above the slit pore is 10.08×10.08×15.00 nm^3, and the region of the slit pore is 4.2×10.08×5.04 nm^3. Periodic boundary conditions are employed in the x and y directions and the mirror boundary condition is used at the top of a unit cell. The solid wall in the Figure consists of three solid layers where the outermost layer is fixed and the temperature of the middle layer is controlled at a constant value of 100 K by the Langevin method. An ensemble of 7500 solid atoms are arrayed in a fcc lattice structure with the (111) surface in contact with the fluid molecules in the unit cell. The solid wall potential parameters are taken to be those of platinum(Pt) and the fluid is assumed to be argon(Ar), and all interactions between molecules or atoms are assumed to obey the 12-6 Lennard-Jones potential(Eq. 3.6) as described in Sec. 3.1.2. The parameters for the fluid-fluid(Ar-Ar) interaction employed are σ_{Ar} = 3.40 Å and ε_{Ar} = 1.67×10^{-21} J, respectively. The Lennard-Jones parameters, σ_{Pt} = 2.54 Å and ε_{Pt} = 109.2×10^{-21} J are used for the solid-solid(Pt-Pt) interaction (Zhu & Philpott 1994). The interaction between the fluid molecules and the wall atoms is also described by the Lennard-Jones

potential form, and the Lorentz-Berthelot combining rule is applied to obtain the standard parameters $\sigma_{Ar\text{-}Pt}=(\sigma_{Ar}+\sigma_{Pt})/2$ and $\varepsilon_{Ar\text{-}Pt}=(\varepsilon_{Ar}\varepsilon_{Pt})^{1/2}$. For controlling the fluid-solid interaction intensity, the relative parameter α is adopted in addition to the standard value $\varepsilon_{Ar\text{-}Pt}$ in the calculation. Hence, the potential energy between the fluid molecules and the wall atoms can be written as,

$$U_{Ar-Pt}(r_{ij}) = 4\alpha\varepsilon_{Ar-Pt}\left[\left(\frac{\sigma_{Ar-Pt}}{r_{ij}}\right)^{12} - \left(\frac{\sigma_{Ar-Pt}}{r_{ij}}\right)^{6}\right]. \tag{4.1}$$

As an initial condition, a liquid film consisting of 12960 liquid molecules(Ar) exists on the solid wall(Pt) with a slit pore as shown in Fig. 4.1. The liquid film is initially kept at 100 K by the velocity scaling control for 100.0 ps, followed by 1.0 ns of the relaxation calculation conducted to equilibrate the system without the velocity scaling control. 3σ is used for the cutoff distance. During the relaxation calculation, the value of α is set to be 0.03, a relatively lower interaction intensity compared with the values employed for the observation of the wetting phenomena. After the relaxation calculation, the interaction parameter α is changed to the target value and the non-equilibrium classical molecular dynamics simulations are conducted for at least 1.0 ns.

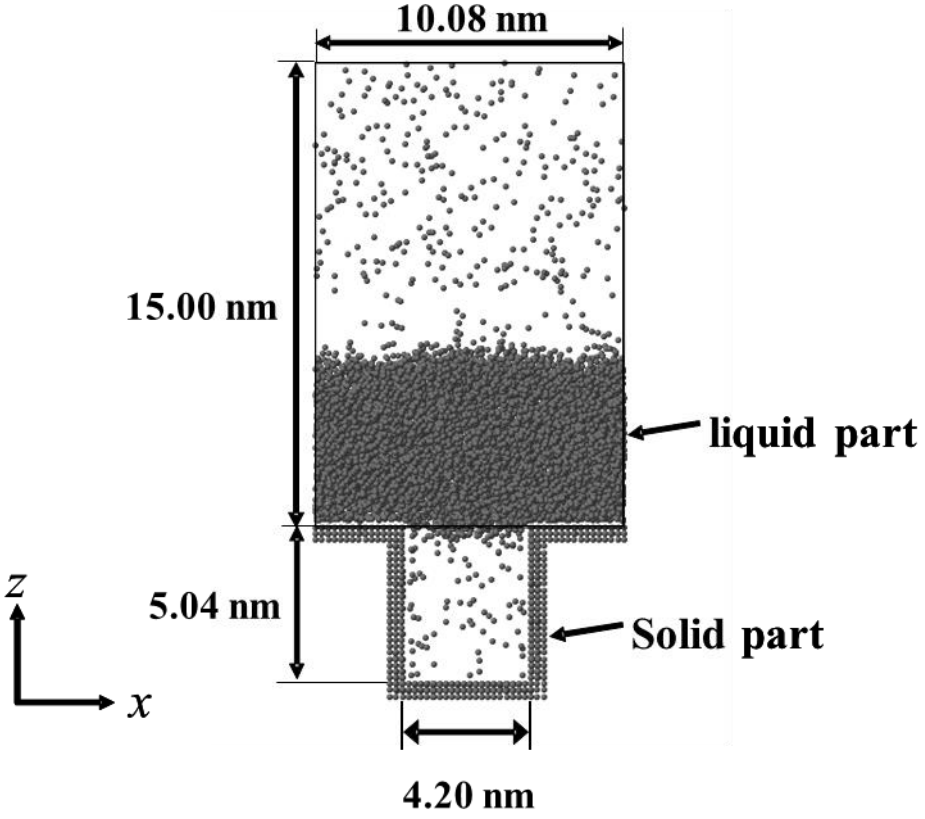

Fig. 4.1 Calculation model (initial condition). Periodic boundary conditions are employed in the *x* and *y* directions and the mirror boundary condition is used at the top of the unit cell.

4.2 Effects of the fluid-solid interaction on the wetting phenomena

Figures 4.2(a) and (b) show typical calculated results for two cases. In Fig. 4.2(a), the inside of the slit pore is unfilled with liquid molecules at t = 1.0 ns, while in Fig. 4.2(b) the pore filling is in progress, and is completed at t = 1.0 ns. When the fluid-solid interaction intensity is relatively low (α = 0.03), the filling of the liquid molecules into the inside of the slit pore doesn't occur as completely as the results checked by the non-equilibrium molecular dynamics simulations during 10.0 ns. Meanwhile, the filling of the liquid molecules into the slit pore occurs only when the value of α exceeds a certain value. Figure 4.2(b) shows the filling-in progress when the time, t, is 150.0 ps. These results show the wetting phenomenon of the slit pore, i.e., whether or not the inside of the slit pore is filled with the liquid molecules within a definite time, depends on the fluid-solid interaction intensity.

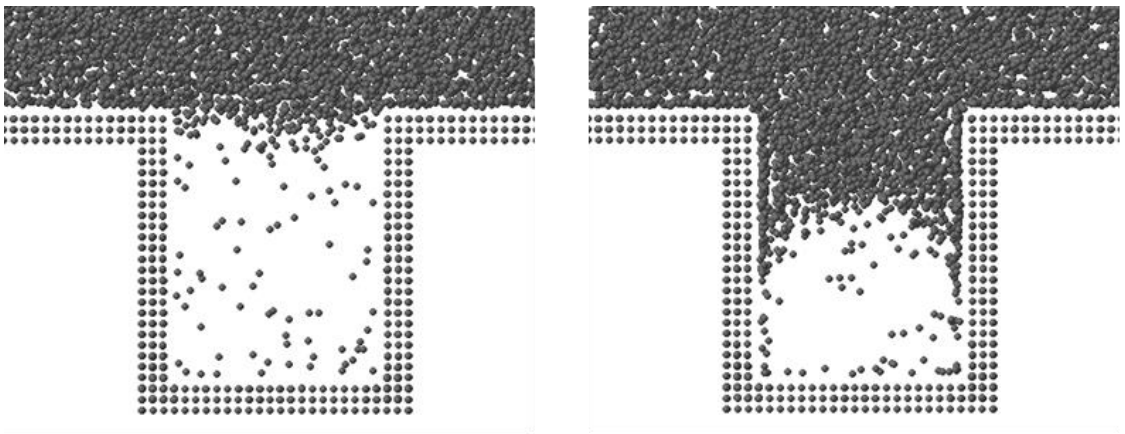

(a) α = 0.03(t = 1.0 ns). (b) α = 0.08(t = 150.0 ps).

Fig. 4.2 Typical calculation results when the inside of the slit pore isn't filled or is filled with liquid molecules: (a) α = 0.03(t = 1.0 ns) and (b) α = 0.08(t = 150.0 ps).

The simulation results of the slit pore wetting obtained by changing the value of α are listed in Table 4.1. The wetting probability in Table 4.1 is defined as the result which shows whether the inside of the slit pore is filled with liquid molecules within 1.0 ns. A white circle indicates that the inside of the pore was filled with the liquid molecules

within 1.0 ns, a white triangle is the case when the filling wasn't completed within 1.0 ns, and a cross indicates a low probability of the filling in the calculation during 1.0 ns. The results indicate that there is a critical value of $\alpha(=\alpha_c)$ which determines whether the inside of the slit pore is filled with the liquid molecules within a definite time.

Table 4.1 The α values and wetting probability. The white circle indicates that the inside of the pore was filled with the liquid molecules within 1.0 ns, the white triangle is the case when the filling wasn't completed within 1.0 ns, and the cross indicates a low probability of the filling in the calculation during 1.0 ns.

α	Probability of wetting phenomenon
0.03	×
0.04	×
0.05	Δ
0.06	Δ
0.07	○
0.08	○
0.09	○
0.10	○

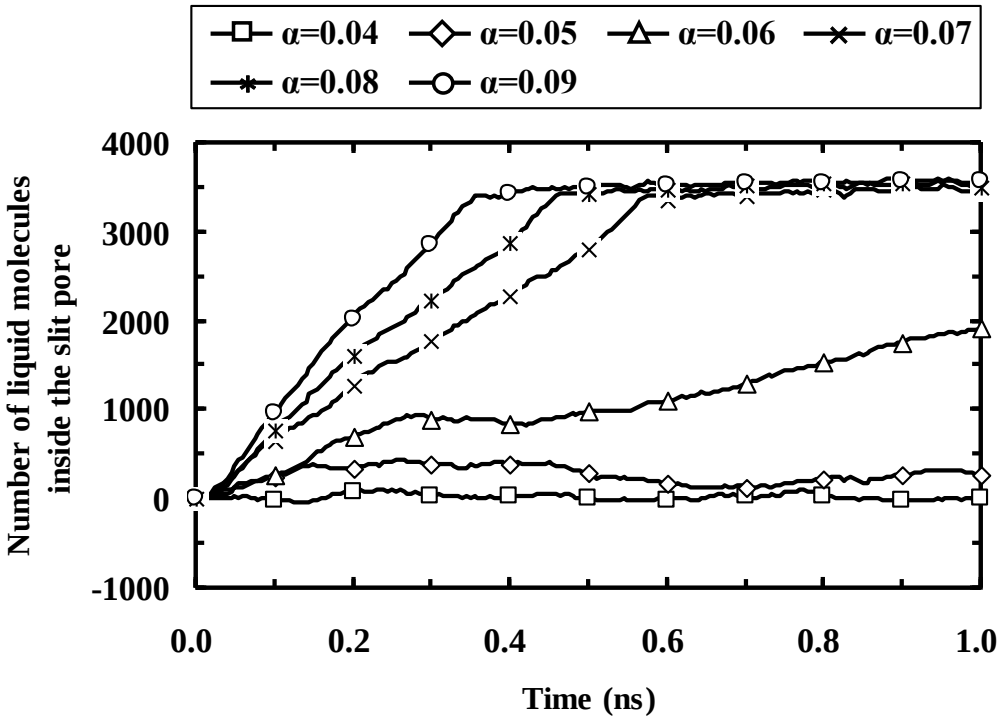

Fig. 4.3 Time evolution of the number of liquid molecules inside the slit pore for various fluid-solid interaction intensity α.

Figure 4.3 shows the time evolution of the number of liquid molecules inside the slit pore for various values of the interaction intensity α(0.04 – 0.09). The initial number of argon molecules inside the slit pore is subtracted from the total number of liquid molecules in Fig. 4.3. When the value of α is relatively low (0.04), there is little deviation in the number of liquid molecules inside the slit pore, and the initial state is stable for at least 1.0 ns. Changing the value of α to 0.05, the number of the liquid molecules inside the slit pore fluctuates, although there seems to be little possibility of complete wetting, judging from the simulation results for 1.0 ns. When the value of α is sufficiently high (0.07, 0.08, and 0.09), the wetting phenomenon of the slit pore is completed within 1.0 ns. These results also suggest that the wetting phenomena, whether or not the inside of the slit pore is filled with liquid molecules within 1.0 ns, as well as the characteristic time of the filling phenomena, are dependent on the fluid-solid interaction intensity α in the present calculation, in which the fluid-solid interaction is assumed to obey Eq. (4.1).

The effects of the fluid-solid interaction intensity α on the progress of wetting phenomenon are shown in Fig. 4.4. Figures 4.4(a,b) indicate that the fluid-solid interaction intensity α has a considerable effect on wetting progress; it can be seen that the higher the interaction intensity α, the more that the filling is driven by the liquid molecules in the vicinity of the solid wall, and the greater the curvature of the gas-liquid interface tends to become. When the value of α is relatively high as shown in Fig. 4.4(c), it can be seen more clearly that a monolayer is formed on the wall surface before the bulk part of the liquid molecules proceeds into the slit pore.

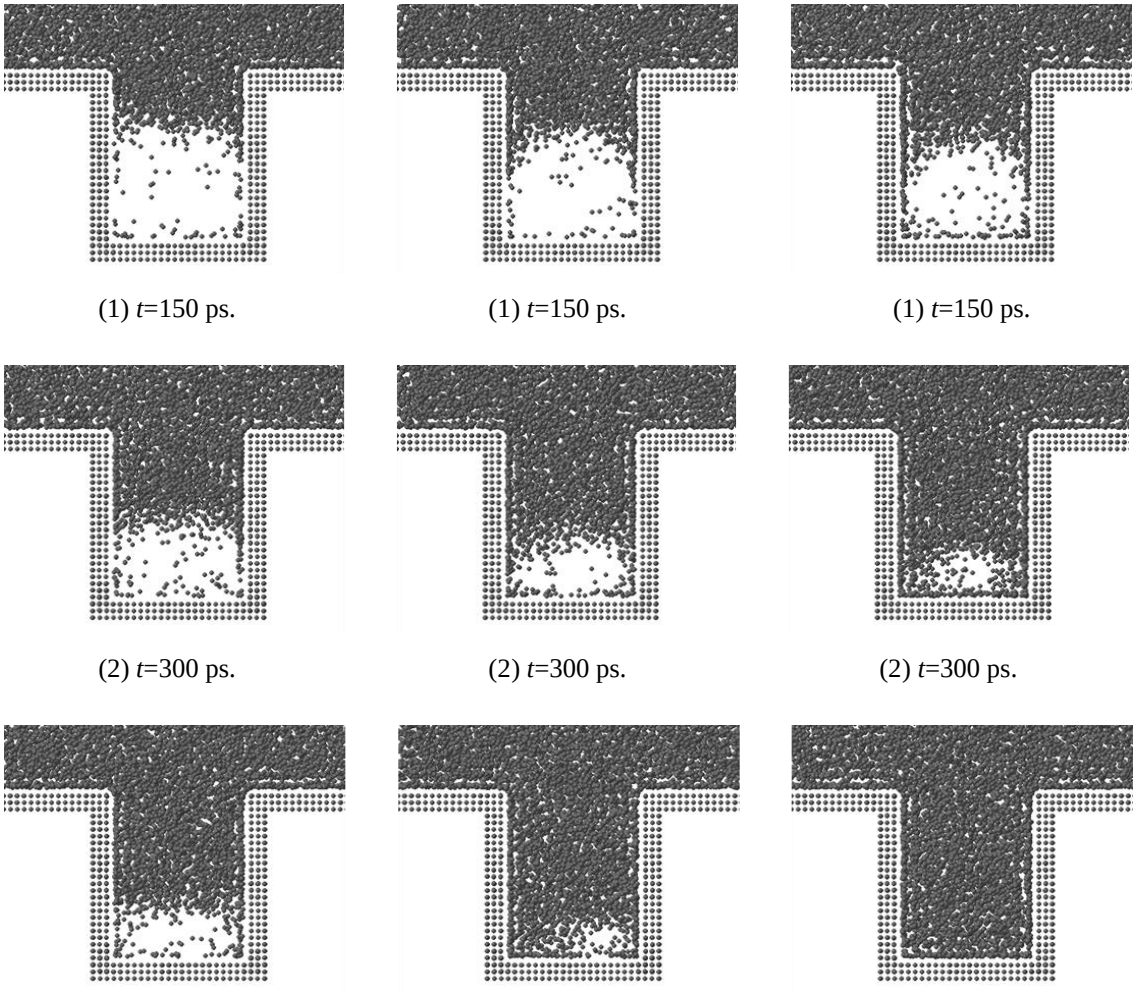

Fig. 4.4 Effect of the fluid-solid interaction intensity on the distribution of liquid molecules when the wetting phenomenon occurs: (a) α = 0.07, (b) α = 0.08, and (c) α = 0.10.

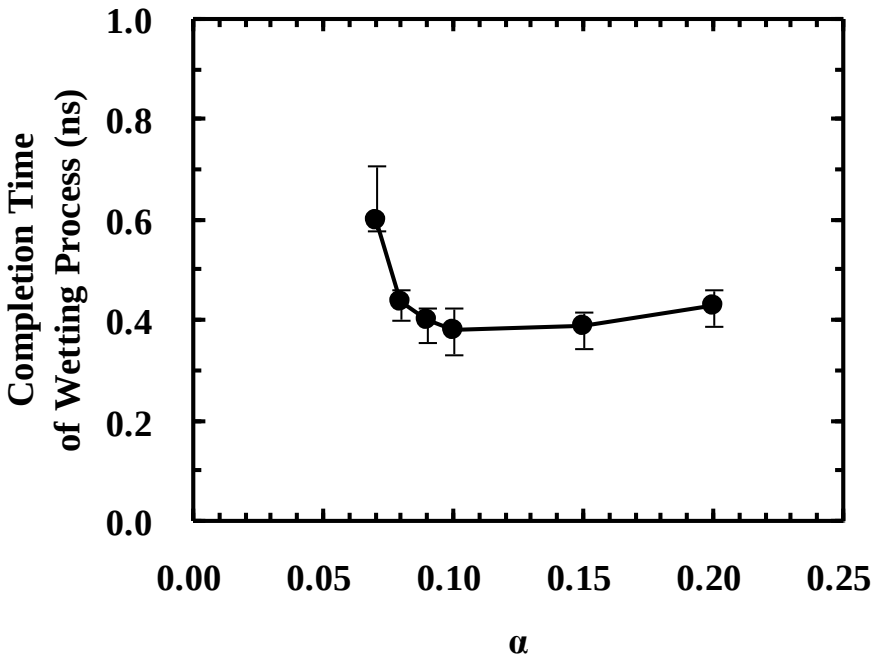

Fig. 4.5 Effect of the fluid-solid interaction intensity on the completion time of the slit pore wetting process in the case of T = 100 K. The completion time is defined by the variation of the total number of the liquid molecules inside the slit pore.

The wetting process completion time when the value of α is changed, is shown in Fig. 4.5. The wetting process completion time used in Fig. 4.5 is defined as the time when the number of liquid molecules inside the slit pore reaches 95% of the final (or equilibrium) value. 10 simulations are conducted for each value of α, and the initial values are chosen at intervals of 50.0 ps after the relaxation calculation. The result shows that when the value of α is relatively low (0.07-0.10), the wetting process completion time decreases with the increase of α. On the other hand, at values of $\alpha >$ 0.10, the completion time does not show pronounced differences in changes in α. This could be due to the formation of a monolayer which precedes the bulk part of the liquid molecules in the slit pore wetting process, and the arrangement of the liquid molecules in the vicinity of the wall surface as shown in Fig. 4.6. In the case of $\alpha > 0.10$, the monolayer is first formed inside the slit pore by the high interaction intensity with solid atoms before the bulk part of the liquid molecules proceeds into the slit pore, and the bulk liquid becomes less directly affected by the fluid-solid interaction intensity. Effects

of temperature are investigated and shown in Fig. 4.7. The profiles of the curves are qualitatively the same when the temperature ranges from 85 to 100 K, and the completion time of the wetting process becomes shorter with the increase of the temperature.

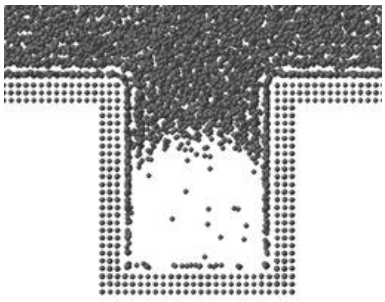

(a) t = 100.0 ps.

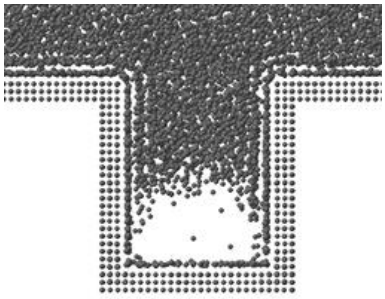

(b) t = 200.0 ps.

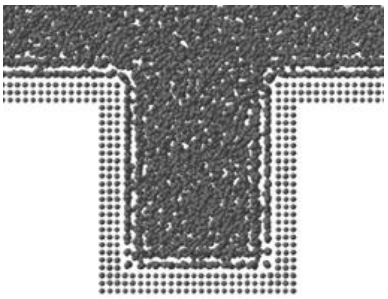

(c) t = 500.0 ps.

Fig. 4.6 Typical configurations and the liquid molecular arrangement during the wetting phenomenon in the case of α = 0.20: (a) t = 100.0 ps, (b) t = 200.0 ps, and (c) t = 500.0 ps.

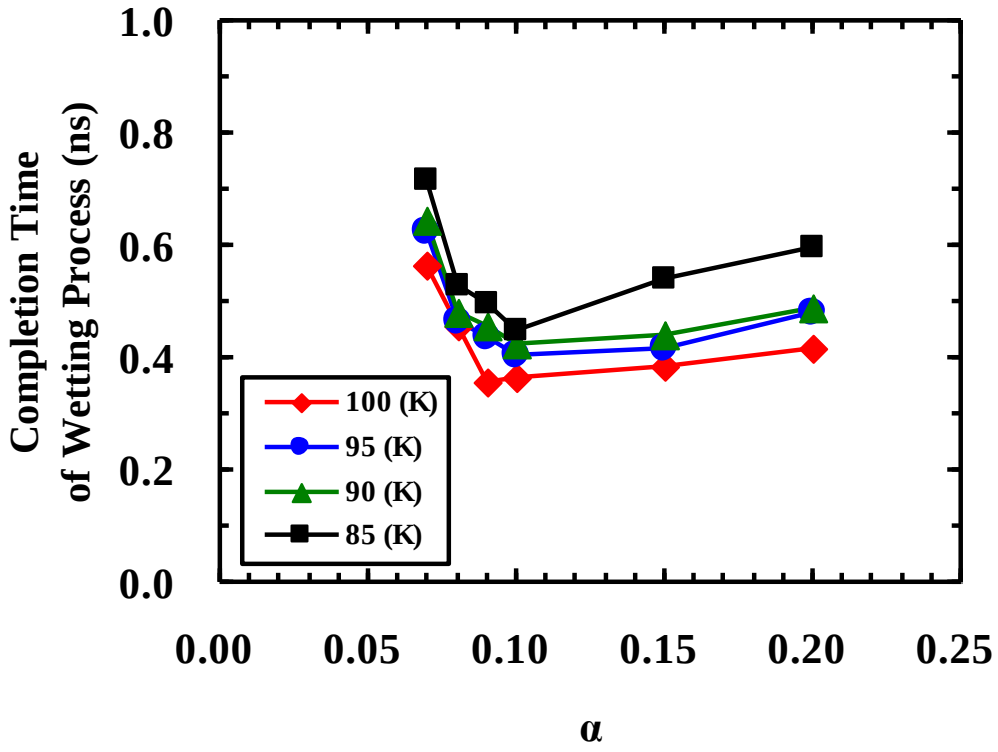

Fig. 4.7 Effect of the fluid-solid interaction intensity on the completion time of the slit pore wetting process in the case of T = 85, 90, 95, and 100 K.

5. Liquid film on a flat solid surface

In this Chapter, the molecular dynamics simulation is conducted for the calculation system in which fluid molecules are confined between two planar solid surfaces. The purpose is to obtain in particular local pressure components and interfacial tension of the liquid film on a flat solid surface, and check the validity of the proposed perturbative method. The calculation system and numerical details are described in Sec. 5.1. In Sec. 5.2, the local pressure components and interfacial tension of the liquid in the vicinity of the solid interface are obtained by the proposed perturbative method based on Eqs. (2.16) and (2.17) in one dimension, and the results are compared with those obtained by two alternative methods: the first method evaluates the intermolecular force acting on a plane, and the second is the conventional method based on the virial expression. The quantities are also obtained in two dimensions and shown in Sec. 5.3.

5.1 System and Numerical details

The classical molecular dynamics simulation is conducted for the system in which 4050 fluid molecules are confined between two planar solid surfaces as shown in Fig. 5.1. The system is in an equilibrium which includes three interfaces (vapor-solid, vapor-liquid, and liquid-solid interfaces) parallel to the solid surfaces (*xy* plane) perpendicularly located along the *z* axis. The Hamiltonian of the system is described as

$$H(\mathbf{r},\mathbf{p}) = \sum_{i}^{N_f} \frac{\left|\mathbf{p}_i\right|^2}{2m_i} + \frac{1}{2}\sum_{i\neq j}^{N_f} u_{ff}(r_{ij}) + u_{ext}, \tag{5.1}$$

where N_f is the number of the fluid molecules, $u_{ff}(r_{ij})$ is the potential energy between the fluid molecules which depends on the distance between the molecules, $r_{ij} = \left|\mathbf{r}_i - \mathbf{r}_j\right|$, and $u_{ext} = \Sigma_{i=1}^{N_f}\Sigma_{j=1}^{N_s} u_{fs}(r_{ij})$ with the number of the solid atoms N_s and the potential energy between the fluid molecules and the solid atoms u_{fs}. All the interactions between

molecules and atoms are assumed to obey the 12-6 Lennard-Jones(LJ) form (Eq. 3.6). The fluid molecules are assumed to be argon (Ar), and reduced units are used as given in Table 5.1 by using the Boltzmann constant k_B, and the LJ parameters of the fluid molecules, m_f, σ_{ff}, and ε_{ff}. The cutoff distance of the LJ potential is 5.0. The solid atoms are assumed to be platinum (Pt), with Lennard-Jones interaction parameters of σ_{ss}=0.746 and ε_{ss}=65.39 (Zhu & Philpott 1994). The fluid-solid interaction is also described by the LJ potential with $\sigma_{fs}=(\sigma_{ff}+\sigma_{ss})/2$= 0.873 and ε_{fs}, in which ε_{fs} is varied as a ratio to the ε_{ff}.

Table 5.1 Reduced units and their values.

Quantity	Unit	Value
Mass	m_f	6.634×10^{-26} kg
Distance	σ_{ff}	3.405×10^{-10} m
Energy	ε_{ff}	1.670×10^{-21} J
Temperature	ε_{ff}/k_B	120.9 K
Time	$\sigma_{ff}\sqrt{m_f/\varepsilon_{ff}}$	2.146×10^{-12} s
Interfacial tension	$\varepsilon_{ff}/\sigma_{ff}^2$	1.440×10^{-2} $\mathrm{Nm^{-1}}$
Pressure	$\varepsilon_{ff}/\sigma_{ff}^3$	4.230×10^{7} $\mathrm{Nm^{-2}}$
Density	m_f/σ_{ff}^3	1.680×10^{3} $\mathrm{kgm^{-3}}$

The volume of the system is defined as $V=L_x\times L_y\times L_z$, where L_x=15.4, L_y=15.4, and L_z=44.1. Periodic boundary conditions are applied in the x and y directions which are tangential to the interfaces. Each solid part consists of 3 layers of the solid atoms where the outermost layer is fixed and the temperature of the middle layer is controlled by the Langevin method, at a constant value T^*=0.8. Artificial forces are not added to the 1st layer, and the atoms in the 1st layer can move freely around the center of oscillation by the interactions with other atoms. The simulation consists of 2028 solid atoms arrayed in an fcc lattice structure with the (111) surface in contact with the fluid molecules.

The temperature of the fluid molecules is kept constant by the velocity scaling control for 500,000 steps with a time interval of Δt=9.3×10^{-4}, followed by 2,000,000 steps of the relaxation calculation conducted to equilibrate the system without the velocity scaling control. The density, pressure, and interfacial tension are obtained as the time averaged values for at least 2,000,000 steps.

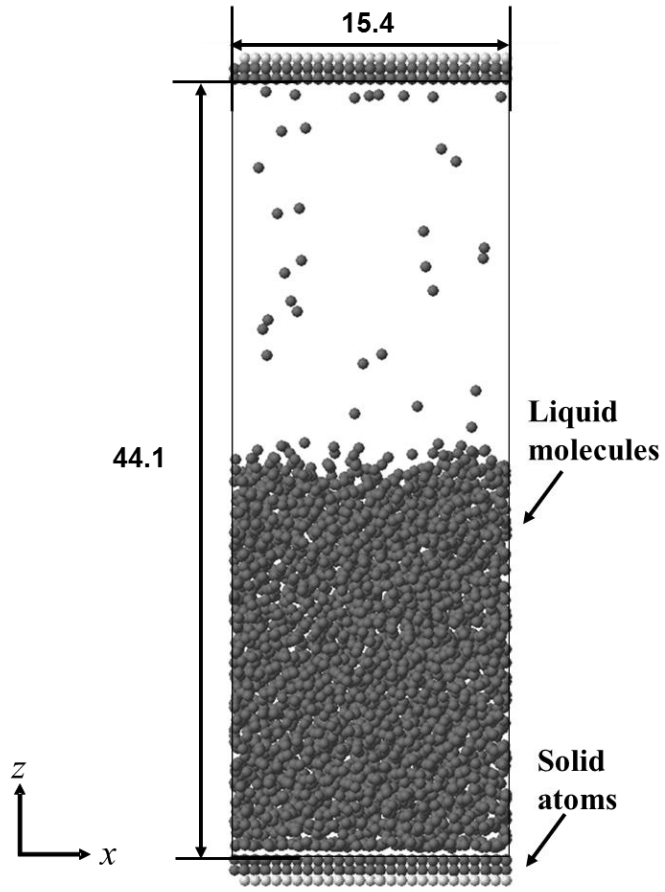

Fig. 5.1 Calculation system(Initial state).

5.2 Analysis in one dimension

Figures 5.2(a) and 5.2(b) present typical results obtained by the perturbative method on the basis of Eq. (2.16). The figures show the normal and tangential components of the reduced pressure and the reduced density of fluid molecules in the *z* direction near the lower substrate for $\lambda = 5.0\times10^{-10}$, and for $\varepsilon_{fs} = 0.25$(Fig. 5.2(a)) and $\varepsilon_{fs}=0.50$(Fig. 5.2(b)). The definition of the perturbation parameter, λ is explained in Sec. 3.2.1. The partial derivatives as expressed in Eqs. (2.4) and (2.11) are evaluated by the central difference method. The results are obtained by averaging the pressure and density values after 5,000,000 time steps. For the pressure results, the Figures show error bars calculated using five averaged results of 1,000,000 time steps. The system is divided into subsystems with the height of 0.088 in the *z* direction, in which the pressure components and density of fluid molecules are calculated. As shown in Fig. 5.2, the normal pressure component $P_N^*(=P_{zz}^*)$ is constant in the *z* direction, ensuring that the system is in equilibrium, while the tangential pressure component $P_T^*(=(P_{xx}^*+P_{yy}^*)/2)$ fluctuates in the vicinity of the liquid-solid interface and is almost constant in the bulk of the liquid. The error bars obtained by the 5 simulation runs indicate that the results are obtained with considerable accuracy in the present study. Comparing Figs. 5.2(a) and 5.2(b), it is evident that the fluctuation of P_T in the vicinity of the liquid-solid interface becomes pronounced with the increase of ε_{fs}.

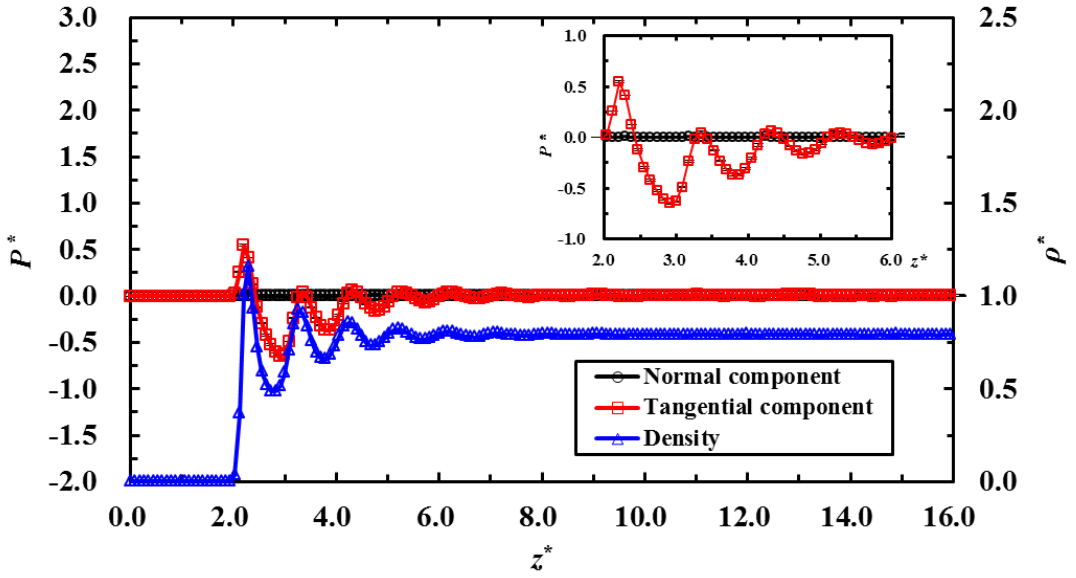

(a) ε_{fs}=0.25.

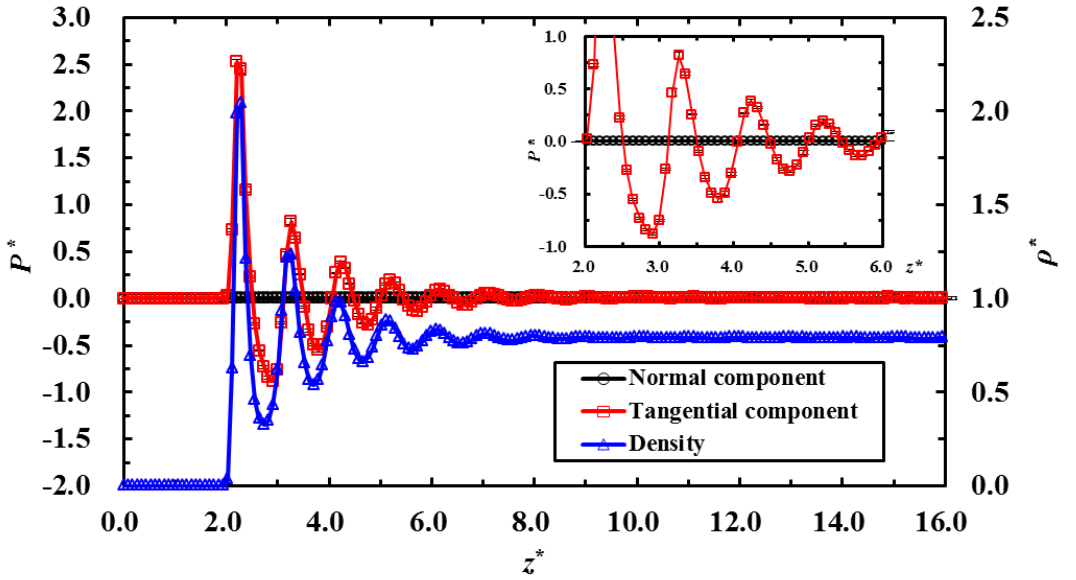

(b) ε_{fs}=0.50.

Fig. 5.2 Normal and tangential components of the reduced pressure P^* and the reduced density of fluid molecules ρ^* in the z direction, obtained on the basis of Eq. (2.16) in the vicinity of the liquid-solid interface for $\lambda=5.0\times10^{-10}$, and for (a) ε_{fs}=0.25 and (b) ε_{fs}=0.50. The circles and squares correspond to the results of the normal and tangential components of the pressure, respectively. The triangles are the results of the density of the fluid molecules. The results of the pressure components and density are calculated as the averaged values of 5,000,000 time steps.

Figure 5.3 shows effects of the perturbation parameter, λ on the reduced local liquid-solid interfacial tension, $\gamma_{V_k}^*$ obtained on the basis of Eq. (2.17) by the forward difference for ε_{fs}=0.25. The figure shows $\gamma_{V_k}^*$ as a function of z^*, and is normalized to the corresponding values for the case of $\lambda=5.0\times10^{-10}$. As shown in Fig. 5.3, with increasing λ, the value of the local interfacial tension differs markedly from that in the case of $\lambda=5.0\times10^{-10}$, especially in the bulk of the liquid; this is due to the quite small values of the local interfacial tension in the bulk. This result suggests that the use of the forward difference alone is not sufficient to obtain accurate local interfacial tension when the value of λ is relatively large ($>5.0\times10^{-6}$), as in the present study. Therefore using smaller values of λ or switching to the central difference method is strongly recommended. The value of $\lambda=5.0\times10^{-10}$ is adopted as the standard in the following calculations.

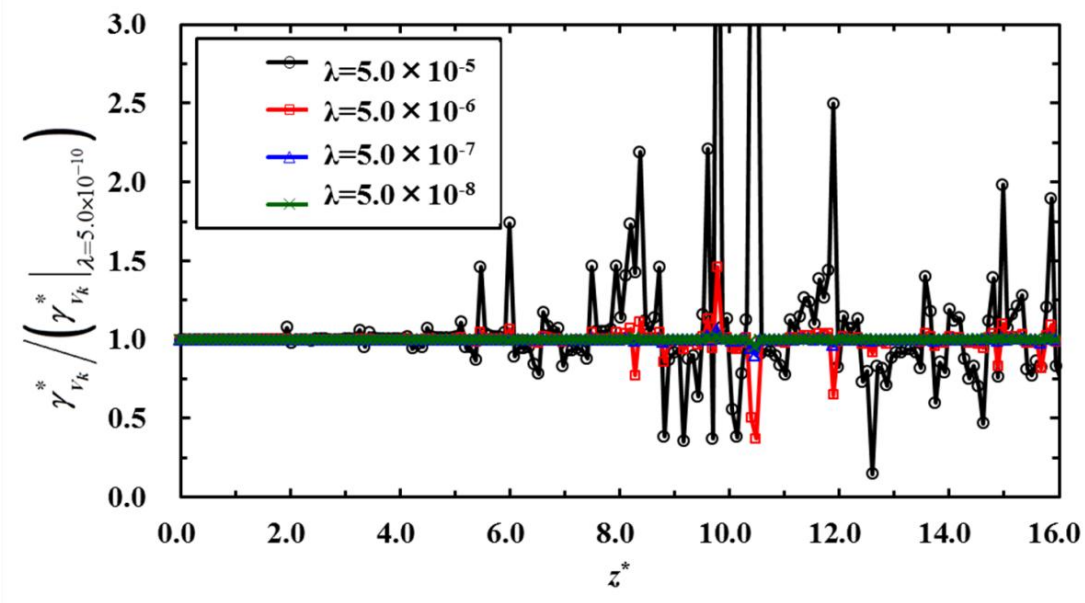

Fig. 5.3 Effects of the perturbation parameter λ on the reduced local liquid-solid interfacial tension $\gamma_{V_k}^*$ obtained on the basis of Eq. (2.17) by the forward difference for ε_{fs}=0.25. Values of $\gamma_{V_k}^*$ are normalized to the value in the case of $\lambda=5.0\times10^{-10}$, $\gamma_{V_k}^*\big|_{\lambda=5\times10^{-10}}$. The circles, squares, triangles, and crosses are the results for $\lambda=5.0\times10^{-5}$, 5.0×10^{-6}, 5.0×10^{-7}, and 5.0×10^{-8}, respectively. Each result is calculated as the averaged value of 2,000,000 time steps.

Figure 5.4 shows effects of using forward and backward differences on the calculated local liquid-solid interfacial tension for λ=5.0×10^{-10} and ε_{fs}=0.25, in which each value is normalized to the value obtained by the central difference. Relatively high peaks are observed in the bulk of the liquid, but the profile is symmetric about the value of the central difference ($\gamma^*_{V_k}$ =1.0), which means that the result obtained by the central difference is the most reliable method compared with the other approaches. However, from the fact that the maximum error was found to be at most 5 % in this study, it can also be said that the forward and backward differences are suitable when such a small value of λ is chosen(λ=5.0×10^{-10}), if high accuracy is not required for the calculation of the local liquid-solid interfacial tension.

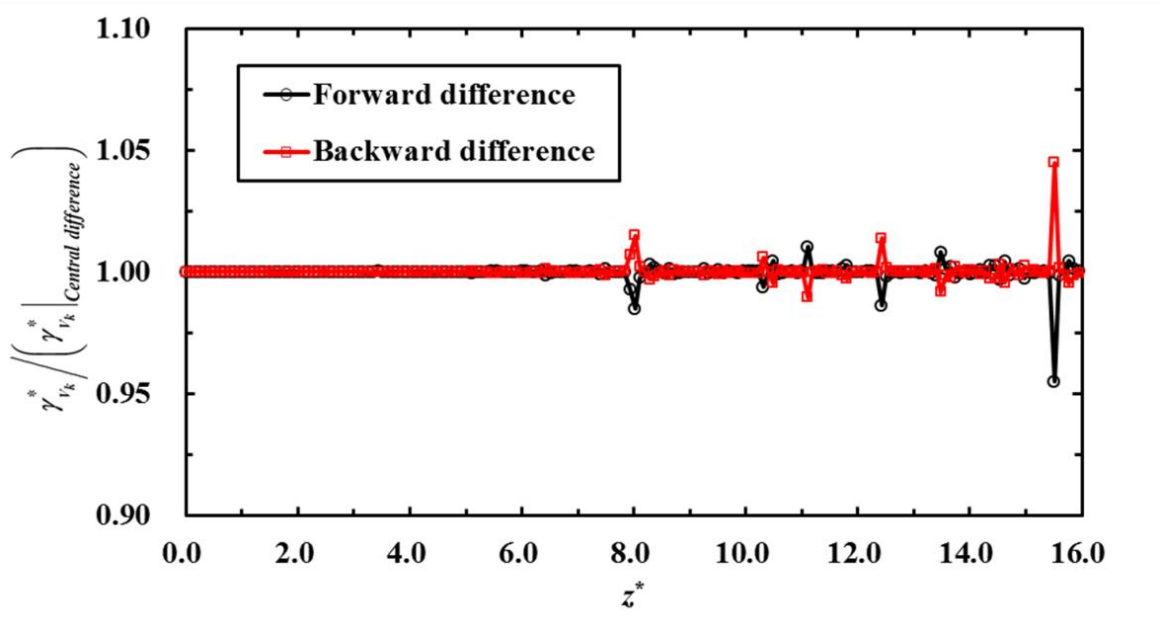

Fig. 5.4 Effects of the forward and backward difference methods on calculating the reduced local liquid-solid interfacial tension $\gamma^*_{V_k}$ obtained on the basis of Eq. (2.17). for λ=5.0×10^{-10} and ε_{fs}=0.25. Each value is normalized to that obtained by the central difference, $\gamma^*_{V_k}\Big|_{Central\ difference}$. The circles and squares indicate the results of using the forward and backward difference methods, respectively. Each result is calculated as the averaged value of 2,000,000 time steps.

Figure 5.5 gives the results of the reduced local liquid-solid interfacial tensions in one dimension calculated by the perturbative method (Eq. (2.17)), the evaluation of the intermolecular force acting on a plane (Eq. (2.19)), and the virial expression based on the Irving and Kirkwood definition (Eq. (2.23)) for ε_{fs}=0.25. These results are shown normalized to the values obtained by the perturbative method in Fig. 5.6. According to Fig. 5.5, all the results have good agreement at each local position, and confirm that the local liquid-solid interfacial tension obtained by the perturbative method in this study is valid in one dimension. A detailed comparison of the results as shown in Fig. 5.6 reveals that the values of the local interfacial tension at each position agree well, but differences are observed in the bulk of the liquid where the values of the local interfacial tension are quite small as shown in Fig. 5.5. In Fig 5.6, effects of the tangential pressure components affected by the solid atoms can be evaluated by the result of Irving & Kirkwood definition obtained based on Eq. (2.23) in which no contributions of the tangential pressure components affected by the fluid-solid interactions are considered. The results of the local liquid-solid interfacial tensions obtained by the perturbative method and the force acting on a plane confirm that the tangential pressure component affected by the solid atoms almost vanishes in one dimension, as indicated in the previous works (Varnik *e. al.* 2000).

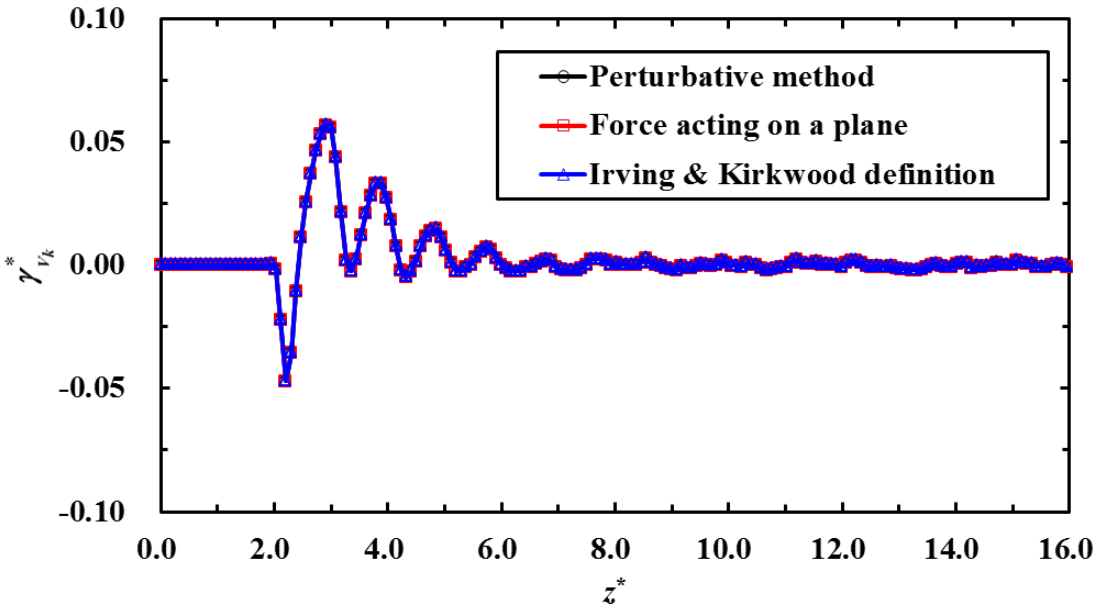

Fig. 5.5 Reduced local liquid-solid interfacial tension $\gamma^*_{V_k}$ calculated by the perturbative method (Eq. (2.17)), the evaluation of the intermolecular force acting on a plane (Eq. (2.19)), and the virial expression based on the Irving and Kirkwood definition (Eq. (2.23)) for ε_{fs}=0.25. The values of the perturbative method are calculated by the central difference method. The circles, squares and triangles indicate the results obtained by the perturbative method, the evaluation of the intermolecular force acting on a plane, and Irving and Kirkwood definition, respectively. Each result is calculated as the averaged value of 5,000,000 time steps.

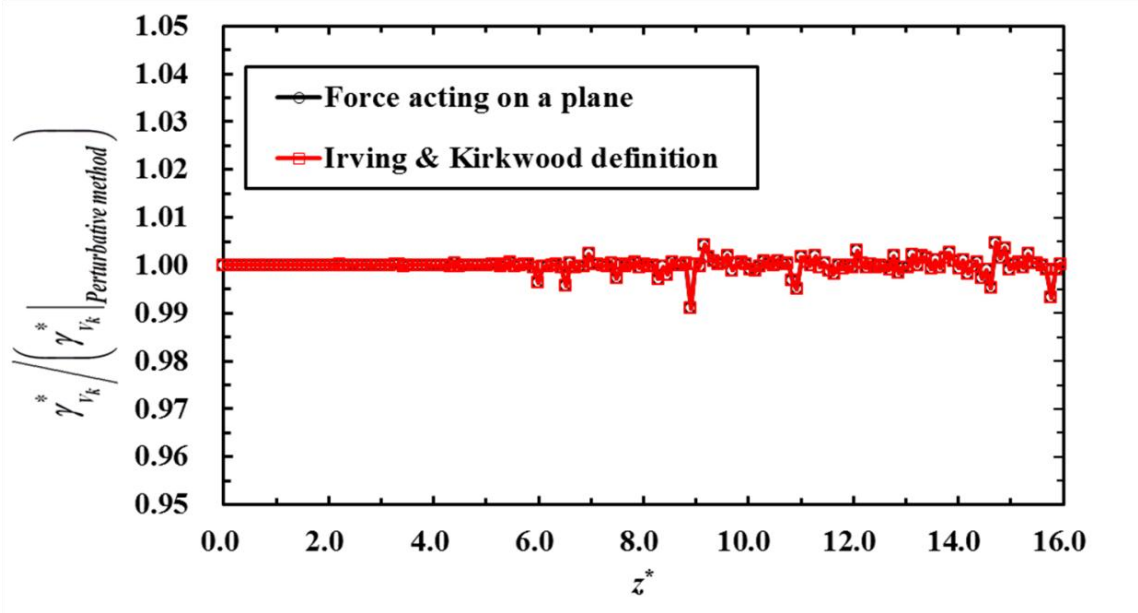

Fig. 5.6 Reduced local liquid-solid interfacial tensions $\gamma^*_{V_k}$ calculated on the basis of Eqs. (2.19) and (2.23) for ε_{fs}=0.25. The results are normalized to that obtained by the perturbative method (Eq. (2.17)), $\gamma^*_{V_k}\big|_{Perturbative\ method}$. The circles and squares indicate the results obtained by the evaluation of the intermolecular force acting on a plane (Eq. (2.19)) and Irving and Kirkwood definition (Eq. (2.23)), respectively. Each result is obtained as the averaged value of 2,000,000 time steps.

5.3 Analysis in two dimensions

The perturbative method based on Eqs. (2.16) and (2.17) is applied to the calculation system to obtain the pressure components and interfacial tension at a liquid-solid interface in two dimensions. The system is divided into subsystems with the area A_k(= $dx_k \times dz_k$=0.088×0.088) in the *xz* plane, and results are obtained as the averaged values of 5,000,000 time steps. Figure 5.7 shows reduced density distributions of the fluid molecules in the vicinity of the liquid-solid interface; Fig. 5.7(a) shows the result for ε_{fs}=0.25 and Fig. 5.7(b) for ε_{fs}=0.50. In Fig. 5.7, the x^* positions of the first layer of the solid atoms facing the fluid molecules are 0.0, 0.592, and 1.184. The results indicate that the density distribution of the fluid molecules fluctuates in the vicinity of the liquid-solid interface and is affected by the positions of the solid atoms in two dimensions.

Figure 5.8 presents two-dimensional contour plots of the local tangential component of the reduced pressure of the fluid, obtained based on Eq. (2.16) using the central difference method for λ=5.0×10^{-10}, and for ε_{fs}=0.25 (Fig. 5.8(a)) and ε_{fs}=0.50 (Fig. 5.8(b)). The tangential pressure component in the *xz* plane fluctuates at the liquid-solid interface and becomes pronounced with the increase of ε_{fs}, displaying the same tendency as that obtained in one dimension.

Three-dimensional contour plots of the local tangential pressure component are shown in Fig. 5.9 for λ=5.0×10^{-10}, and for ε_{fs}=0.25 (Fig. 5.9(a)) and ε_{fs}=0.50 (Fig. 5.9(b)). The latter shows that the peaks of the tangential pressure component fluctuate in the *x* direction due to the effects of the solid atoms, while the effect is weak in the case of ε_{fs}=0.25 as shown in Fig. 5.9(a).

Figure 5.10 gives the results of the reduced local interfacial tension in the vicinity of the liquid-solid interface in the *xz* plane; results are obtained on the basis of Eq. (2.17) for λ=5.0×10^{-10}, and for ε_{fs}=0.25 (Fig. 5.10(a)) and ε_{fs}=0.50 (Fig. 5.10(b)). The profiles of the local interfacial tension are the same as those obtained in one dimension, which ensures the validation of the method in two dimensions.

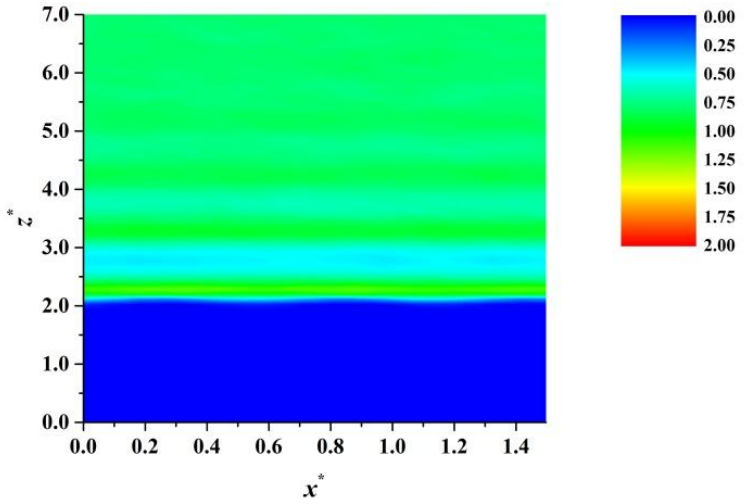

(a) ε_{fs}=0.25.

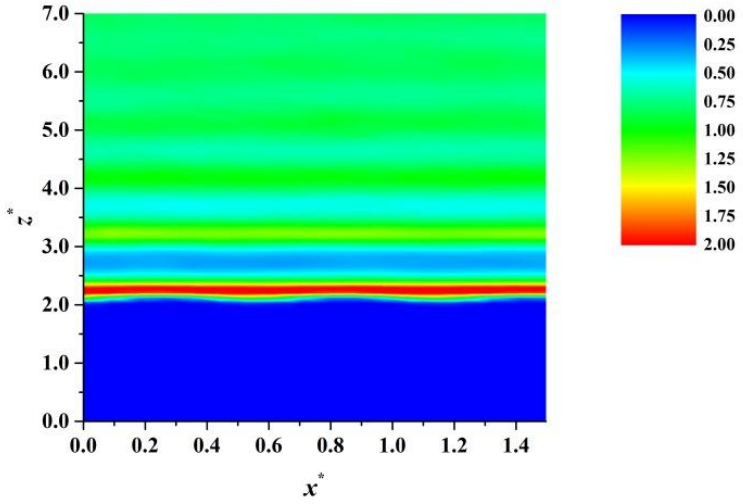

(b) ε_{fs}=0.50.

Fig. 5.7 Reduced density distributions of fluid molecules in the vicinity of the liquid-solid interface, for (a) ε_{fs}=0.25 and (b) ε_{fs}=0.50. Each result is obtained as the averaged value of 5,000,000 time steps and shown on each area A_k(= $dx_k \times dz_k$=0.088×0.088).

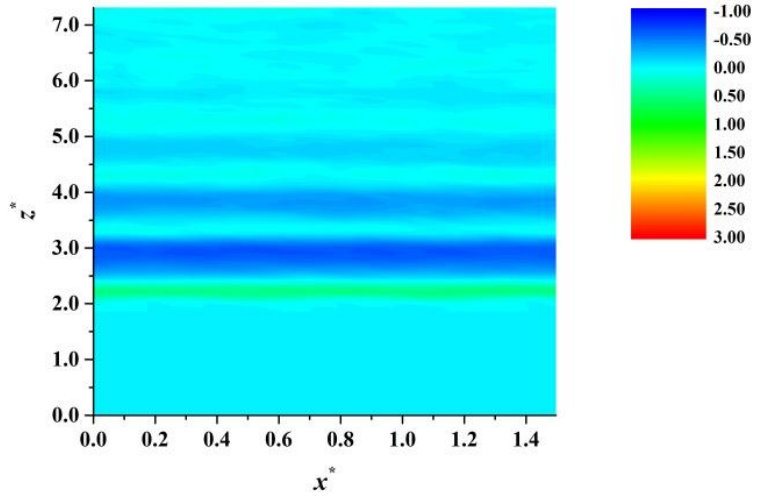

(a) ε_{fs}=0.25.

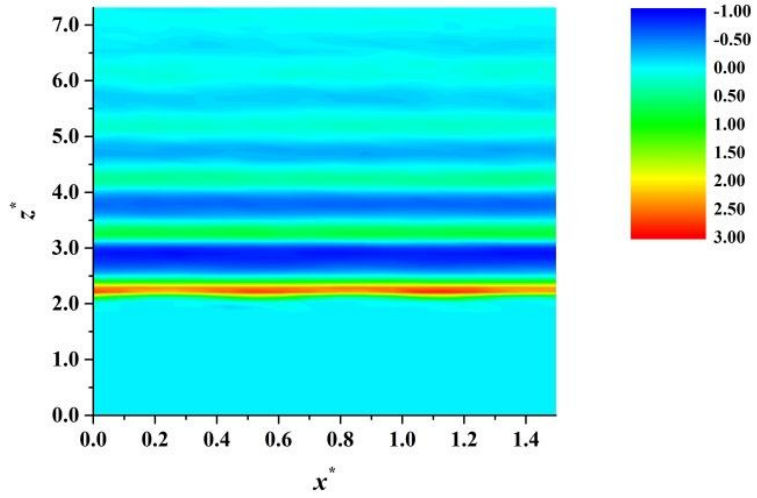

(b) ε_{fs}=0.50.

Fig.5.8 Two-dimensional contour plots of the reduced local tangential pressure component P_T^* in the vicinity of the liquid-solid interface in the *xz* plane, obtained on the basis of Eq. (2.16) for λ=5.0×10^{-10}, and for (a) ε_{fs}=0.25 and (b) ε_{fs}=0.50. Each result is obtained as the averaged value of 5,000,000 time steps.

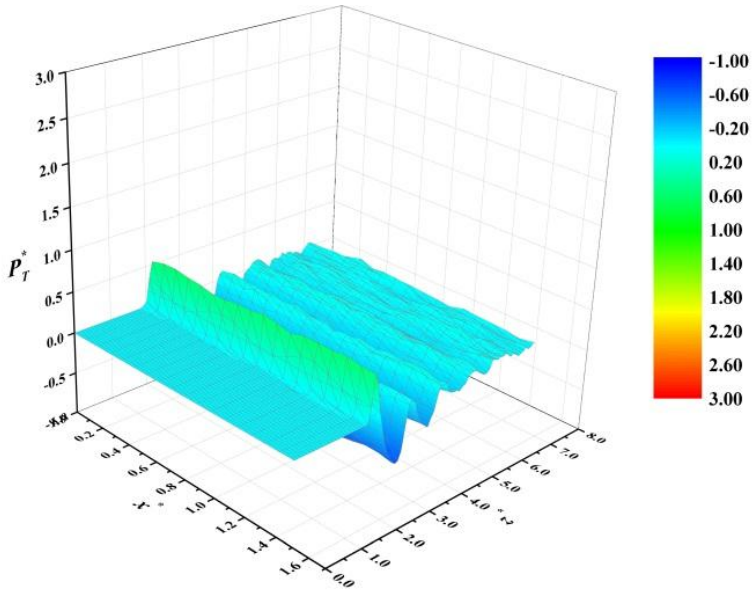

(a) ε_{fs}=0.25.

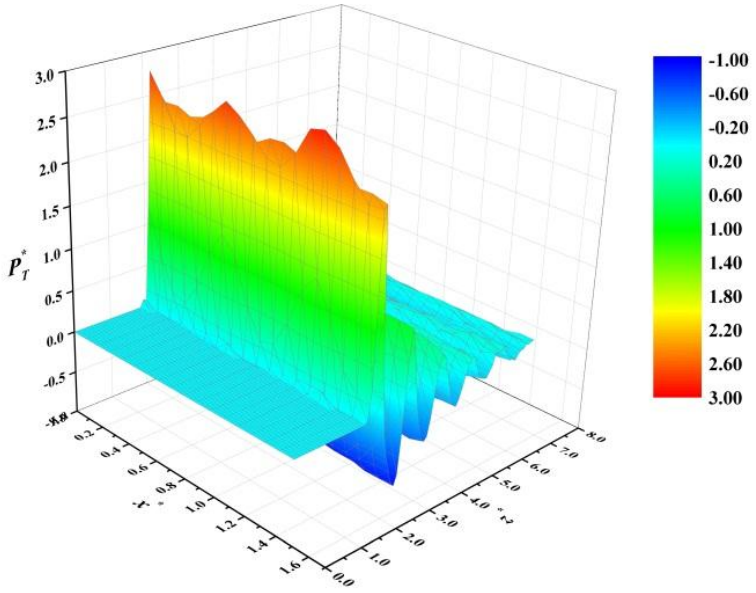

(b) ε_{fs}=0.50.

Fig. 5.9 Three-dimensional contour plots of the reduced local tangential pressure component P_T^* in the vicinity of the liquid-solid interface in the *xz* plane, obtained on the basis of Eq. (2.16) for λ=5.0×10^{-10}, and for (a) ε_{fs}=0.25 and (b) ε_{fs}=0.50. Each result is the averaged value of 5,000,000 time steps.

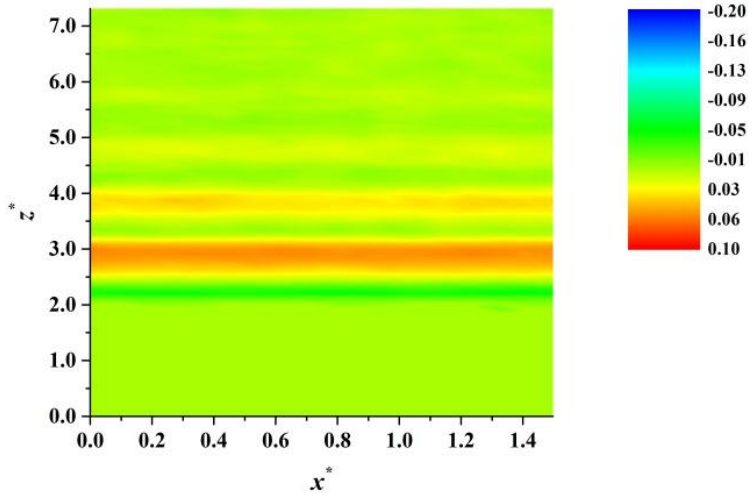

(a) ε_{fs}=0.25.

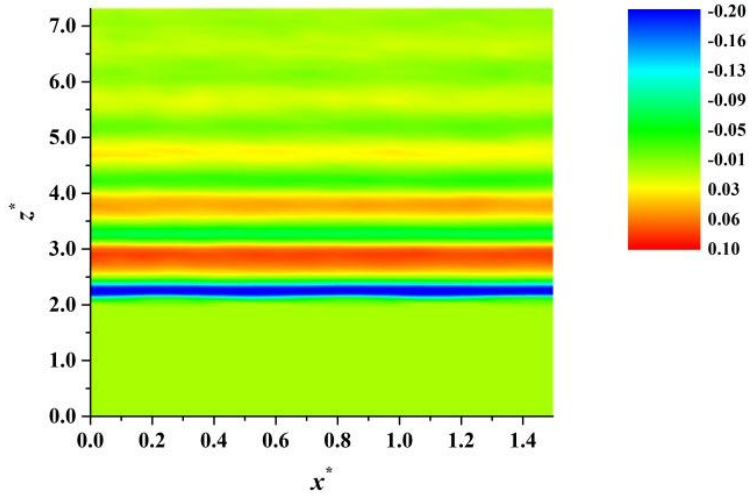

(b)ε_{fs}=0.50.

Fig. 5.10 Two-dimensional contour plots of the reduced local interfacial tension $\gamma^*_{V_k}$ in the vicinity of the liquid-solid interface in the *xz* plane, obtained on the basis of Eq. (2.17) for λ=5.0×10^{-10}, and for (a) ε_{fs}=0.25 and (b) ε_{fs}=0.50. Each result is the averaged value of 5,000,000 time steps.

Figure 5.11 gives the three-dimensional contour plot of the reduced local liquid-solid interfacial tension in the *xz* plane obtained by the evaluation of the intermolecular force acting on a plane, using Eq. (2.19) with λ=5.0×10^{-10} and ε_{fs}=0.25. The result is normalized to the value obtained by the perturbative method (Eq. (2.17)). According to the result, the difference between the two methods becomes relatively pronounced toward the bulk part of the fluid, but the error is under 2 % in the calculation region. The result suggests that the proposed perturbative method is valid for the calculation of the local liquid-solid interfacial tension in this study, even if the values are evaluated in two dimensions.

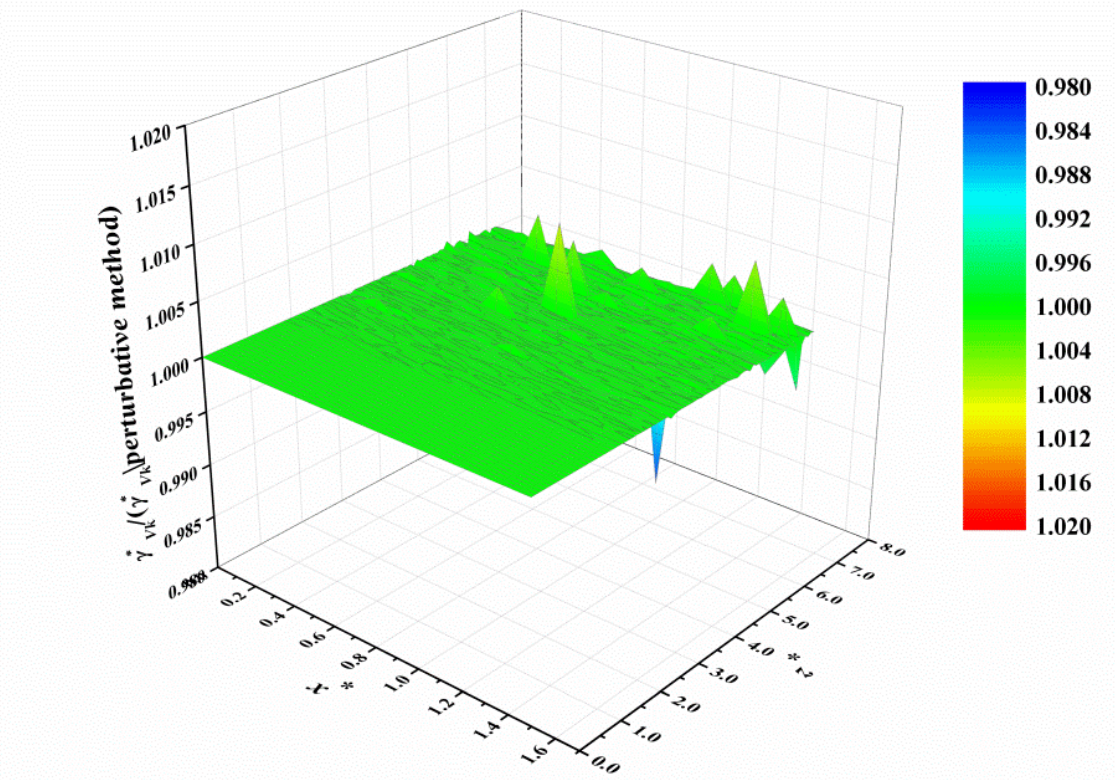

Fig. 5.11 Three-dimensional contour plot of the reduced local interfacial tension $\gamma^*_{V_k}$ in the vicinity of the liquid-solid interface in the *xz* plane, obtained on the basis of Eq. (2.19) for λ=5.0×10^{-10} and ε_{fs}=0.25. The result is normalized to the value obtained by the perturbative method, $\gamma^*_{V_k}\big|_{Perturbative\,method}$. The result is the averaged value of 5,000,000 time steps.

6. Liquid film in the vicinity of a structured solid surface

In this Chapter, as the local thermodynamic quantities, the time-averaged local density and pressure components of the fluid are obtained for the two states of the liquid film: (a) liquid film on the slit and (b) liquid film in the slit, based on the instantaneous expression of the pressure components (Eq. (2.27)). Sec. 6.1 describes the system and numerical details used in this Chapter. The results of the density and pressure distributions of the liquid film on the slit are given in a two dimensional plane in Sec. 6.2 and the results of the liquid film in the slit are given in Sec. 6.3.

6.1 System and numerical details

Classical molecular dynamics simulations are conducted for a system in which a liquid film exists in the vicinity of the solid surface with a slit pore as shown in Fig. 6.1(a). The liquid film exists, as the initial state either on, or in, the slit, and there is a planar solid surface at the top of the calculation system. The periodic boundary conditions are applied in the *x* and y directions. The number of the fluid molecules, upper and lower solid atoms are 6300, 5670, and 12915, respectively.

The potential function and parameters are the same as those in Sec. 5.1. The volume above the slit, $V^u(=L_x^u \times L_y^u \times L_z^u)$ is 24.87×17.76×44.05, and the volume of the slit is 11.84×17.76×12.43. The definition of the coordinates in the system is illustrated in Fig. 6.1(b), on the zoomed figure in the vicinity of the entrance of the slit. The x^* position of the solid atoms facing the inside of the slit at the left side of the slit is 6.51, and the center of the slit is at x^* =12.43. The upper and lower solid parts consist of 9 and 30 layers of the solid atoms, respectively, and the solid atoms are arrayed in an fcc lattice structure with the (111) surface in contact with the fluid part. The solid atoms in the 1st layers facing the fluid part can move freely around the center of oscillation by the interactions with other atoms, the temperature of the solid atoms in the 2nd layers is controlled by the Langevin

method, at a constant value T^*=0.8, and the other solid atoms are fixed. The perturbation parameter, λ, which is needed to evaluate the difference of the energy in Eq. (2.27), is chosen to have the value of 1.0×10^{-10}, and the difference is numerically evaluated by the central difference method.

The procedure to make the initial condition is as follows. Firstly, the temperature of the fluid molecules is kept constant by the velocity scaling control for 500,000 time steps with a time interval of Δt=9.3×10^{-4}. Secondly, the relaxation calculation is conducted for 1,500,000 time steps without the velocity scaling control. The quantities: density, pressure, and interfacial tension are obtained as the time averaged values for at least 2,000,000 time steps.

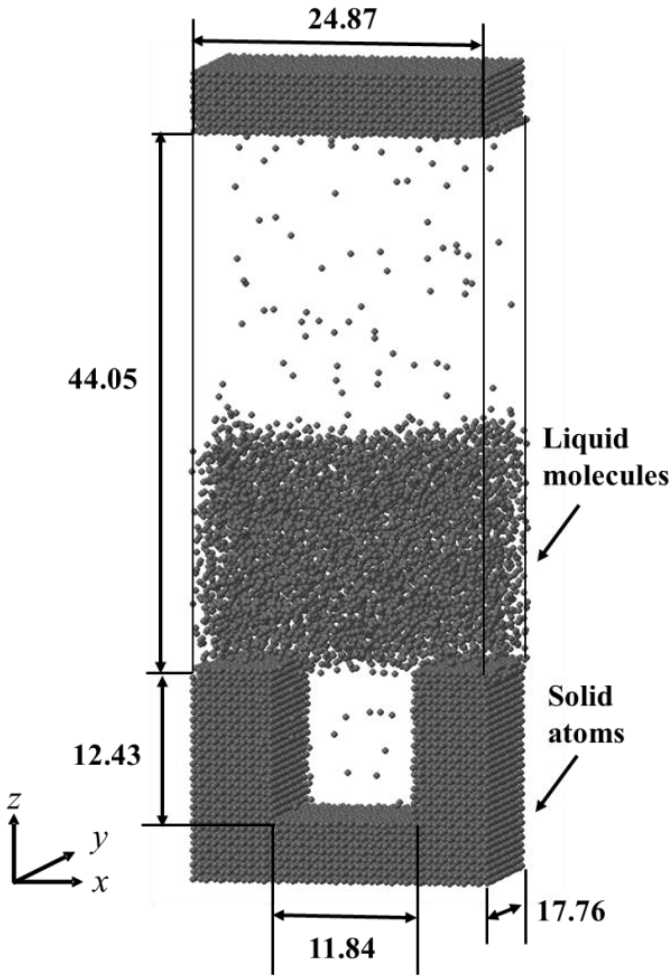

(a) Liquid film on a slit pore (Initial condition).

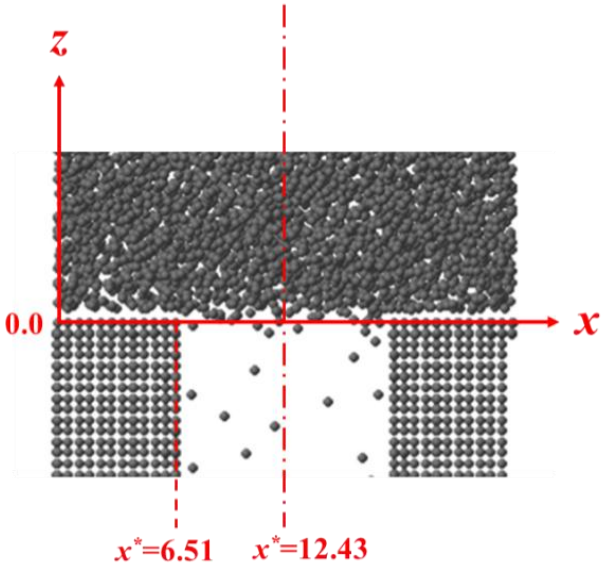

(b) Definition of the location of the coordinates.

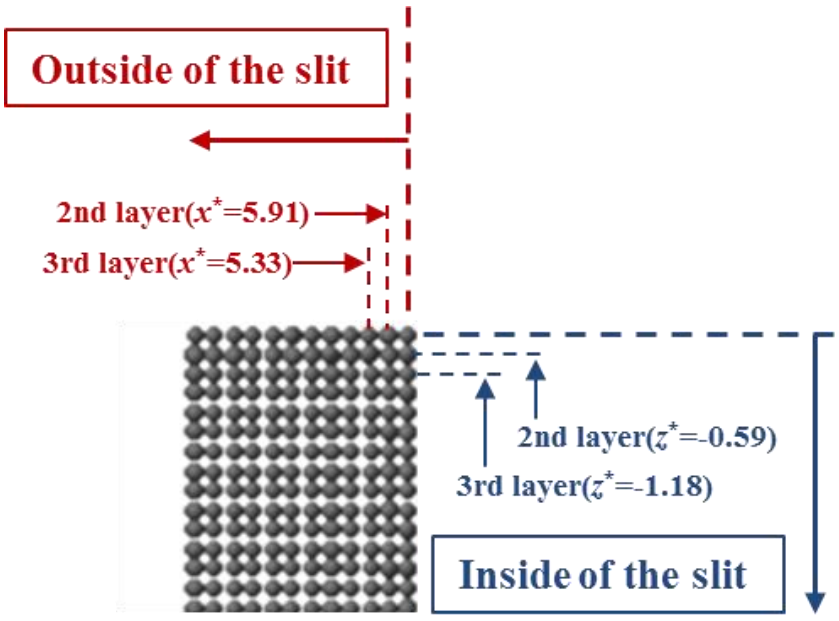

(c) Arrangement of solid atoms at the left side of the entrance of the slit, and definition of the 2nd and 3rd layers of the solid atoms inside and outside of the slit.

Fig. 6.1 Calculation system, and definition of the coordinates and of the positions of the solid atoms at the left side of the slit.

6.2 Liquid film on the slit pore

The distributions of the density and pressure components in the vicinity of the left entrance of the slit are obtained on the basis of Eq. (2.27), for each subsystem with the area A_k(= dx_k ×dz_k=0.073×0.073) in the x-z plane. The results are obtained as the time averaged values of 2,000,000 steps after the relaxation calculation. Figure 6.2 presents reduced density ρ^* (Fig. 6.2(a)), and pressure components: $\left\langle \hat{P}_{xx}^* \right\rangle$ (Fig. 6.2(b)), $\left\langle \hat{P}_{yy}^* \right\rangle$ (Fig. 6.2(c)), and $\left\langle \hat{P}_{zz}^* \right\rangle$ (Fig. 6.2(d)), of the liquid film on the slit pore for ε_{fs}=0.20. In Figs. 6.2(a-d), the solid atoms of the left side of the slit are shown as the white circles. Figure 6.2(a) shows the vapor-liquid interface in the vicinity of the slit is situated above the slit for the relatively weak fluid-solid interaction intensity(ε_{fs}=0.20). Figures 6.2(b,c) confirm that the variation of the pressure components tangential to the liquid-solid interface is significant and the distribution of the pressure components: $\left\langle \hat{P}_{xx}^* \right\rangle$ and $\left\langle \hat{P}_{yy}^* \right\rangle$ are almost the same. $\left\langle \hat{P}_{zz}^* \right\rangle$ in Fig. 6.2(d) represents no significant distribution, because it is not the component tangential to the liquid-solid interface outside the slit. The same tendency is observed in that the variations of the pressure components tangential to the liquid-solid interface are significant, for the cases of stronger interaction intensities (ε_{fs}=0.30(Figs. 6.3(a-d)), ε_{fs}=0.40 (Figs. 6.4(a-d)), and ε_{fs}=0.42 (Figs. 6.5(a-d))).

In addition, the results of the density distribution show that the liquid film is situated on the slit and partially filling the inside of the slit particularly in the cases of ε_{fs}=0.40 and 0.42 (Figs. 6.4(a) and 6.5(a)). On increasing the fluid-solid interaction intensity ε_{fs}, the local density outside the slit in the vicinity of the corner becomes higher, and with this, the local density inside the slit also becomes higher (Figs. 6.2(a), 6.3(a), 6.4(a), and 6.5(a)). The results also confirm that the shape of the vapor-liquid interface is almost flat excluding the layers in the vicinity of the solid surface (Figs. 6.2(a), 6.3(a), 6.4(a), and 6.5(a)).

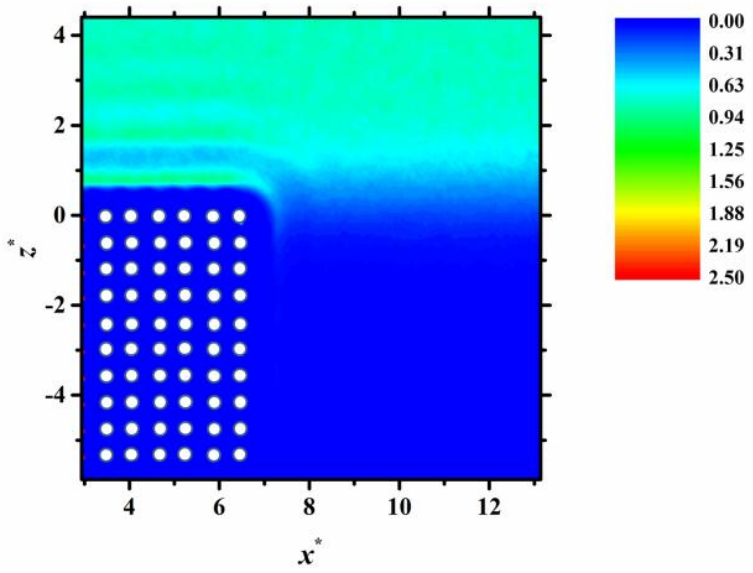

(a) ρ^*.

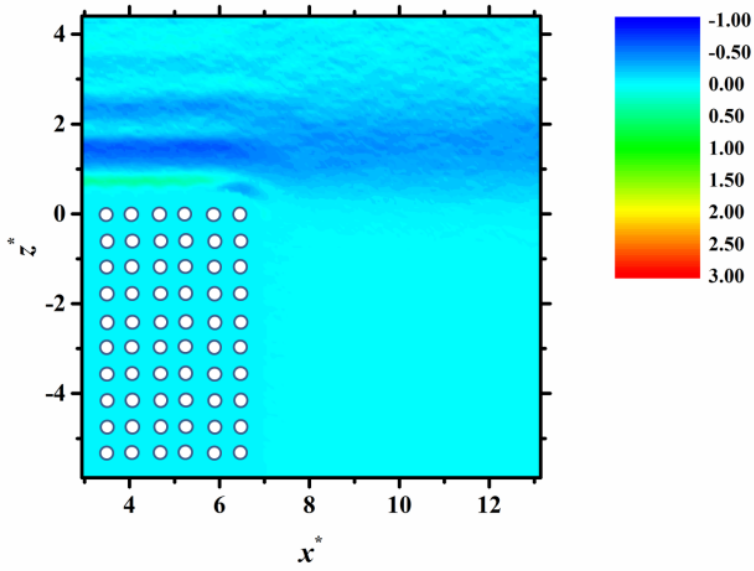

(b) $\left\langle \hat{P}_{xx}^{*} \right\rangle$.

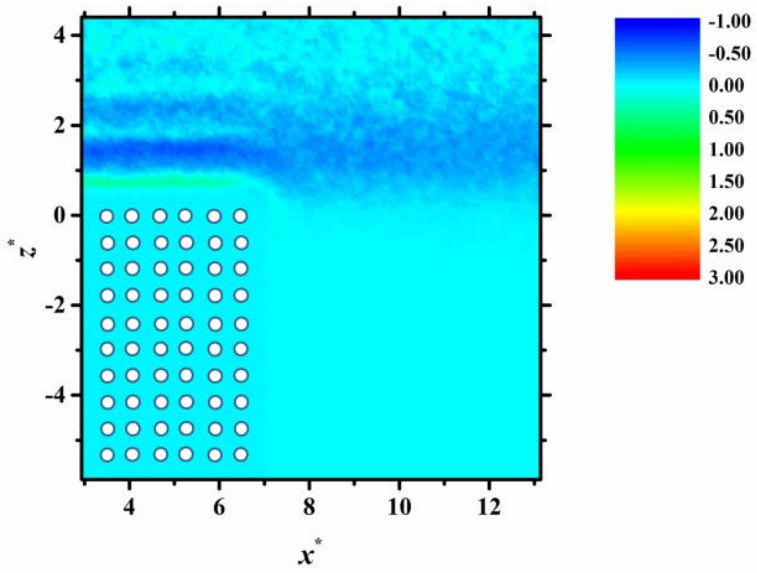

(c) $\left\langle \hat{P}_{yy}^{*} \right\rangle$.

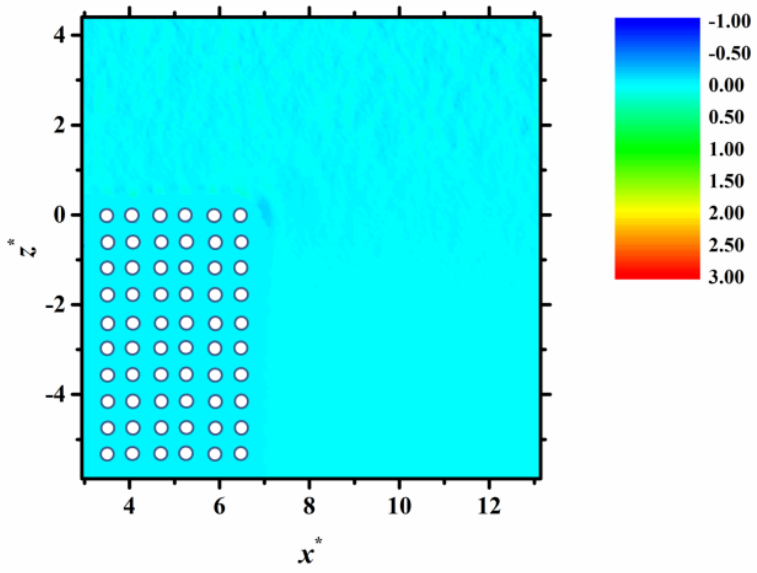

(d) $\left\langle \hat{P}_{zz}^{*} \right\rangle$.

Fig. 6.2 Reduced density and pressure components of the fluid in the *x*-*z* plane for $\varepsilon_{fs} = 0.20$: (a) ρ^{*}, (b) $\left\langle \hat{P}_{xx}^{*} \right\rangle$, (c) $\left\langle \hat{P}_{yy}^{*} \right\rangle$, and (d) $\left\langle \hat{P}_{zz}^{*} \right\rangle$.

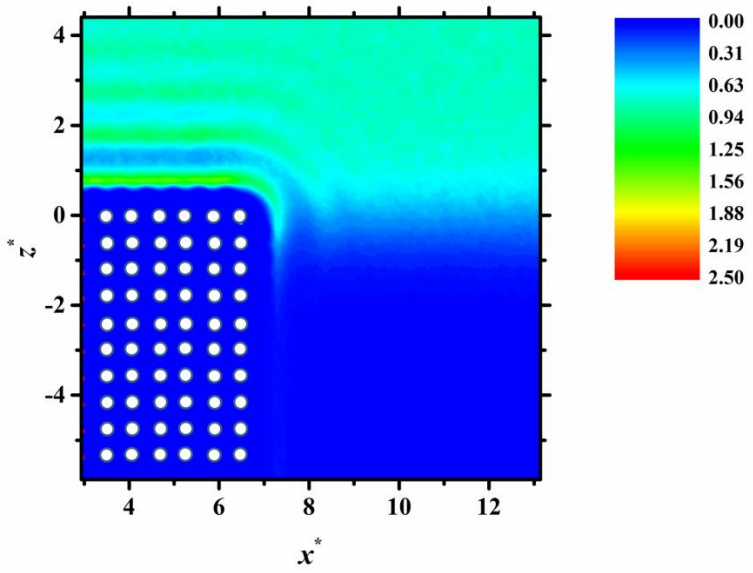

(a) ρ^*.

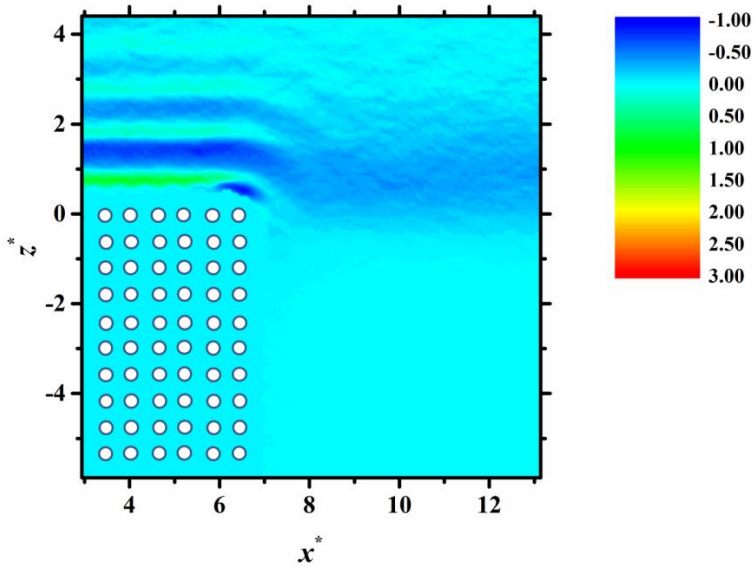

(b) $\left\langle \hat{P}_{xx}^{*} \right\rangle$.

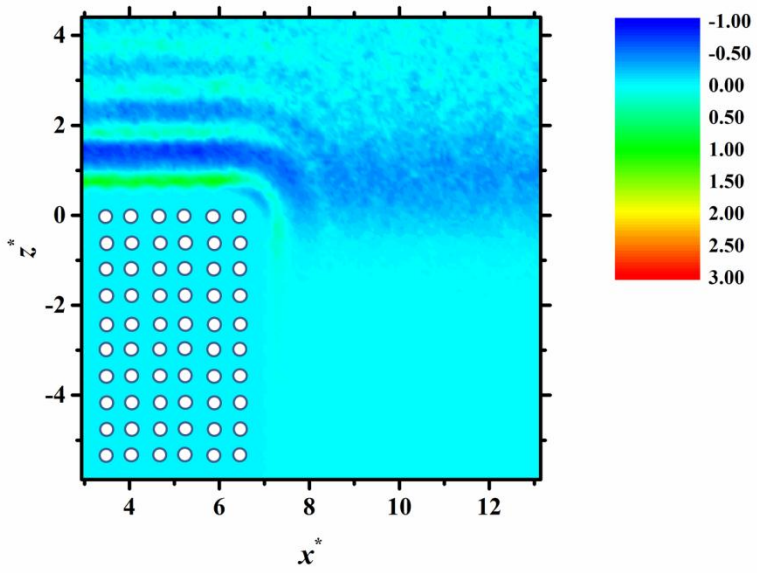

(c) $\left\langle \hat{P}_{yy}^{*} \right\rangle$.

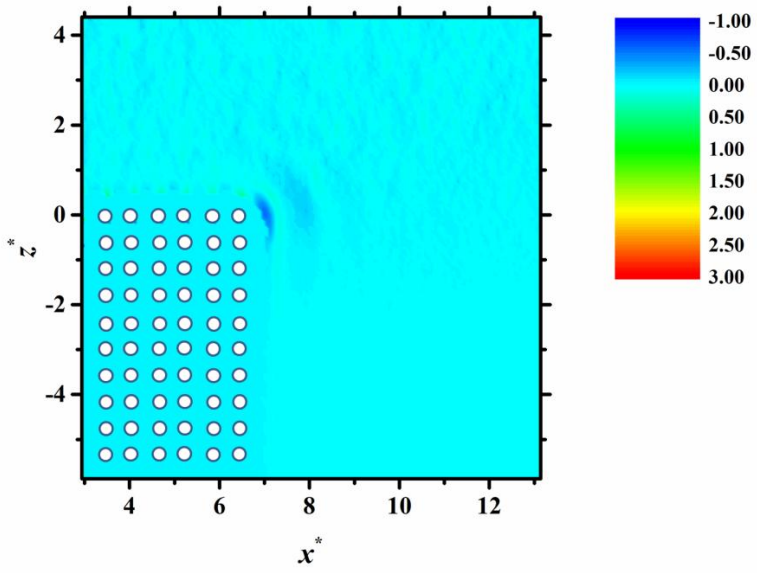

(d) $\left\langle \hat{P}_{zz}^{*} \right\rangle$.

Fig. 6.3 Reduced density and pressure components of the fluid in the *x*-*z* plane for $\varepsilon_{fs} = 0.30$: (a) ρ^{*}, (b) $\left\langle \hat{P}_{xx}^{*} \right\rangle$, (c) $\left\langle \hat{P}_{yy}^{*} \right\rangle$, and (d) $\left\langle \hat{P}_{zz}^{*} \right\rangle$.

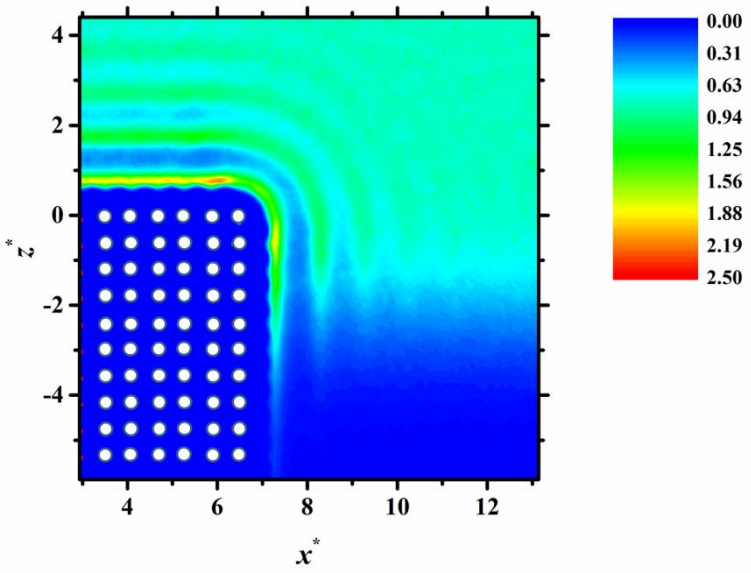

(a) ρ^*.

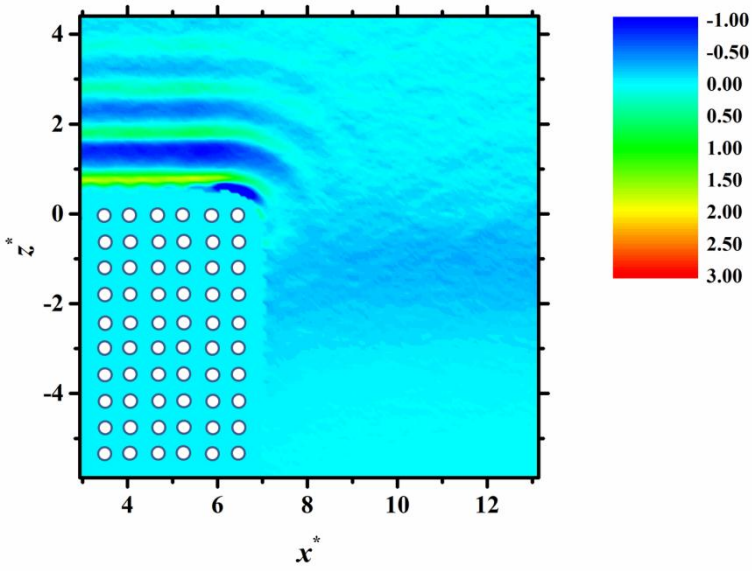

(b) $\left\langle \hat{P}_{xx}^{*} \right\rangle$.

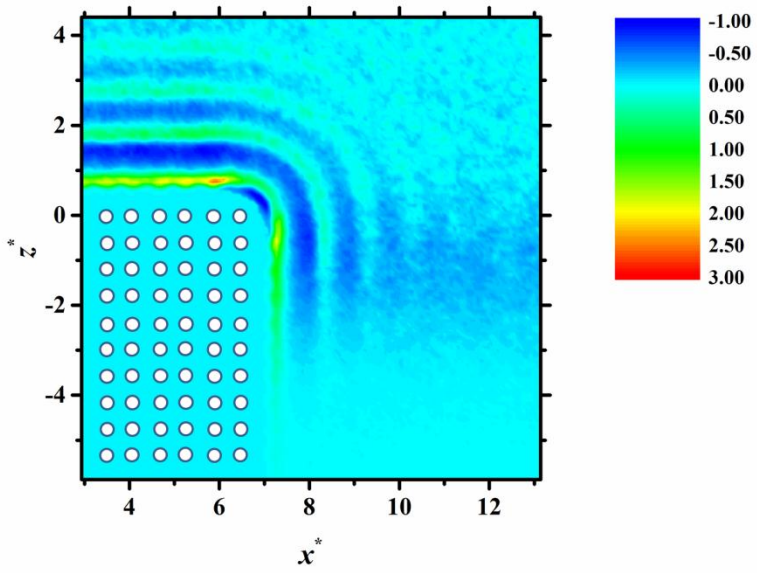

(c) $\left\langle \hat{P}_{yy}^{*} \right\rangle$.

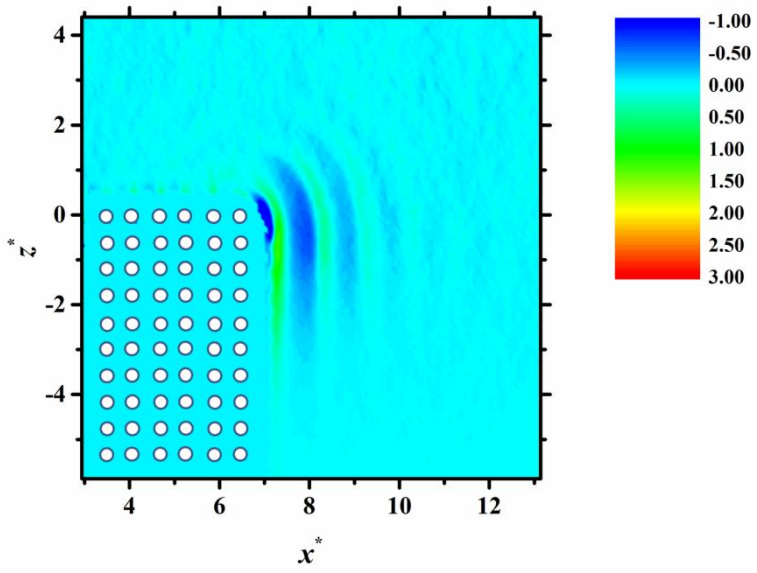

(d) $\left\langle \hat{P}_{zz}^{*} \right\rangle$.

Fig. 6.4 Reduced density and pressure components of the fluid in the *x*-*z* plane for $\varepsilon_{fs} = 0.40$: (a) ρ^{*}, (b) $\left\langle \hat{P}_{xx}^{*} \right\rangle$, (c) $\left\langle \hat{P}_{yy}^{*} \right\rangle$, and (d) $\left\langle \hat{P}_{zz}^{*} \right\rangle$.

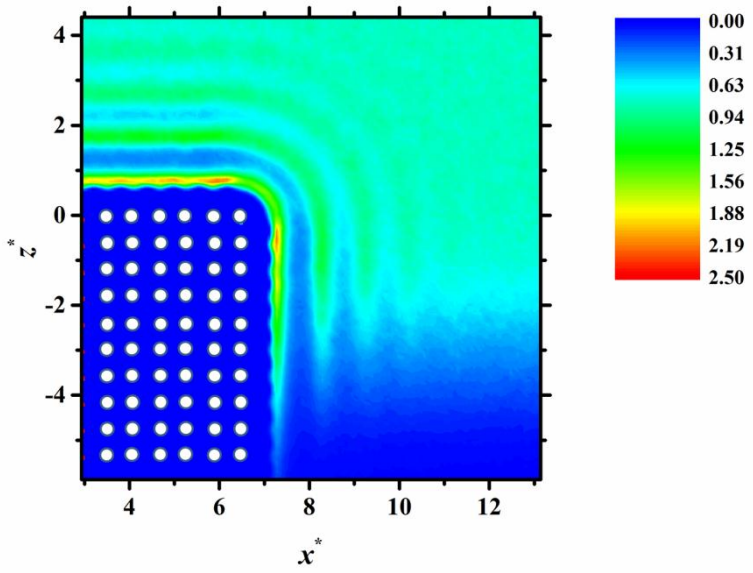

(a) ρ^*.

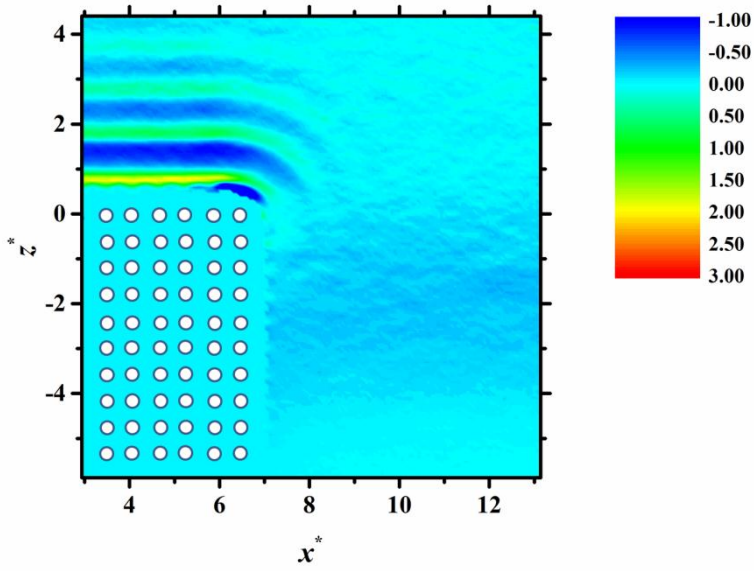

(b) $\left\langle \hat{P}_{xx}^{*} \right\rangle$.

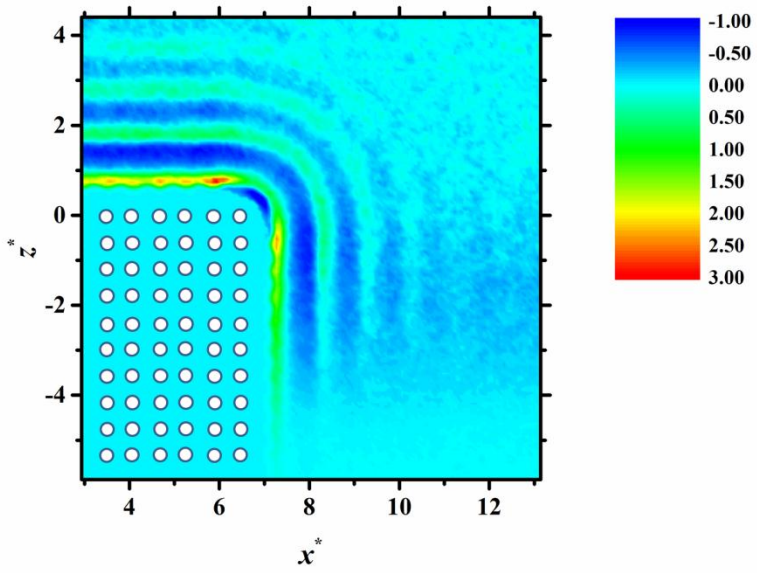

(c) $\left\langle \hat{P}_{yy}^{*} \right\rangle$.

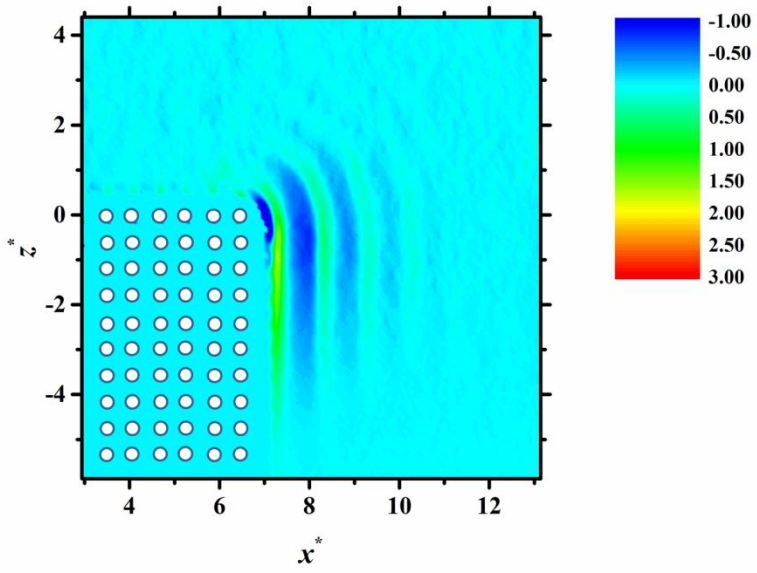

(d) $\left\langle \hat{P}_{zz}^{*} \right\rangle$.

Fig. 6.5 Reduced density and pressure components of the fluid in the *x*-*z* plane for $\varepsilon_{fs} = 0.42$: (a) ρ^{*}, (b) $\left\langle \hat{P}_{xx}^{*} \right\rangle$, (c) $\left\langle \hat{P}_{yy}^{*} \right\rangle$, and (d) $\left\langle \hat{P}_{zz}^{*} \right\rangle$.

6.3 Liquid film in the slit pore

Figures 6.6 and 6.7 present the reduced density distribution (Figs. 6.6(a) and 6.7(a)), and pressure components: $\left\langle \hat{P}_{xx}^{*} \right\rangle$ (Fig. 6.6(b) and 6.7(b)), $\left\langle \hat{P}_{yy}^{*} \right\rangle$ (Fig. 6.6(c) and 6.7(c)), and $\left\langle \hat{P}_{zz}^{*} \right\rangle$ (Fig. 6.6(d) and 6.7(d)), of the liquid film in the slit pore for ε_{fs}=043 and ε_{fs}=0.50, respectively. As is evident from Figs. 6.6(a) and 6.7(a), the inside of the slit pore is filled with liquid molecules under the influence of the strong fluid-solid interaction intensity (ε_{fs}=0.43 and 0.50). The same tendency is observed in Figs. 6.6(b-d) and 6.7(b-d) in that the variations of the pressure components tangential to the liquid-solid interface are significant, and it should also be noted that $\left\langle \hat{P}_{yy}^{*} \right\rangle$ has two observable liquid-solid interfaces because the *y* direction is normal to the *x*-*z* plane. The pressure component, $\left\langle \hat{P}_{yy}^{*} \right\rangle$ in Figs. 6.6(c) and 6.7(c) has a characteristic profile at the liquid-solid interface inside and outside the slit, corresponding to the density distribution in Figs. 6.6(a) and 6.7(a), and it shows the two highest values in the vicinity of the 2nd solid layer from the corner at both the inside and outside the slit (see also Fig. 6.1(c)). This suggests that the local pressure components tangential to the solid surface, $\left\langle \hat{P}_{xx}^{*} \right\rangle$ and $\left\langle \hat{P}_{yy}^{*} \right\rangle$, in the vicinity of the 1st layer of the fluid from the solid surface, are different in a two dimensional plane for a relatively strong fluid-solid interaction intensities(ε_{fs}=0.43 and 0.50), and the difference becomes pronounced in the vicinity of the corner of the slit.

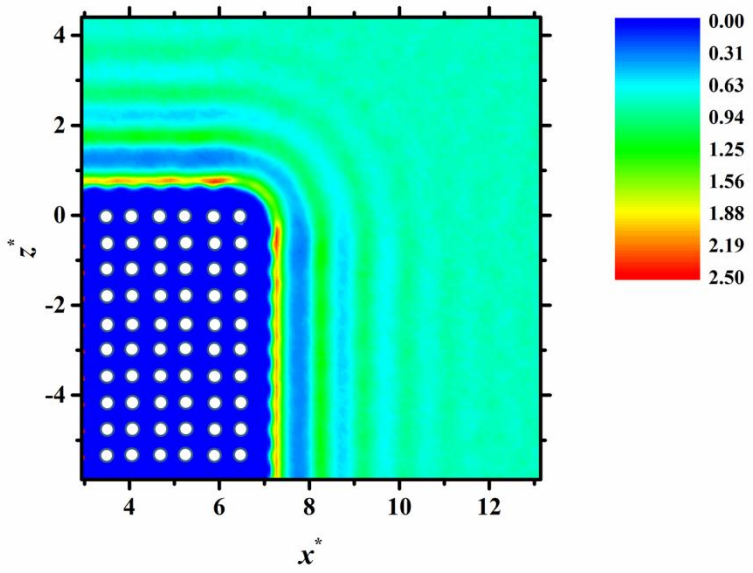

(a) $\rho.^{*}$

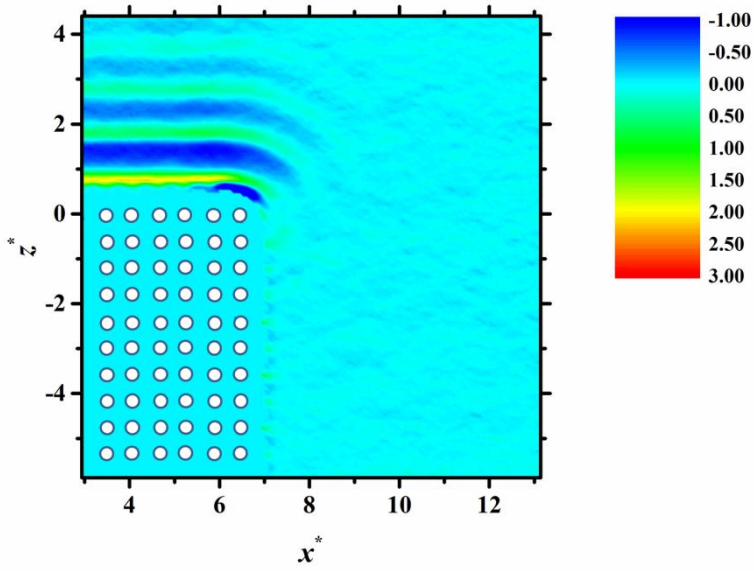

(b) $\left\langle \hat{P}_{xx}^{*} \right\rangle$.

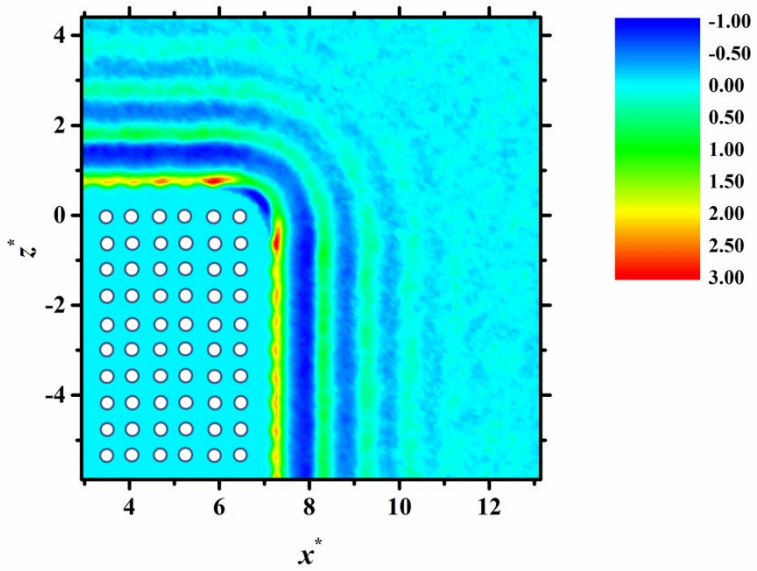

(c) $\left\langle \hat{P}_{yy}^{*} \right\rangle$.

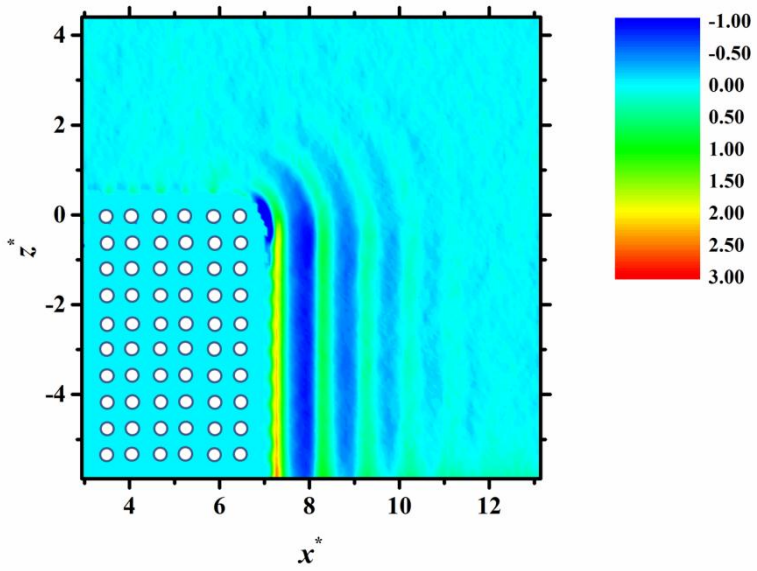

(d) $\left\langle \hat{P}_{zz}^{*} \right\rangle$.

Fig. 6.6 Reduced density and pressure components of the fluid in the *x*-*z* plane for $\varepsilon_{fs} = 0.43$: (a) ρ^{*}, (b) $\left\langle \hat{P}_{xx}^{*} \right\rangle$, (c) $\left\langle \hat{P}_{yy}^{*} \right\rangle$, and (d) $\left\langle \hat{P}_{zz}^{*} \right\rangle$.

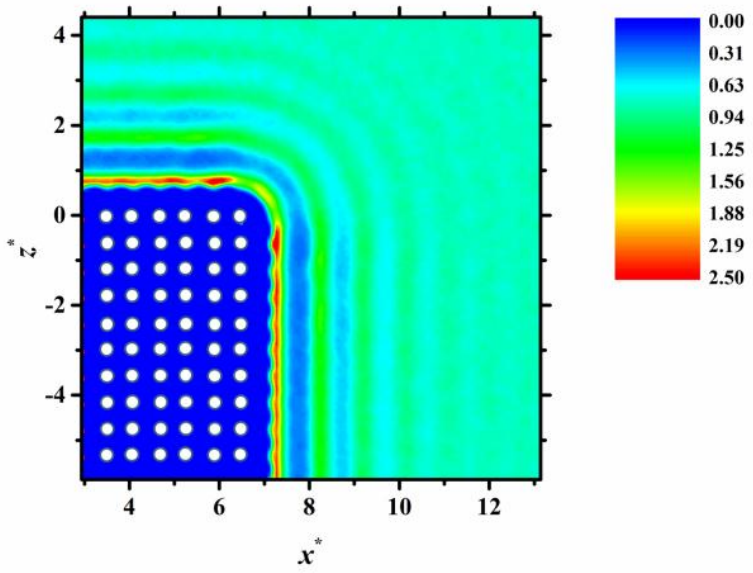

(a) $\rho.^{*}$

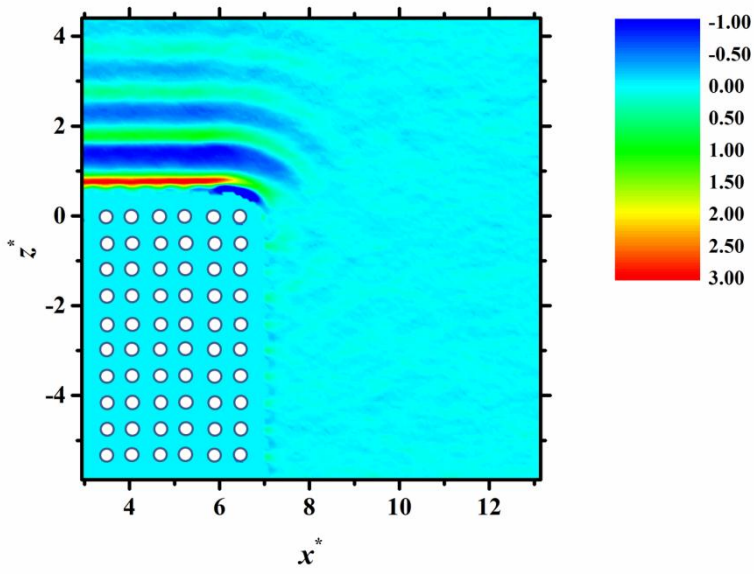

(b) $\left\langle \hat{P}_{xx}^{*} \right\rangle$.

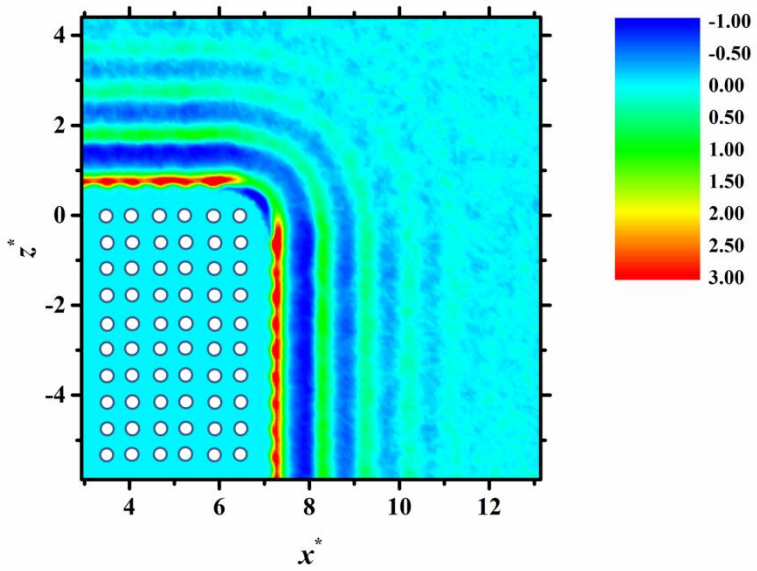

(c) $\left\langle \hat{P}_{yy}^{*} \right\rangle$.

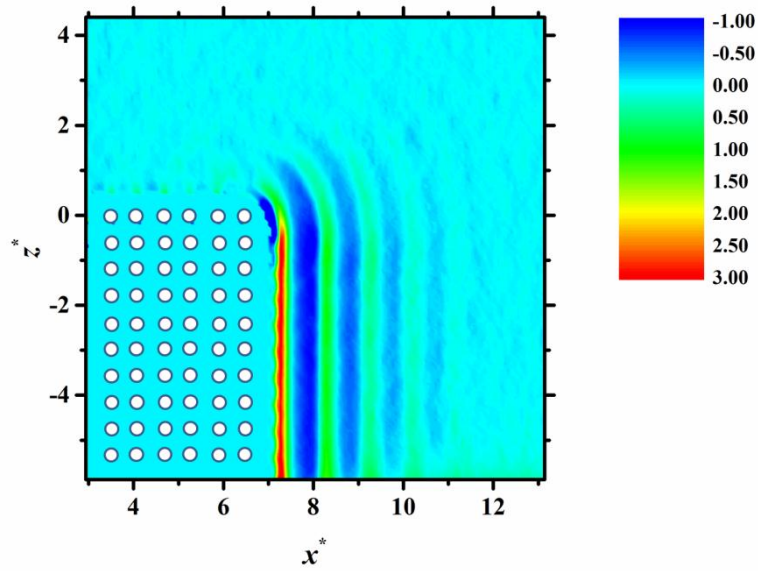

(d) $\left\langle \hat{P}_{zz}^{*} \right\rangle$.

Fig. 6.7 Reduced density and pressure components of the fluid in the *x*-*z* plane for $\varepsilon_{fs} = 0.50$: (a) ρ^{*}, (b) $\left\langle \hat{P}_{xx}^{*} \right\rangle$, (c) $\left\langle \hat{P}_{yy}^{*} \right\rangle$, and (d) $\left\langle \hat{P}_{zz}^{*} \right\rangle$.

7. Transition mechanism between the states of the liquid film based on the local thermodynamic states

This chapter examines the molecular transition mechanism between the two states of the liquid film: (a) liquid film on the slit and (b) liquid film in the slit, based on the thermodynamic states of the liquid film in the vicinity of the slit. First, in Sec. 7.1, effects of the fluid-solid interaction intensity on the states of the liquid film are investigated for the calculation model introduced in Sec. 6.1. Next, the relationship between interfacial tensions based on a macroscopic concept and the states of the liquid film are examined under a varying fluid-solid interaction intensity. In Sec. 7.2, as the local thermodynamic quantities, the local pressure components, and interfacial tensions of the liquid film in the vicinity of the slit, are obtained as the time-averaged values based on the instantaneous expressions (Eqs. (2.27) and (2.30)), and which are investigated in detail, to reveal a beginning of the transition process between the two states of the condensed matter from a molecular point of view.

7.1 Relationship between the interfacial tensions and the states of the liquid film

In this section, effects of the fluid-solid interaction intensity on the states of the liquid film in the vicinity of the slit are examined based on the density, pressure, and interfacial tensions of the fluid. The calculation model is introduced in Sec. 6.1. Figure 7.1 shows the time evolution of the number of fluid molecules in the slit after the relaxation calculation for ε_{fs}=0.20-0.50. The number of the fluid molecules in the slit is defined as the number of the fluid molecules below z^*=0.0 (see Fig. 6.1(b)). The large numbers in the cases of ε_{fs}=0.43 and 0.50 indicate that the inside of the slit is filled with fluid molecules, on the other hand, the inside of the slit is not fully filled with the fluid

molecules in the cases of ε_{fs}=0.20-0.42, which are the states of the liquid film on the slit. The number of the fluid molecules fluctuates with the passage of time on this time scale, and the fluctuation becomes pronounced with an increase in ε_{fs}.

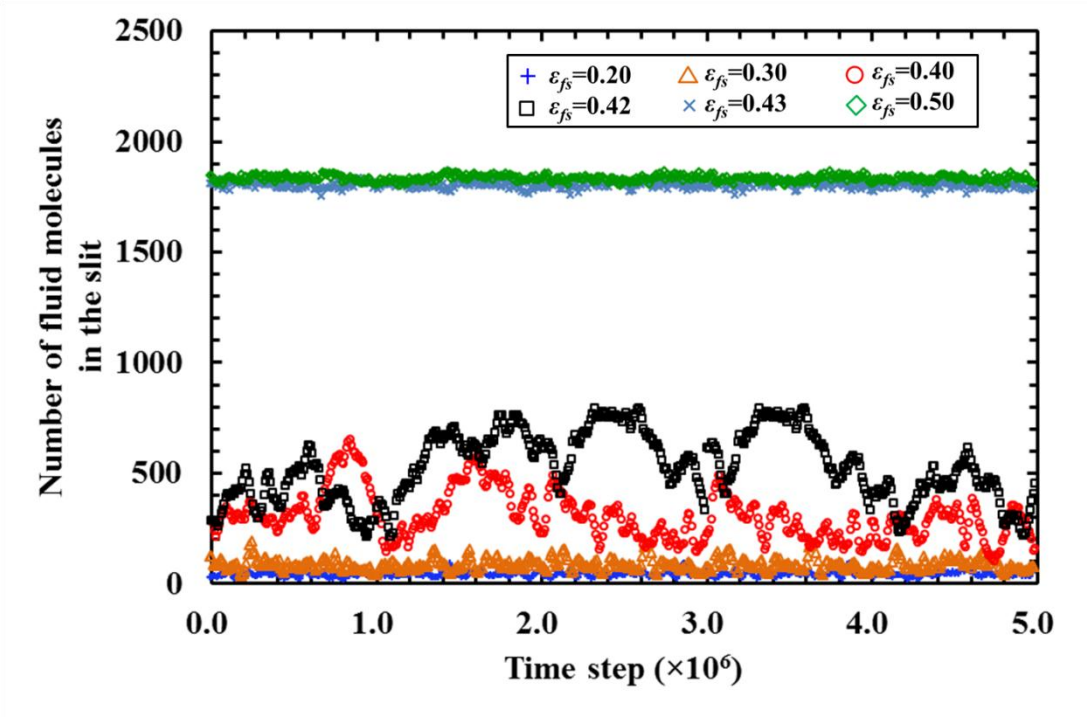

Fig. 7.1 Time evolution of the number of fluid molecules in the slit for ε_{fs}=0.20-0.50.

As revealed in Sec. 6.2, on increasing the fluid-solid interaction intensity ε_{fs}, the local density outside the slit in the vicinity of the corner becomes higher, and with this, the local density inside the slit also becomes higher. In order to examine the increase of the local density of the fluid in the vicinity of the corner, the reduced density of the fluid molecules, ρ^* in the x direction at z^*=0.77(e.g. see Fig. 6.2(a)), where the 1st layer of the fluid from the solid surface exists outside the slit, is obtained for ε_{fs}=0.20-0.43, and the results are presented in Fig. 7.2. The density profile of the fluid outside the slit in Fig. 7.2 clearly indicates that the fluid density in the vicinity of the 2nd layer of solid atoms from the corner of the slit becomes higher with an increase in ε_{fs} (see also Fig. 6.1(c)).

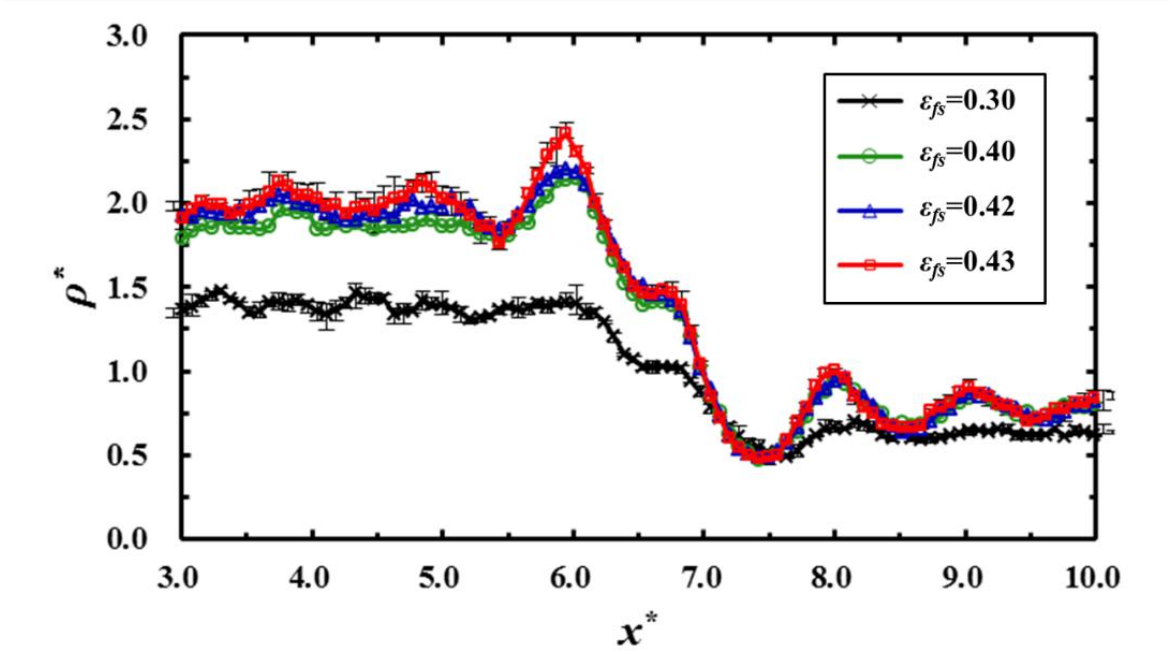

Fig. 7.2 Reduced density profile of the fluid molecules, ρ^* in the x direction at z^*=0.77, for ε_{fs}=0.30-0.43. The values are obtained as the averaged values of 5,000,000 time steps, and the error bars show the five averaged results of 1,000,000 time steps for ε_{fs}=0.30 and 0.43.

The reduced pressure component $\left\langle \hat{P}_{zz}^{*} \right\rangle$ of the vapor region above the liquid film, is calculated to investigate effects of fluid-solid interaction intensity ε_{fs} on the pressure in the system, and the results are given in Fig. 7.3. The pressure is calculated in the vapor region above the liquid film in the system, defined as the range: 25.0 < z^* < 35.0, for ε_{fs}=0.20-0.50. The result indicates that $\left\langle \hat{P}_{zz}^{*} \right\rangle$ in the vapor region is almost constant, although the vapor-liquid interface in the vicinity of the slit fluctuates with increasing ε_{fs}, as shown in Fig. 7.1.

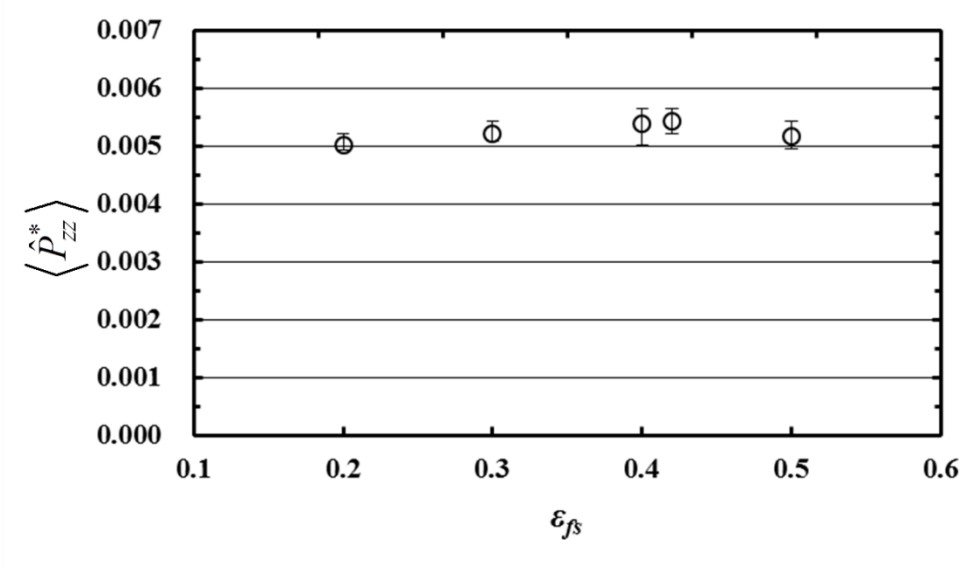

Fig. 7.3 Reduced pressure component $\left\langle \hat{P}^*_{zz} \right\rangle$ in the vapor region above the liquid film in the system for ε_{fs}=0.20, 0.30, 0.40, 0.42, and 0.50. The values of the pressure component are averaged for 5,000,000 time steps, and the error bars show the five averaged results of 1,000,000 time steps. The pressure is calculated in the vapor region above the liquid film in the system, defined as the range: $25.0 < z^* < 35.0$.

In order to clarify the relationship between the interfacial tensions and the state of the liquid film on or in the slit, first, reduced local interfacial tensions of the fluid at the liquid-solid interface, $\left\langle \hat{\gamma}^*_{z\text{-}x} \right\rangle$ and $\left\langle \hat{\gamma}^*_{z\text{-}y} \right\rangle$, are calculated based on Eq. (2.30) for ε_{fs}=0.20 and 0.40, and are shown in Figs. 7.4(a,b). The local interfacial tensions are obtained at each local slab, along the z direction, with the height of 0.073: dz^*=0.073, and the values are averaged at the outside of the slit, in the range: $0.0<x^*<4.7$, where effects of the corner of the silt can be ignored. It can be seen that $\left\langle \hat{\gamma}^*_{z\text{-}x} \right\rangle$ is identical to $\left\langle \hat{\gamma}^*_{z\text{-}y} \right\rangle$ for each ε_{fs}, which indicates the space-averaged local liquid-solid interfacial tension is isotropic in the x and y directions at each z position.

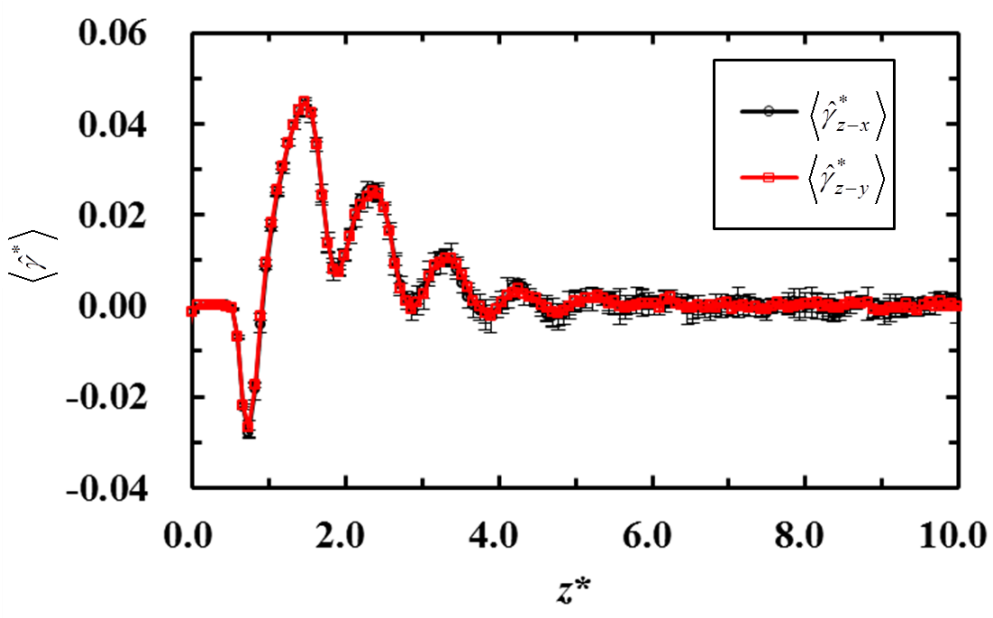

(a) ε_{fs}=0.20.

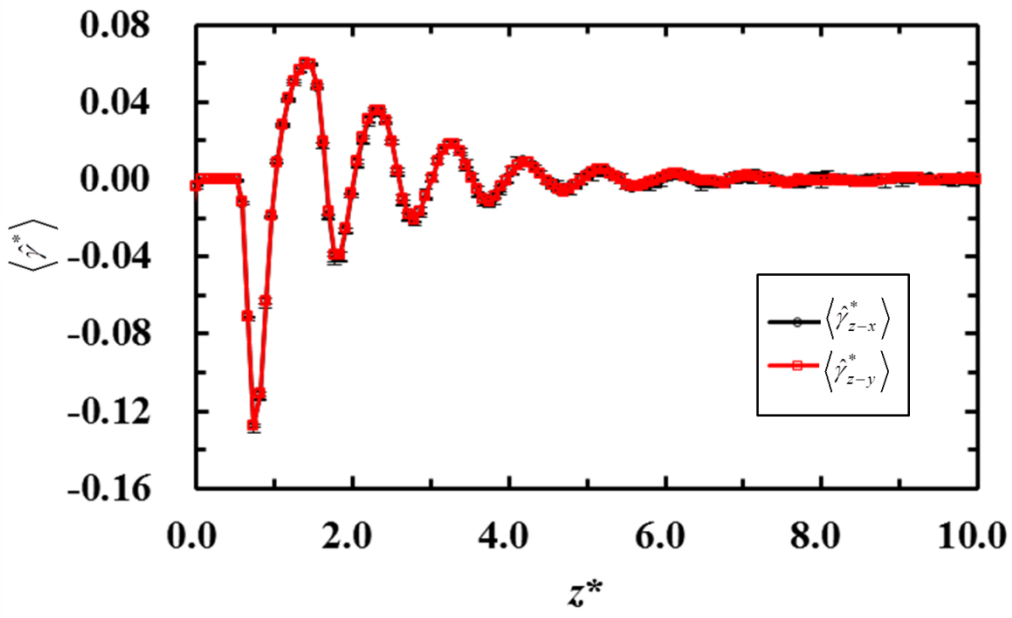

(b) ε_{fs}=0.40.

Fig. 7.4 Reduced interfacial tension, $\langle \hat{\gamma}^*_{z\text{-}x} \rangle$ and $\langle \hat{\gamma}^*_{z\text{-}y} \rangle$ of the fluid at the liquid-solid interface for (a) ε_{fs}=0.20 and (b) ε_{fs}=0.40. The values are obtained in the range: $0.0<x^*<4.7$, and are averaged values for 5,000,000 time steps. The error bars are shown by the five averaged results of 1,000,000 time steps.

From a macroscopic point of view, the slit becomes impregnated with liquid, when the condition below is satisfied in the slit (de Gennes *et al.* 2004),

$$I = \gamma_{vs} - \gamma_{ls} > 0, \tag{12.1}$$

where I represents the impregnation parameter, and is defined as the difference of the vapor-solid and liquid-solid interfacial tensions, $\gamma_{vs} - \gamma_{ls}$. Eq. (12.1) is valid for γ_{vs} and γ_{ls}, defined as the values inside the slit, but under the macroscopic condition, the values inside and outside the slit are almost the same for a flat vapor-liquid interfacial system. It suggests that the two states of the liquid film, (a) liquid film on the slit, and (b) liquid film in the slit, are predictable from the values of γ_{vs} and γ_{ls} outside the slit. Based on this macroscopic concept, the time-averaged value of the instantaneous expression of the impregnation parameter,

$$\left\langle \hat{I} \right\rangle = \left\langle \hat{\gamma}_{vs} \right\rangle - \left\langle \hat{\gamma}_{ls} \right\rangle, \tag{12.2}$$

which is defined as the values outside the slit, is investigated in the present calculation system, and the reduced results for ε_{fs}=0.20-0.50 are shown in Fig. 7.5(a). Here, the vapor-solid and liquid-solid interfacial tensions are obtained as the integrated values of the local quantities in the area defined in Fig. 7.5(b), and are described based on Eqs. (2.20) and (2.30):

$$\begin{aligned} \hat{\gamma}_{vs} &= \int_{Vapor-Solid} \left(\hat{P}_{zz,V_k} - \hat{P}_{xx,V_k} \right) \mathrm{d}z_k, \\ \hat{\gamma}_{ls} &= \int_{Liquid-Solid} \left(\hat{P}_{zz,V_k} - \hat{P}_{xx,V_k} \right) \mathrm{d}z_k. \end{aligned} \tag{12.3}$$

Comparing Fig. 7.5(a) and Fig. 7.1 reveals that the two states of the liquid film are almost predictable by the time-averaged impregnation parameter obtained from the interfacial tensions outside the slit, but this parameter does not determine a definite threshold between the two states on a molecular time-space scale, i.e., it does not predict the fluctuations of the liquid film as shown in Fig. 7.1.

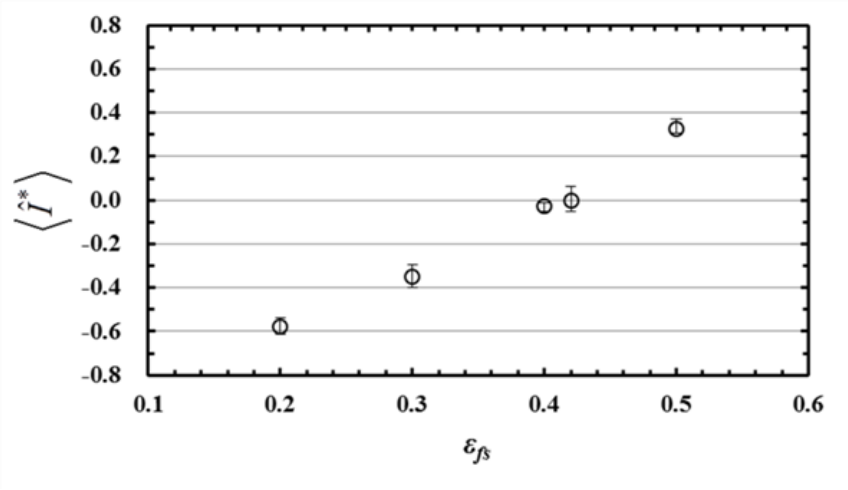

(a) Effects of ε_{fs} on the reduced impregnation parameter, $\langle I^* \rangle = \langle \hat{\gamma}_{vs}^* \rangle - \langle \hat{\gamma}_{ls}^* \rangle$.

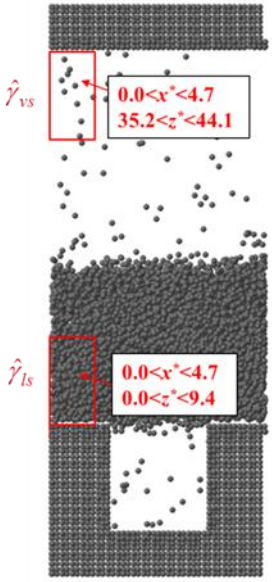

(b) Definition of the calculation area for $\hat{\gamma}_{vs}$ and $\hat{\gamma}_{ls}$.

Fig. 7.5 Effects of the fluid-solid interaction intensities(ε_{fs}=0.20-0.50) on the reduced impregnation parameter, $\langle I^* \rangle = \langle \hat{\gamma}_{vs}^* \rangle - \langle \hat{\gamma}_{ls}^* \rangle$, and the definition of the area in which $\hat{\gamma}_{vs}$ and $\hat{\gamma}_{ls}$ are calculated. The values of the impregnation parameters are averaged for 5,000,000 time steps, and the error bars are shown by the five averaged results of 1,000,000 steps.

7.2 Relationship between the local interfacial tensions and the states of the liquid film

In order to reveal in more detail the transition mechanism between the two states of the liquid film: (a) liquid film on the slit and (b) liquid film in the slit, the local interfacial tensions in the vicinity of the left entrance of the slit are obtained as the time-averaged values by using Eq. (2.30), and investigated in this Section. Figures 7.6-7.10 show the reduced local interfacial tensions, $\langle \hat{\gamma}^*_{x-y} \rangle$ and $\langle \hat{\gamma}^*_{x-z} \rangle$, in the *x*-*z* plane for ε_{fs}=0.20, 0.30, 0.40, 0.42, and 0.43. The fluid-solid interaction intensity ε_{fs}=0.42 is the case that the liquid film is the state before reaching the wetting process as shown in Fig. 7.1. The results in Figs. 7.9(a,b) show characteristic distributions of $\langle \hat{\gamma}^*_{x-y} \rangle$ and $\langle \hat{\gamma}^*_{x-z} \rangle$ around the corner inside the slit, and it can be seen that there exists a minimum value in the vicinity of the 2nd layer of the solid atoms inside the slit as shown in Fig. 7.9(a). To investigate the local interfacial tensions in detail, $\langle \hat{\gamma}^*_{x-y} \rangle$ and $\langle \hat{\gamma}^*_{x-z} \rangle$ in the vicinity of the 1st fluid layer from the solid surface inside the slit, along the *z* direction (at x^*=7.30), are shown in Fig. 7.11 for ε_{fs}=0.40, 0.42, and 0.43, where the inside of the slit is filled with liquid molecules in the case of ε_{fs}=0.43. Figure 7.11 reveals that there are points where the values of $\langle \hat{\gamma}^*_{x-y} \rangle$ and $\langle \hat{\gamma}^*_{x-z} \rangle$ are locally low (at around z^*=-0.5 for $\langle \hat{\gamma}^*_{x-y} \rangle$ and z^*=-1.0 for $\langle \hat{\gamma}^*_{x-z} \rangle$), for each value of ε_{fs}, and the values in the case of the liquid film on the slit (ε_{fs}=0.40) approach the values of the case that the inside of the slit is filled with the fluid molecules (ε_{fs}=0.43). The minimum value of $\langle \hat{\gamma}^*_{x-y} \rangle$ is lower than that of $\langle \hat{\gamma}^*_{x-z} \rangle$ for each ε_{fs}, which corresponds to the density profile of the fluid molecules in the *x*-*z* plane in Figs. 6.4(a) and 6.5(a). It suggests that the local interfacial tensions $\langle \hat{\gamma}^*_{x-y} \rangle$ at around z^*=-0.5: in the vicinity of the 2nd layer of solid atoms inside the slit, and $\langle \hat{\gamma}^*_{x-z} \rangle$ at around z^*=-1.0: in the vicinity of the 3rd layer of solid atoms, act as a trigger to cause the transition between the two states of the liquid film (see also Fig. 6.1(c)).

In order to examine the relationships of the local interfacial tensions between inside and outside the slit in the vicinity of the corner, $\left\langle \hat{\gamma}^*_{z-x} \right\rangle$ and $\left\langle \hat{\gamma}^*_{z-y} \right\rangle$ in the vicinity of the 1st fluid layer from the solid surface outside the slit (z^*=0.77), along the x direction, are shown in Fig. 7.12 for ε_{fs}=0.40, 0.42, and 0.43. Here the local interfacial tension $\left\langle \hat{\gamma}^*_{z-y} \right\rangle$ for each ε_{fs} represents locally low values, as is the case for $\left\langle \hat{\gamma}^*_{x-y} \right\rangle$ in Fig. 7.11, and it corresponds to the density profile as shown in Fig. 7.2. It's also found that the minimum values of $\left\langle \hat{\gamma}^*_{z-y} \right\rangle$ for ε_{fs}=0.40 and 0.42, obtained outside the slit, are lower than those of $\left\langle \hat{\gamma}^*_{x-y} \right\rangle$ obtained inside the slit, when the transition between the two states doesn't occur.

Focusing on the point where $\left\langle \hat{\gamma}^*_{x-y} \right\rangle$ is the lowest value along the z direction, i.e., in the vicinity of the 2nd layer of the solid atoms inside the slit, the local interfacial tensions, $\left\langle \hat{\gamma}^*_{x-y} \right\rangle$ and $\left\langle \hat{\gamma}^*_{x-z} \right\rangle$ at z^*=-0.55 are calculated along the x direction for ε_{fs}=0.42 and 0.43, and the results are presented in Fig. 7.13. It can be seen from Fig. 7.13 that $\left\langle \hat{\gamma}^*_{x-y} \right\rangle$ (ε_{fs}=0.42) almost satisfies the state of $\left\langle \hat{\gamma}^*_{x-y} \right\rangle$ (ε_{fs}=0.43) excluding the minimum value at x^*=7.30, although $\left\langle \hat{\gamma}^*_{x-z} \right\rangle$ (ε_{fs}=0.42) is different from that of ε_{fs}=0.43 at each y position. In particular, it can also be seen that $\left\langle \hat{\gamma}^*_{x-z} \right\rangle$ (ε_{fs}=0.42) is lower than 0.0 in the vicinity of the center of the slit (x^*=12.0). In order to investigate $\left\langle \hat{\gamma}^*_{x-y} \right\rangle$ and $\left\langle \hat{\gamma}^*_{x-z} \right\rangle$ for ε_{fs}=0.42 in detail, the local pressure components, $\left\langle \hat{P}^*_{xx} \right\rangle$, $\left\langle \hat{P}^*_{yy} \right\rangle$, and $\left\langle \hat{P}^*_{zz} \right\rangle$ are obtained by using Eq. (2.27), and the results are shown in Fig. 7.14. According to Fig. 7.14, $\left\langle \hat{P}^*_{xx} \right\rangle$ and $\left\langle \hat{P}^*_{yy} \right\rangle$ are lower than 0.0 in the vicinity of the center of the slit, due to the effects of the vapor-liquid interface, and that is why $\left\langle \hat{\gamma}^*_{x-z} \right\rangle$ (ε_{fs}=0.42) is lower than 0.0 in the vicinity

of the center of the slit as seen in Fig. 7.13. It should be noted that $\left\langle \hat{P}_{xx}^{*} \right\rangle$ is not lower than 0.0 in the vicinity of the 1st layer of fluid molecules from the solid surface, and which means the effect of the low value of $\left\langle \hat{P}_{xx}^{*} \right\rangle$ is weak in the vicinity of the 1st fluid layer from the solid surface.

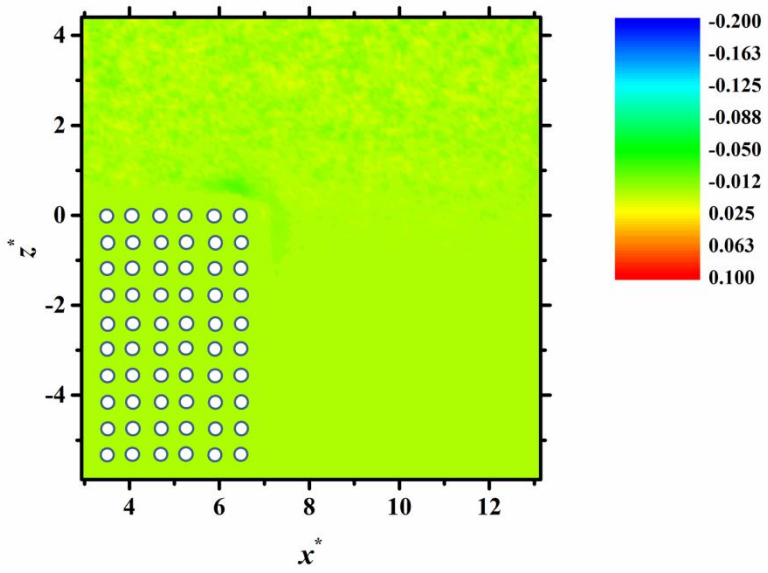

(a) $\left\langle \hat{\gamma}^*_{x-y} \right\rangle$.

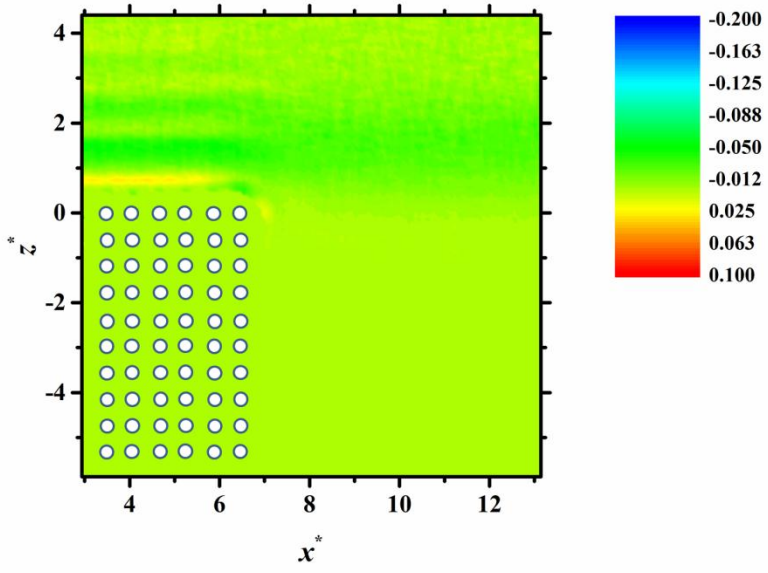

(b) $\left\langle \hat{\gamma}^*_{x-z} \right\rangle$.

Fig. 7.6 Reduced local interfacial tensions in the *x*-*z* plane in the vicinity of the left corner of the entrance of the slit for ε_{fs}=0.20: (a) $\left\langle \hat{\gamma}^*_{x-y} \right\rangle$ and (b) $\left\langle \hat{\gamma}^*_{x-z} \right\rangle$. The values are obtained as the averaged values of 2,000,000 time steps.

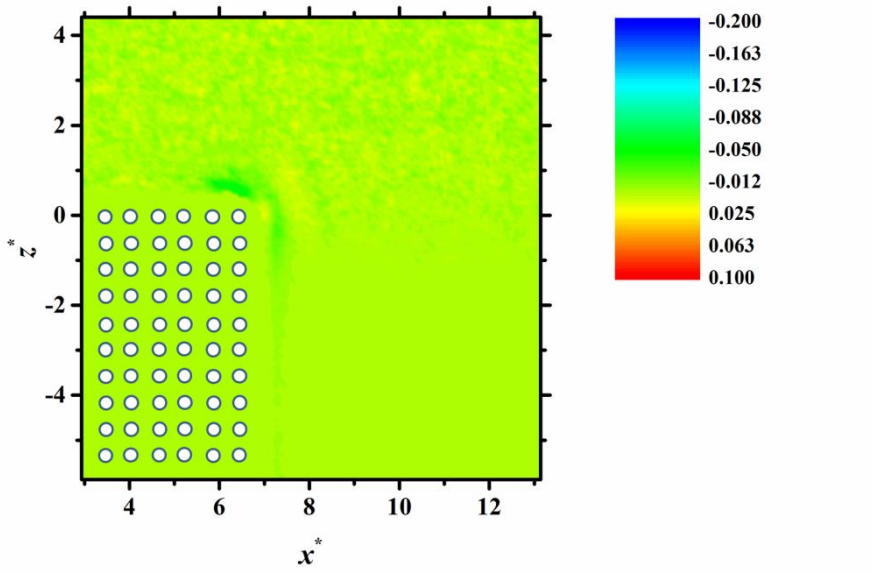

(a) $\left\langle \hat{\gamma}^*_{x-y} \right\rangle$.

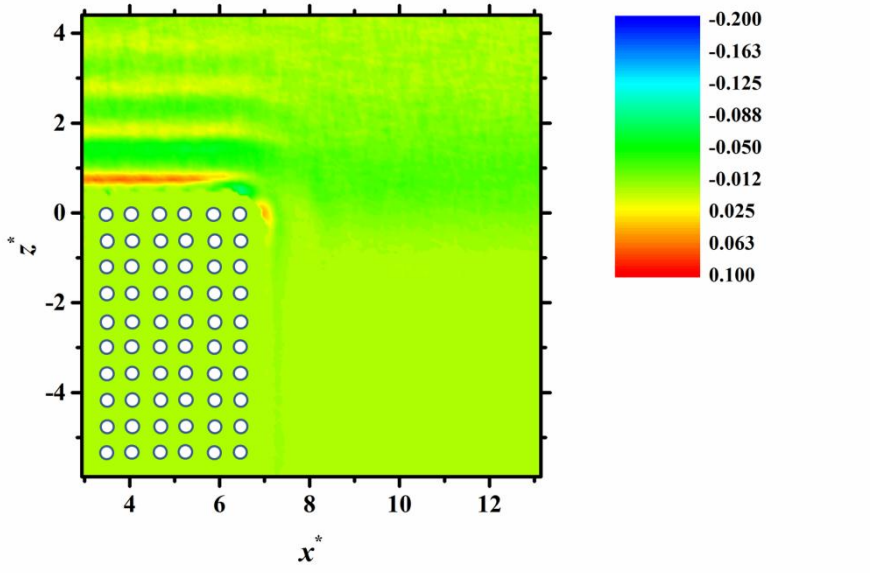

(b) $\left\langle \hat{\gamma}^*_{x-z} \right\rangle$.

Fig. 7.7 Reduced local interfacial tensions in the *x*-*z* plane in the vicinity of the left corner of the entrance of the slit for ε_{fs}=0.30: (a) $\left\langle \hat{\gamma}^*_{x-y} \right\rangle$ and (b) $\left\langle \hat{\gamma}^*_{x-z} \right\rangle$. The values are obtained as the averaged values of 2,000,000 time steps.

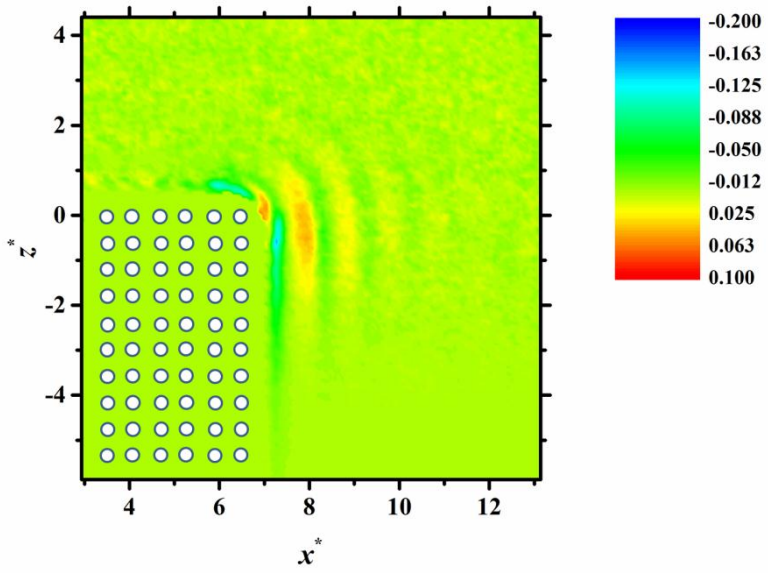

(a) $\langle \hat{\gamma}^*_{x-y} \rangle$.

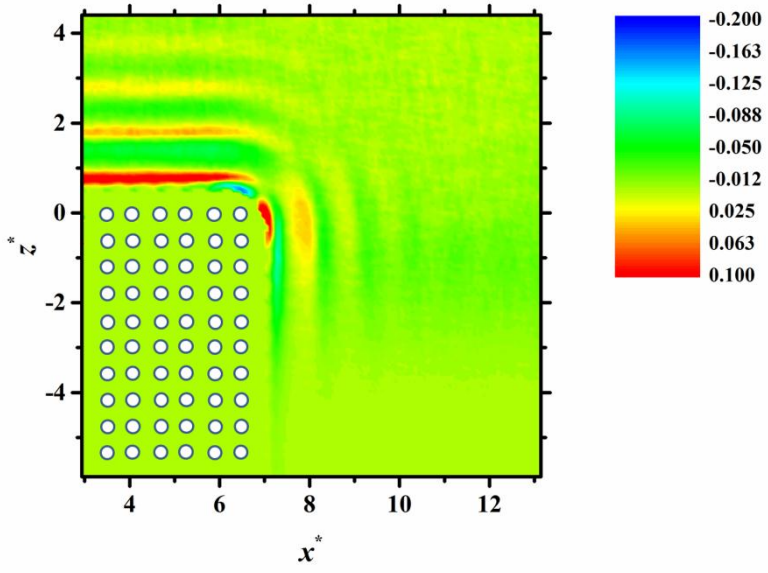

(b) $\langle \hat{\gamma}^*_{x-z} \rangle$.

Fig. 7.8 Reduced local interfacial tensions in the *x*-*z* plane in the vicinity of the left corner of the entrance of the slit for ε_{fs}=0.40: (a) $\langle \hat{\gamma}^*_{x-y} \rangle$ and (b) $\langle \hat{\gamma}^*_{x-z} \rangle$. The values are obtained as the averaged values of 2,000,000 time steps.

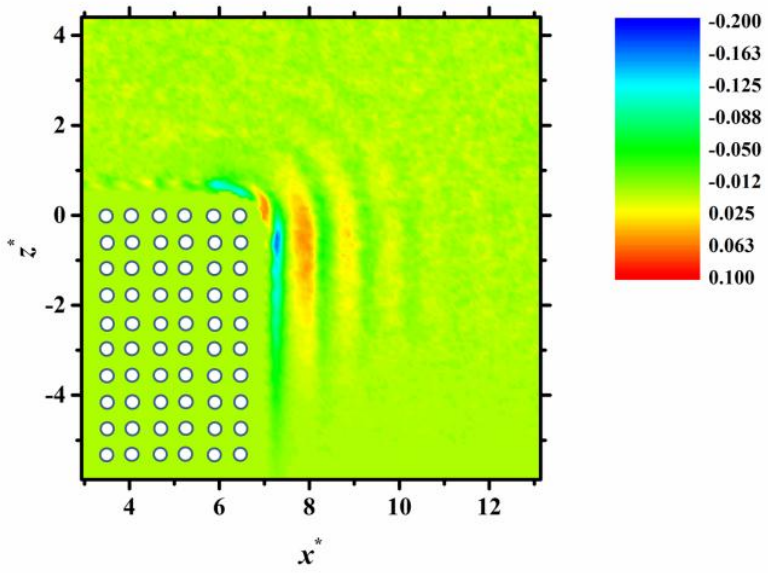

(a) $\langle \hat{\gamma}^*_{x-y} \rangle$.

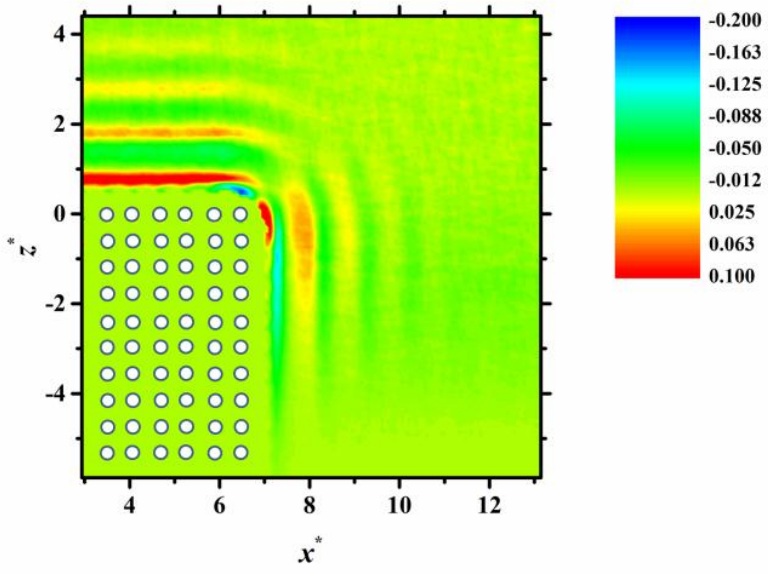

(b) $\langle \hat{\gamma}^*_{x-z} \rangle$.

Fig. 7.9 Reduced local interfacial tensions in the *x*-*z* plane in the vicinity of the left corner of the entrance of the slit for ε_{fs}=0.42: (a) $\langle \hat{\gamma}^*_{x-y} \rangle$ and (b) $\langle \hat{\gamma}^*_{x-z} \rangle$. The values are obtained as the averaged values of 2,000,000 time steps.

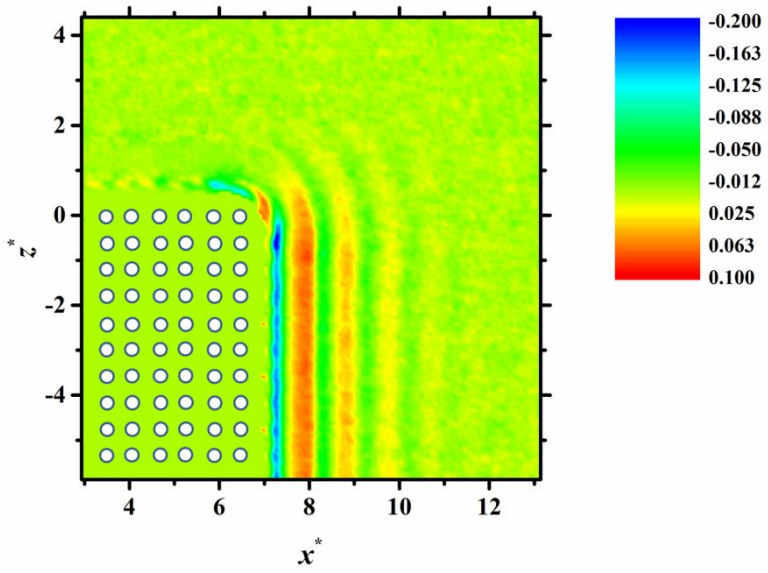

(a) $\left\langle \hat{\gamma}^*_{x-y} \right\rangle$.

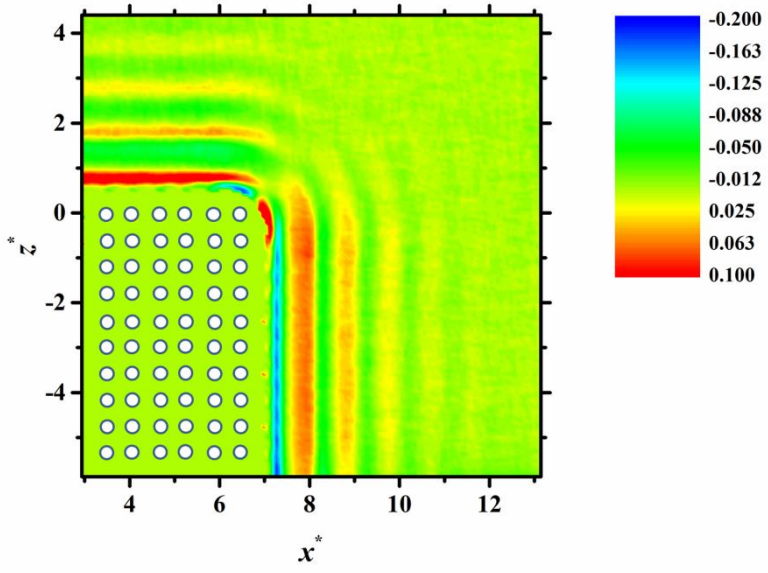

(b) $\left\langle \hat{\gamma}^*_{x-z} \right\rangle$.

Fig. 7.10 Reduced local interfacial tensions in the *x*-*z* plane in the vicinity of the left corner of the entrance of the slit for ε_{fs}=0.43: (a) $\left\langle \hat{\gamma}^*_{x-y} \right\rangle$ and (b) $\left\langle \hat{\gamma}^*_{x-z} \right\rangle$. The values are obtained as the averaged values of 2,000,000 time steps.

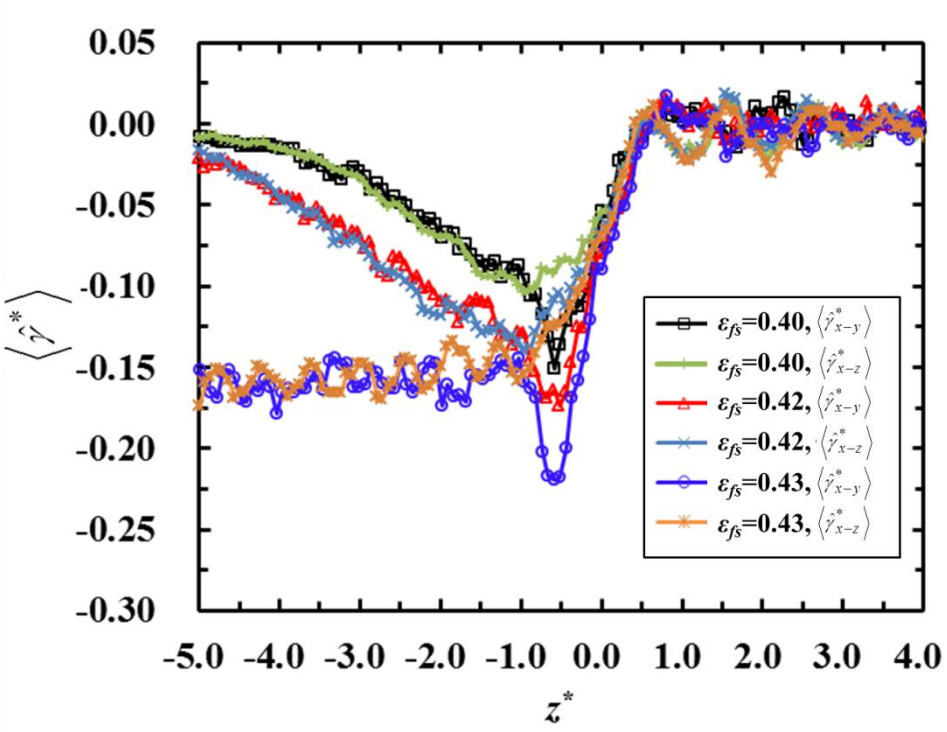

Fig. 7.11 Reduced local interfacial tensions, $\left\langle \hat{\gamma}^*_{x-y} \right\rangle$ and $\left\langle \hat{\gamma}^*_{x-z} \right\rangle$, along the z direction, at the 1st layer of the fluid from the solid surface inside the slit(x^*=7.30), for ε_{fs}=0.40, 0.42, and 0.43. The values are obtained as the averaged values of 2,000,000 time steps.

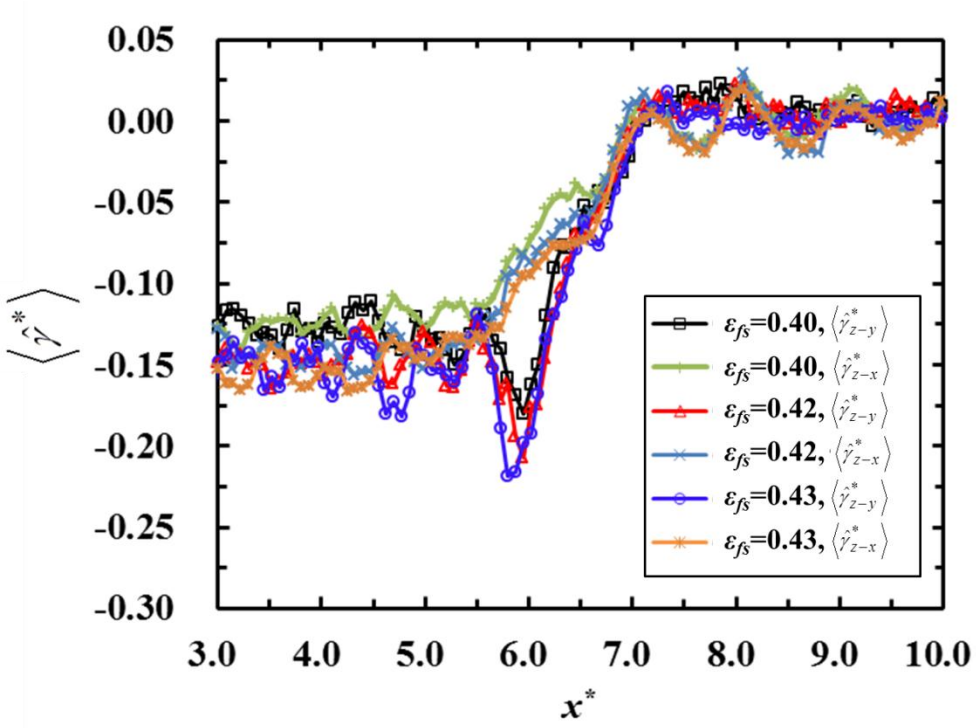

Fig. 7.12 Reduced local interfacial tensions, $\langle \hat{\gamma}^*_{z-x} \rangle$ and $\langle \hat{\gamma}^*_{z-y} \rangle$, along the *x* direction, at the 1st layer of the fluid from the solid surface outside the slit(z^*=0.77), for ε_{fs}=0.40, 0.42, and 0.43. The values are obtained as the averaged values of 2,000,000 time steps.

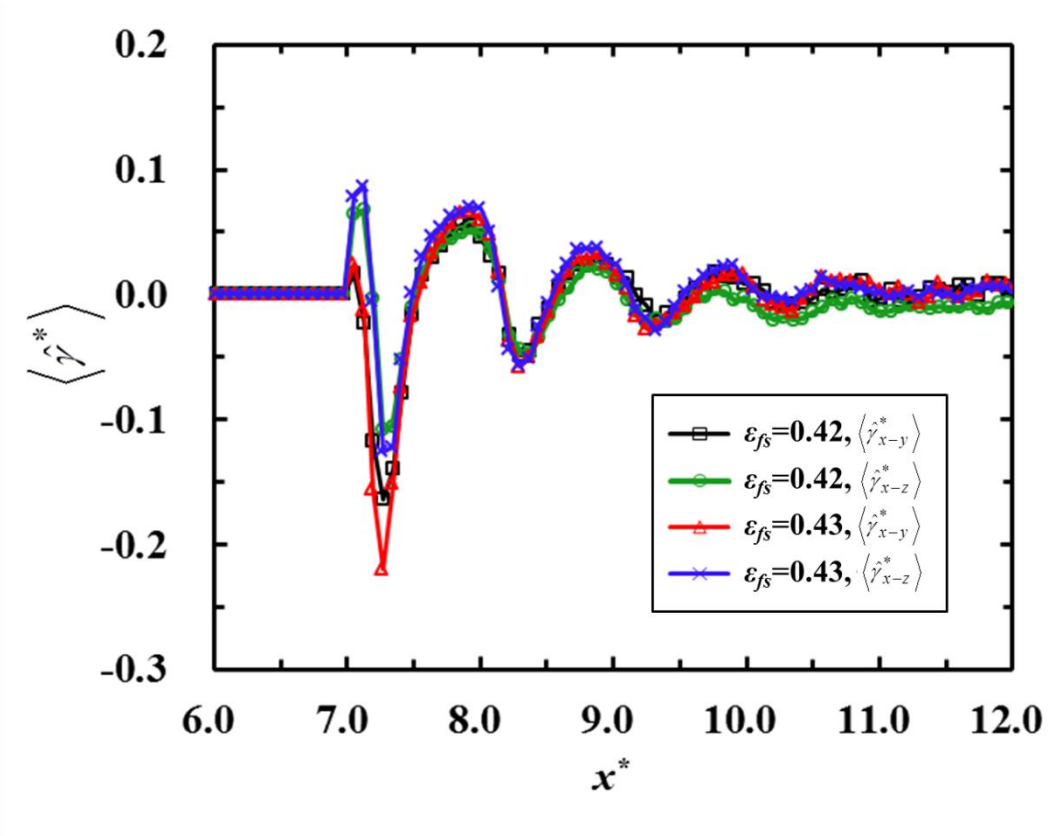

Fig. 7.13 Reduced local interfacial tensions, $\left\langle \hat{\gamma}^*_{x-y} \right\rangle$ and $\left\langle \hat{\gamma}^*_{x-z} \right\rangle$ along the x direction at z^*=-0.55, for ε_{fs}=0.42 and 0.43. The values are obtained as the averaged values of 2,000,000 time steps.

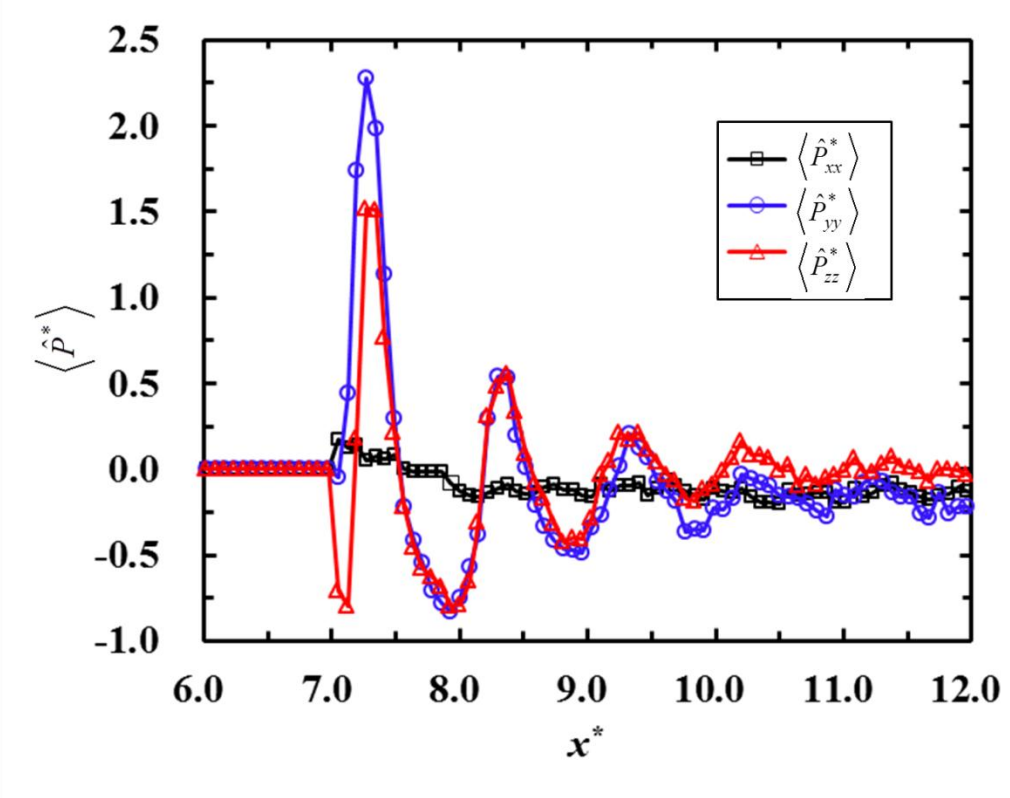

Fig. 7.14 Reduced pressure components, $\langle \hat{P}^*_{xx} \rangle$, $\langle \hat{P}^*_{yy} \rangle$, and $\langle \hat{P}^*_{zz} \rangle$ along the x direction at z^*=-0.55, for ε_{fs}=0.42. The values are obtained as the averaged values of 2,000,000 time steps.

8. Summaries

The results obtained in this thesis are summarized below.

The results in relation to theories and methods for numerical analyses are summarized as follows:

- A general perturbative method on the basis of statistical thermodynamics is proposed for a fluid-solid interfacial system in the canonical and grand canonical ensembles. This method allows us to obtain the local pressure components and interfacial tensions acting on the fluid at a fluid-solid interface which includes contributions of pressure components tangential to the interface affected by interactions with solid atoms.

- An instantaneous expression of the local pressure components and interfacial tensions, which is based on a volume perturbation, is presented to investigate time-dependent phenomena in molecular simulations. The relationship between the description in equilibrium and the time-averaged expression of the instantaneous expression of the pressure, reveals that the two expressions are different in that it contains “ln” in the averaged part in the equation or not.

Numerical analyses are conducted by the classical molecular dynamics method for fluid-solid interfacial systems, where fluid-fluid, fluid-solid, and solid-solid interactions are described by the 12-6 Lennard-Jones potential. Firstly, before detailed analyses of the liquid film on a flat and structured solid surface, a phenomenological analysis of dynamic wetting phenomena at a solid surface with a slit pore is conducted in order to understand dynamic characteristics of a liquid film consisting of fluid molecules, and effects of the fluid-solid interaction intensity on the dynamic wetting phenomena are examined. The results are summarized as follows:

- The wetting phenomena of the slit pore, i.e., whether the inside of the slit pore is filled with liquid molecules within a definite time, as well as the characteristic time of the phenomena, are dependent on the intensity of the fluid molecule–solid atom interaction.

- Increasing the fluid-solid interaction intensity, the number of fluid molecules inside the slit fluctuates before reaching the state of the wetting process.

- The completion time of the slit pore wetting process tends to become short when the interaction intensity between fluid molecules and solid atoms is relatively strong.

Secondly, local pressure components and interfacial tension at a liquid-solid interface are obtained by the proposed perturbative method, and examined in one- and two-dimensions for a system composed of fluid molecules between two planar solid surfaces. In addition, the validity of the proposed perturbative method is investigated by comparison with two alternative methods: the first method evaluates the intermolecular force acting on a plane, and the second is the conventional method based on the virial expression. The accuracy of the numerical results is discussed comprehensively through the comparison of the results obtained by each method. The results are summarized as follows:

- From the results obtained in one dimension, the local interfacial tension of the fluid in the vicinity of the solid surface reveals that quite a small value (on the order of 1.0×10^{-10}) of the perturbation parameter is required to obtain relatively accurate values of the local interfacial tension using the forward or backward difference method. On the other hand, the results obtained by the central difference method are not almost dependent on the values of the perturbation parameter. The calculated local interfacial tension agrees well with the results of the two alternative methods at each local position.

- The results in two dimensions show a characteristic profile of the tangential pressure component which depends on the direction tangential to the liquid-solid interface. In addition, the result of the local interfacial tension calculated by the perturbative method, agrees with that obtained by the evaluation of the force acting on a plane. Such good agreement indicates that the perturbative method proposed in this study is valid to obtain the local pressure components and interfacial tension at a liquid-solid interface.

Thirdly, as the local thermodynamic quantities, time-averaged local pressure components and interfacial tensions are obtained by using the instantaneous expressions of the local pressure components and interfacial tensions, for the two states of the liquid film: (a) liquid film on the slit and (b) liquid film in the slit. Furthermore, the molecular transition mechanism between the two states is examined in detail based on those local thermodynamic quantities. The results are summarized as follows:

- The results of the time-averaged density distribution of the fluid show that there are

states where the liquid film is situated on the slit partially filling the inside of the slit, before reaching the wetting process. Increasing the fluid-solid interaction intensity, leads to the local density of the fluid outside the slit in the vicinity of the corner becoming higher, and with this, the local density inside the slit also becomes higher, before reaching the wetting process. The state of the liquid film in the slit has two peaks of the fluid density in the vicinity of the one corner of the slit.

- The local pressure components tangential to the solid surface in the vicinity of the 1st layer of the fluid from the solid surface are different in a two dimensional plane, and the difference becomes pronounced in the vicinity of the corner of the slit, for cases where the fluid-solid interaction intensities are relatively strong.

- The occurrence of the liquid film in one state or the other depends for the most part on the impregnation parameter outside the slit, which is defined, based on the macroscopic concept, as the difference between the integrated vapor-solid and liquid-solid interfacial tensions acting on the fluid. However it does not determine a definite threshold between the two states on a molecular temporal-spatial scale, i.e., it does not predict fluctuations of the liquid film and variations of the local quantities in the vicinity of the corner of the slit.

- The local interfacial tensions in the vicinity of the 1st layer of the fluid from the solid surface inside the slit, $\langle \hat{\gamma}^*_{x-y} \rangle$ and $\langle \hat{\gamma}^*_{x-z} \rangle$, which are defined by the difference of the pressure components in the width(x), depth(y), and height(z) directions of the slit respectively, indicate that there are points where the values of $\langle \hat{\gamma}^*_{x-y} \rangle$ and $\langle \hat{\gamma}^*_{x-z} \rangle$ are locally low in the vicinity of the 2nd and 3rd layers of solid atoms from the entrance of the slit respectively, for each fluid-solid interaction intensity.

- The minimum value of $\langle \hat{\gamma}^*_{z-y} \rangle$ in the vicinity of the 1st fluid layer from the solid surface outside the slit, is lower than that of $\langle \hat{\gamma}^*_{x-y} \rangle$ obtained inside the slit, for the cases that the liquid film is on the slit, and with an increase in the fluid-solid interaction intensity, the minimum value obtained inside the slit approaches the value of the case that the inside of the slit is filled with the fluid molecules. Furthermore, the pressure components along the width(x) direction in the slit, at the minimum value of

$\left\langle \hat{\gamma}^*_{x-y} \right\rangle$, reveal that the pressure components tangential to a vapor-liquid interface influence the values of $\left\langle \hat{\gamma}^*_{x-y} \right\rangle$ and $\left\langle \hat{\gamma}^*_{x-z} \right\rangle$ in the vicinity of the center of the slit, but the effect is weak for the minimum value of $\left\langle \hat{\gamma}^*_{x-y} \right\rangle$ and $\left\langle \hat{\gamma}^*_{x-z} \right\rangle$. It indicates that the local interfacial tensions inside the slit, $\left\langle \hat{\gamma}^*_{x-y} \right\rangle$ and $\left\langle \hat{\gamma}^*_{x-z} \right\rangle$, in the vicinity of the 2nd and 3rd layers of solid atoms from the entrance of the slit respectively, act as a trigger to cause the transition between the two states of the liquid film.

9. Conclusions

In this thesis, a general perturbative method on the basis of statistical thermodynamics is proposed for a fluid-solid interfacial system in the canonical and grand canonical ensembles. This method allows us to obtain the local pressure components and interfacial tensions acting on the fluid at a fluid-solid interface which includes contributions of pressure components tangential to the interface affected by interactions with solid atoms. In the molecular dynamics simulation, the perturbative method directly evaluates the time-averaged Boltzmann factor of the potential energy difference due to the small perturbation of the local volume, instead of using the conventional method which evaluates the force acting on a plane or virial terms. Comparisons between the results obtained by the proposed perturbative method and by the alternative two methods, indicate that the proposed perturbative method is applicable and suitable for practical use in molecular simulations in equilibrium states, to obtain the local pressure components and interfacial tensions at a fluid-solid interface. However, it should be noted that the description of the pressure components $P_{\xi\eta}$ based on the perturbative method doesn't consider effects of the kinetic part of particles correctly in the case of $\xi \neq \eta$.

Ibergay *et al.* (2007) calculated local quantities by the perturbative method for a vapor-liquid interface in one dimension, and investigated local spatial correlation function defined between the local volumes. Based on the results, they insist that the local quantities obtained by the perturbative method are applicable under the condition that the local quantities are uncorrelated. However, considering the results obtained in this thesis, the nature of the perturbative method is that the quantities are evaluated through one system, which enables us to remove statistical relationships between the local volumes. Spatial dependences of the local quantities should be investigated by the perturbative method, and a comparison with the results of Bennett (1976) could be beneficial to understand deeply the statistically-correlated effects.

An artificial operation, changing the fluid-solid interaction intensity, for the initial state of the liquid film on a solid surface with a slit pore, let the liquid film consisting of molecules move spontaneously, keeping the liquid form in a molecular scale. Such an operation reveals that wetting phenomena of the slit, i.e., whether the inside of the slit pore is filled with liquid molecules within a definite time, as well as the characteristic

time of the phenomena, are dependent on the intensity of the fluid molecule–solid atom interaction. It also reveals that with the increase of the fluid-solid interaction intensity, the number of liquid molecules inside the slit fluctuates before reaching the state of the wetting process, which is unpredictable from macroscopic theories.

In order to examine such phenomena, an instantaneous expression of the local pressure components, which is based on a volume perturbation, is presented, and an instantaneous expression of the local interfacial tensions is defined in this thesis based on the instantaneous pressure components. Then, the time-averaged local pressure components and interfacial tensions are obtained by using them to elucidate the molecular transition mechanism between the two states of the liquid film: (a) liquid film on the slit and (b) liquid film in the slit. The results reveal that the local thermodynamic quantities in the vicinity of the corner of the slit: density, pressure components, and interfacial tensions, are different from those obtained in other areas, for cases where the fluid-solid interaction intensities are relatively strong. The impregnation parameter outside the slit, which is defined, based on the macroscopic concept, as the difference between the integrated vapor-solid and liquid-solid interfacial tensions acting on the fluid outside the slit, predicts for the most part the occurrence of the liquid film in one state or the other. However, it does not determine a definite threshold between the two states on a molecular temporal-spatial scale, i.e., it does not predict fluctuations of the liquid film and variations of the local quantities in the vicinity of the corner of the slit. The results of the time-averaged local interfacial tensions reveal that the minimum values of the local interfacial tensions inside the slit, in the vicinity of the 2nd and 3rd layers of solid atoms from the entrance of the slit respectively, act as a trigger to cause the transition between the two states. These results reveal that there exist the phenomena on a molecular temporal-spatial scale which are not comprehended through the thermodynamic quantities based on the macroscopic concept, and which lead to the transport of the condensed matter.

The effects of the temporal and spatial dependences of the obtained local thermodynamic quantities in this study, on the thermodynamic quantities based on the macroscopic concept, should be investigated for further understanding of fundamentals of molecular transport phenomena of condensed matters.

References

Allen, M. P. and Tildesley, D. J. (1987). *Computer Simulation of Liquids.* Oxford University Press, Oxford.

Bennett, C. H. (1976). Efficient estimation of free energy differences from Monte Carlo data. *J. Compt. Phys.* **22**, 245-268.

Biscay, F., Ghoufi, A., Goujon, F., Lachet, V., and Malfreyt, P. (2009). Calculation of the surface tension from Monte Carlo simulations: Does the model impact on the finite-size effects? *J. Chem. Phys.* **130**, 184710/1-13.

Bohlen, H., Parry, A. O., Díaz-Herrera, E., and Schoen, M. (2008). Intrusion of fluids into nanogrooves: How geometry determines the shape of the gas-liquid interface. *Eur. Phys. J. E* **25**, 103-115.

Callen, H. B. (1985). *Thermodynamics and an Introduction to Thermostatistics,* 2nd ed. John Wiley & Sons, New York.

Cassie, A. B. D. and Baxter, S. (1944). Wettability of porous surfaces. *Trans. Faraday Soc.* **40**, 546-551.

Choi, C. and Kim, M. (2011). Wettability Effects on Heat Transfer. *Two Phase Flow, Phase Change and Numerical Modeling,*edited by Dr. Amimul Ahsan, 311-340.

Choi, G. M. (2014). Necessity of cleaning and its application in future memory devices. *Solid State Phenomena* **219**, 3-10.

de Gennes, P. G., Brochard-Wyart, F., and Quéré, D. (2004). *Capillarity and Wetting Phenomena: Drops, Bubbles, Pearls, Waves.* Springer, New York.

de Groot, S. R. and Mazur, P. (1984). *Non-Equilibrium Thermodynamics.* Dover, New York.

de Miguel, E. and Jackson, G. (2006). The nature of the calculation of the pressure in molecular simulations of continuous models from volume perturbations. *J. Chem. Phys.* **125**, 164109/1-11.

Eppenga, R. and Frenkel, D. (1984). Monte Carlo study of the isotropic and nematic phases of infinitely thin hard platelets. *Mol. Phys.* **52**, 1303-1334.

Evans, D. J. and Morriss, G. (2008). *Statistical Mechanics of Nonequilibrium Liquids*, 2nd ed. Cambridge University Press, Cambridge.

Gloor, G. J., Jackson, G., Blas, F. J., and de Miguel, E. (2005). Test-area simulation method for the direct determination of the interfacial tension of systems with continuous or discontinuous potentials. *J. Chem. Phys.* **123**, 134703/1-19.

Hansen, J.-P. and McDonald, I. R. (2013). *Theory of Simple Liquids*, 4th ed. Academic Press, Oxford.

Harismiadis, V. I., Vorholz, J., and Panagiotopoulos, A. Z. (1996). Efficient pressure estimation in molecular simulations without evaluating the virial. *J. Chem. Phys.* **105**, 8469/1-2.

Hill, T. L. (1986). *An Introduction to Statistical Thermodynamics*. Dover, New York.

Ibergay, C., Ghoufi, A., Goujon, F., Ungerer, P., Boutin, A., Rousseau, B., and Malfreyt, P. (2007). Molecular simulations of the *n*-alkane liquid-vapor interface: Interfacial properties and their long range corrections. *Phys. Rev. E* **75**, 051602/1-18.

Ito, T., Yamada, T., Inao, Y., Yamaguchi, T., Mizutani, N., and Kuroda, R. (2006). Fabrication of half-pitch 32 nm resist patterns using near-field lithography with *a*-Si mask. *Appl. Phys. Lett.* **89**, 033113/1-3.

Irving, J. H. and Kirkwood, J. G. (1950). The statistical mechanical theory of transport processes. IV. The equations of hydrodynamics. *J. Chem. Phys.* **18**, 817-829.

Kirkwood, J. G. and Buff, F. P. (1949). The statistical mechanical theory of surface tension. *J. Chem. Phys.* **17**, 338-343.

Koishi, T., Yasuoka, K., Fujikawa, S., Ebisuzaki, T., and Zeng, X. C. (2009). Coexistence and transition between Cassie and Wenzel state on pillared hydrophobic surface. *Proc. Natl. Acad. Sci. USA* **106**, 8435-8440.

Kumar, V., Sridhar, S., and Errington, J. R. (2011). Monte Carlo simulation strategies for computing the wetting properties of fluids at geometrically rough surfaces. *J. Chem. Phys*. **135**, 184702/1-14.

Ma, X., Wang, S., Lan, Z., Peng, B., Ma, H. B., and Cheng, P. (2012). Wetting mode evolution of steam dropwise condensation on superhydrophobic surface in the presence of noncondensable gas. *J. Heat Trans.* **134**, 021501/1-9.

Maruyama, S. (2000). Molecualr dynamics method for microscale heat transfer. *Advances in Numerical Heat Transfer* **2**, 189-226.

Mickel, W., Joly, L., and Biben, T. (2011). Transport, phase transitions, and wetting in micro/nanochannels: A phase field/DDFT approach. *J. Chem. Phys.* **134**, 094105/1-14.

Míguez, J. M., Piñeiro, M. M., Moreno-Ventas Bravo, A. I., and Blas, F. J. (2012). On interfacial tension calculation from the test-area methodology in the grand canonical ensemble. *J. Chem. Phys.* **136,** 114707/1-8.

Nair, A. R. and Sathian, S. P. (2012). A molecular dynamics study to determine the solid-liquid interfacial tension using test area simulation method (TASM). *J.*

Chem. Phys. **137**, 084702/1-9.

Nijmeijer, M. J. P., Bruin, C., Bakker, A. F., and van Leeuwen, J. M. J. (1990). Wetting and drying of an inert wall by a fluid in a molecular-dynamics simulation. *Phys. Rev. A* **42**, 6052-6059.

Ohara, T. (1999). Intermolecular energy transfer in liquid water and its contributions to heat conduction: A molecular dynamics study. *J. Chem. Phys.***111**, 6492-6500.

Ould-Kaddour, F. and Levesque, D. (2011). Molecular simulation of fluid-solid interfaces at nanoscale. *J. Chem. Phys.* **135**, 224705/1-7.

Plawsky, J. L., Fedorov, A. G., Garimella, S. V., Ma, H. B., Maroo, S. C., Chen, L., and Nam, Y. (2014). Nano- and microstructures for thin-film evaporation-A review. *Nano. Micro. Thermophys. Eng.* **18**, 251-269.

Prigogine, I. (1955). *Introduction to Thermodynamics of Irreversible Processes,* 3rd ed. John Wiley & Sons, New York.

Rowlinson, J. S. and Widom, B. (1982). *Molecular Theory of Capillarity.* Clarendon Press, Oxford.

Schoch, R. B., Han, J., and Renaud, P. (2008). Transport phenomena in nanofluidics. *Rev. Mod. Phys.* **80**, 839-883.

Shi, B. and Dhir, V. K. (2009). Molecular dynamics simulation of the contact angle of liquids on solid surfaces. *J. Chem. Phys.* **130**, 034705/1-5.

Shibahara, M. and Takeuchi, K. (2008). A molecular dynamics study on the effects of nanostructural clearances on thermal resistance at a liquid water-solid interface. *Nano. Micro. Thermophys. Eng.* **12**, 311-319.

Shibahara, M. and Ohara, T. (2011). Effects of the nanostructural geometry at a liquid-solid interface on the interfacial thermal resistance and the liquid molecular non-equilibrium behaviors. *J. Therm. Sci. & Tech.* **6**, 247-255.

Todd, B. D., Evans, D. J., and Daivis, P. J. (1995). Pressure tensor for inhomogeneous fluids. *Phys. Rev. E* **52**, 1627-1638.

Torii, D. and Ohara, T. (2007). Molecular dynamics study on ultrathin liquid water film sheared between platinum solid walls: Liquid structure and energy and momentum transfer. *J. Chem Phys.* **126**, 154706/1-10.

Tully, J. C. (1980). Dynamics of gas-surface interactions: 3D generalized Langevin model applied to fcc and bcc surfaces. *J. Chem. Phys.* **73**, 1975-1985.

Varnik, F., Baschnagel, J., and Binder, K. (2000). Molecular dynamics results on the pressure tensor of polymer films. *J. Chem. Phys.* **113**, 4444-4453.

Verplanck, N., Coffinier, Y., Thomy, V., and Boukherroub, R. (2007). Wettability switching techniques on superhydrophobic surfaces. *Nano. Res. Lett.* **2**, 577-596.

Walton, J. P. R. B., Tildesley, D. J., and Rowlinson, J. S. (1982). The pressure tensor at the planar surface of a liquid. *Mol. Phys.* **48**, 1357-1368.

Wenzel, R. N. (1936). Resistance of solid surfaces to wetting by water. *Ind. Eng. Chem.* **28**, 988-994.

Zhu, S. and Philpott, M. R. (1994). Interaction of water with metal surfaces. *J. Chem. Phys.* **100**, 6961-6968.

Zubarev, D. N. (1974). *Nonequilibrium Statistical Thermodynamics*. Plenum Press, New York.

Zwanzig, R. W. (1954). High-temperature equation of state by a perturbation method. I. Nonpolar gases. *J. Chem. Phys.* **22**, 1420-1426.

List of publications

Papers

1. K. Fujiwara and M. Shibahara, Local pressure components and interfacial tension at a liquid-solid interface obtained by the perturbative method in the Lennard-Jones system, *The Journal of Chemical Physics* **141**, 034707/1-11, 2014.

2. K. Fujiwara and M. Shibahara, A molecular dynamics study on wetting phenomena at a solid surface with a nanometer-scale slit pore, *Nanoscale and Microscale Thermophysical Engineering* **17**, 1-9, 2013.

3. K. Fujiwara and M. Shibahara, A molecular dynamics study on wetting phenomena at a solid surface with a nanometer-scale slit pore, *Journal of Nanoscience and Nanotechnology* **15**, 3143-3146, 2015(in press).

4. K. Fujiwara and M. Shibahara, Local pressure components and interfacial tensions of a liquid film in the vicinity of a solid surface with a nanometer-scale slit pore obtained by the perturbative method, *The Journal of Chemical Physics*(submitted).

Peer-reviewed conference papers

1. K. Fujiwara and M. Shibahara, A molecular dynamics study on wetting phenomena at a solid surface with a nanometer-scale slit pore, *proceedings of The 4th International Symposium on Micro and Nano Technology(ISMNT)*, ID-45, Shanghai, China, October 2013.

2. K. Fujiwara and M. Shibahara, A molecular dynamics study on the wetting phenomena at a soild surface with a nanometer scale slit pore, *proceedings of The 3rd Asian Symposium on Computational Heat Transfer and Fluid Flow(ASCHT)*, ID-037, Kyoto, Japan, September 2011.

3. K. Nakahashi, K. Fujiwara, and M. Shibahara, Effects of the local state of liquid molecules on wetting phenomena at a solid surface with a nanometer-scale slit pore,

proceedings of The 4th Asian Symposium on Computational Heat Transfer and Fluid Flow(ASCHT), 0172-T04-1-P, Hong Kong, June 2013.

Non peer-reviewed conference paper

1. K. Nakahashi, K. Fujiwara, and M. Shibahara, A molecular dynamics simulation on the mechanical balance of the force applied to a thin liquid film on a nanometer-scale slit pore, *The 24th International Symposium on Transport Phenomena(ISTP)*, 95-174, Yamaguchi, Japan, November 2013.

List of publications in Japanese

1. 藤原邦夫，芝原正彦，微細構造を有する固液界面に存在する液膜の熱力学的状態に関する分子動力学解析，日本流体力学会年会 2014 講演論文集，236, 2014.
2. 藤原邦夫，芝原正彦，微細構造を有する固液界面に存在する液膜の熱力学的状態に関する分子論的描像，第 51 回日本伝熱シンポジウム講演論文集，E313, 2014.
3. 藤原邦夫，芝原正彦，微細構造を有する固液界面における液膜の状態遷移に関する分子動力学的研究，日本流体力学会年会 2013 講演論文集，215, 2013.
4. 藤原邦夫，芝原正彦，微細構造物を有する固液界面における液体分子の安定性に関する分子動力学的研究, 第 26 回数値流体力学シンポジウム講演論文集, E01-3, 2012.
5. 佐々木翔平，藤原邦夫，芝原正彦，固体壁面と静的に接する液膜の状態に影響を与える因子に関する分子動力学解析，日本機械学会熱工学コンファレンス 2014 講演論文集, B221, 2014.
6. 中橋和樹，藤原邦夫，芝原正彦，微細構造が固液界面での液体挙動と力の均衡に及ぼす影響に関する分子動力学的研究，日本機械学会熱工学コンファレンス 2013 講演論文集, G111, 2013.
7. 神谷崇仁，藤原邦夫，芝原正彦，界面微細構造が固液界面での液体分子挙動に及ぼす影響に関する分子動力学的研究，日本機械学会熱工学コンファレンス 2012 講演論文集, B115, 2012.
8. 神谷崇仁，藤原邦夫，芝原正彦，界面微細構造が固液界面での液体分子挙動に及ぼす影響に関する分子動力学的研究，第 25 回数値流体力学シンポジウム講演論文集, B10-1, 2011.